MAXIMUM ENTROPY BASED ANALYSIS OF A DS/SSMA DIVERSITY SYSTEM

by

PIETER GERT WESSEL VAN ROOYEN

A thesis submitted as partial fulfilment
of the requirements for the degree

DOCTOR OF ENGINEERING

in

ELECTRICAL AND ELECTRONIC ENGINEERING

in the

FACULTY OF ENGINEERING

at the

RAND AFRIKAANS UNIVERSITY

SUPERVISOR: Prof. J.S. Kunicki
CO-SUPERVISOR: Prof. H.C. Ferreira

November 1994

To Babu

Therefore go forth my little companion,
when you find no highway more, no track,
all being blind, the way to go
shall glimmer in the mind...

SUMMARY

This thesis sets out to propose and analyze a cellular Direct Sequence Spread Spectrum Multiple Access (DS/SSMA) system for the Indoor Wireless Communication (IWC) Nakagami fading channel. The up- and downlink of the system implement Differential Phase Shift Keying (DPSK) and Coherent Phase Shift Keying (CPSK) as modulation schemes respectively, and are analyzed using Maximum Entropy (MaxEnt) principles due to its reliability and accuracy. As a means to enhance system capacity and performance, different forms of diversity are investigated; for the up- and downlink, respectively, RAKE reception and Maximum Ratio Combining (MRC) diversity together with Forward Error Control (FEC) coding are assumed.

Further, the validity of the Gaussian Assumption (GA) is quantified and investigated under fading and non-fading conditions by calculating the missing information, using Minimum Relative Entropy (MRE) principles between the Inter-User Interference (IUI) distribution and a Gaussian distribution of equal variance.

OPSOMMING

Hierdie proefskrif evalueer en stel 'n sellulêre Direkte Sekwensie Sprei Spektrum stelsel voor vir koordlose binnenshuise kommunikasie met Nakagami verspreide kanaal statistieke. Vir die basis-tot-gebruiker en gebruiker-tot-basis verbinding word Koherente Fase Skuif Sleuteling en Differentiële Fase Skuif Sleuteling onderskeidelik voorgestel. Om akkurate evalueringsresultate te verkry word Maksimum Entropie beginsels toegepas a.g.v. die betroubaarheid en akkuraatheid van die tegniek. Om aanvaarbare deurset van die stelsel te verkry word 'n RAKE onvanger en Maksimale Verhoudings Kombineerder saam met foutkorreksie kodering ondersoek as vorms van diversiteit.

Verder word die sogenaamde Gaussiese Aanname (GA) ondersoek en gekwantifiseer onder multi- en enkelpad kondisies deur die entropie tussen die Intergebruiker Interferensie verspreiding en die Gausiese verspreiding, met gelyke variansies, te vergelyk. Hierdie vergelyking word aan die hand van die Minimum Relatiewe Entropie beginsels ondersoek.

ACKNOWLEDGMENTS

I am indebted to many people for their advice and assistance during the period of this work.

In particular to both my supervisors, Professors Jan Kunicki and Hendrik Ferreira, for directing this research and assisting me with invaluable help and suggestions, to Doctor Fritz Solms of the Department of Applied Physics for extensive help with the Maximum Entropy concept, and to Professor Vijay Bhargava (from the University of Victoria, Canada) for affording me the opportunity to work with him for several months.

For financial assistance and unique opportunities I thank Alcatel Altech Telecoms and the Altron Technology Development fund.

Last, but not least, to my parents who taught me that one on God's side is a majority - I hope they will look back and smile at ignorance past.

CONTENTS

LIST OF FIGURES

LIST OF TABLES

CHAPTER 1

INTRODUCTION

"What have I done!?", exclaimed Alexander Graham Bell, examining the latest pocket-size mobile telephone and Dick Tracy like wrist-watch phone. Surely, if Bell was still alive, he would have uttered this, and certainly, we, the "new age" people of the nineties, can only stand amazed at the current telecommunication revolution.

Truly, the invention of telephone in the 19th century was the first step towards shattering the barriers of space and time in communication between individuals. The second step was the successful deployment of radio communications. To date, however, the location barrier has not been completely surmounted; people are more or less tied to telephone sets or "fixed wireline" equipment for communication. The astonishing success of analog cellular radio in providing telecommunication services to the mobile and handheld portable units in the last decade has paved the way towards breaking the location barrier in telecommunications. The ultimate goal of Personal Communication Services (PCS) is to provide instant communication between individuals located anywhere in the world, and at any time.

With an annual growth rate of 40% per year, wireless (mobile) communication is the fastest growing sector of the communication industry [1]. This is in part due to the enormous worldwide success of cellular mobile radio systems and in part due to rapid advances in microelectronics, microprocessors and software engineering in the past decade, which make the design and operation of sophisticated lightweight portable radio systems feasible.

Industry and research organizations worldwide are collectively facing great challenges in providing PCS to industrialised and third world socio-economic communities. Evidence that the latter is in fact being realized is evident; "Mobile communications have grown fastest where few phones went before: in Eastern Europe and Asia. Instead of digging up roads and laying down cables, which would take months or even years, the plan has been to erect base stations for wireless communications that can connect people within a day ..." [2]. Although an important consideration in successful implementation of the PCS is Indoor Wireless Communications (IWC) (i.e. transmission

of voice and data to people on the move inside buildings), it does not, conceptually, exclude the third world scenario. IWC covers a wide variety of situations ranging from communication with individuals walking in residential or office buildings, supermarkets or shopping malls, etc., to fixed stations sending messages to factory workers, robots in assembly lines and the factory environment in general.

Further, as stated in [3], most mobile communication activities take place in dense built up areas or inside buildings. The propagation in both these two environments can be characterised as IWC channels [1] and it is therefore very important to consider these channels when designing a mobile communication system.

Network architecture for in-building communications are evolving. The European-initiated systems such as the Digital European Cordless Telecommunications (DECT), Groupe Special Mobile (GSM), and the Cordless Telecommunications second and third generations (CT2 and CT3) are primarily in-building communication systems, while the Universal Portable Digital Communications (UPDC) in the United States calls for a unification of indoor and outdoor portable radio communications into an overall integrated system. Practical radio communication requires lightweight units with long operation time between battery recharges. Digital communication technology can meet this requirement, in addition to offering many other advantages. There is little doubt that future indoor and outdoor radio communication systems will be digital.

System trade-offs are fundamental to all digital communication designs. The goals, especially for PCS, are minimized required power, which has significance on the power consumption of the portable, minimized system bandwidth, maximized system utilization, that is, to provide reliable service for the maximum number of users, to minimized system complexity and cost; a tall order for any system! It is clear that only a cellular architecture will be able to maximize system utilization, although at the expense of increased system complexity.

The above arguments for the importance of digital cellular IWC systems agree well with related studies in the literature, i.e. [1, 2, 4, 5] to mention a few. This study will therefore concentrate on an application of digital cellular indoor wireless communications.

In a typical indoor portable radio telephone/data system a fixed antenna (basestation), installed in an elevated position, communicates with a number of portable radios (mobiles) inside the building. Due to reflection, refraction and scattering of radio waves by structures inside the building, the transmitted signal most often reaches the receiver by more than one path, resulting in a phenomenon known as multipath fading. As can be expected multipath seriously degrades the performance of communication systems operating inside buildings. Unfortunately, one can do little to eliminate multipath disturbances. However, if the multipath medium is well characterised, the transmitter-receiver pair can be designed to "match" the channel and to reduce the effect of these disturbances. Detailed characterisation of radio propagation is therefore a major requirement for successful design

of indoor communication systems. The signal components from indirect paths, and the direct path (if it exists), combine and produce a distorted version of the transmitted signal. In narrow-band transmission the multipath medium causes fluctuations in the received signal envelope and phase. In wide-band pulse transmission, on the other hand, the effect is to produce a series of uncorrelated pulses (under certain conditions) for each transmitted pulse. Immediately it is clear that wideband signalling has certain inherent characteristics that make it attractive for the IWC channel. The received signal is further corrupted by other unwanted random effects like noise and co-channel interference.

Having described the environment in which PCS for IWC channels operate, let us ponder a moment at current PCS systems. The European systems, like GSM and DECT, standardised on the use of Time Division Multiple Access (TDMA) [6] with higher order modulation schemes, such as GMSK [7] and QPSK respectively. Direct Sequence Code Division Multiple Access (DS/CDMA), also called Direct Sequence Spread Spectrum Multiple Access (DS/SSMA), one of the positive consequences of electronic warfare, is favoured by North American telecommunication companies, notably Qualcomm [8] and PacTel [9]. It is therefore clear that the two leading digital multiple access technologies are TDMA and CDMA. Let us consider some of the advantages and disadvantages of the two techniques.

The capacity of DS/SSMA has long been debated. In the mid eighties a straightforward comparison of the capacity of DS/SSMA to that of conventional TDMA and FDMA for satellite applications suggested a reasonable edge in capacity for the latter two more conventional techniques [10]. This edge was shown to be illusory shortly thereafter [11] when it was recognized that DS/SSMA capacity is only interference limited (unlike FDMA and TDMA capacities which are primarily bandwidth limited); any reduction in interference converts directly and linearly into an increase in capacity [12]. Therefore, since voice signals are intermittent with a duty factor of approximately 3/8, capacity can be increased by an amount inversely proportional to this factor by suppressing transmission during the quiet periods of each speaker. Similarly, any spatial isolation through use of multi-beamed or multi-sectored antennas, which reduces interference, also provides a proportional increase in capacity, especially in a cellular environment [13]. These two factors, voice activity and spatial isolation, were shown to be sufficient to render DS/SSMA capacity at least double that of FDMA and TDMA under similar assumptions for mobile satellite applications [11].

Further, DS/SSMA exhibits its greatest advantage over TDMA and FDMA in terrestrial digital cellular systems, for here isolation among cells is provided by path loss, which in terrestrial UHF propagation typically increases with the fourth power of the distance. Consequently, while conventional techniques must provide for different frequency allocation for contiguous cells (only reusing the same channel in one of every 7 cells [9] in present systems), DS/SSMA can reuse the same spectrum in all cells, thereby increasing the capacity by a large percentage of the normal frequency reuse factor. The net improvement in capacity, due to all the above features, of DS/SSMA over

digital TDMA or FDMA is on the order of four to six and over current analog FM/FDMA, nearly a factor of twenty [9]. Let us briefly summarise some specific advantages and disadvantages of DS/SSMA as opposed to TDMA and analog FDMA.

The advantages can be summarised as follows:

- DS/SSMA can be used in a frequency band that has existing users, therefore it is an effective and efficient mode of frequency band utilisation, making the transition from analog to digital easier [14],
- DS/SSMA does not need the network synchronisation that TDMA requires [15],
- it is simple to generate since no frequency synthesizer is required [16],
- privacy is achieved since each user has his own unique signal set [17],
- in DS/SSMA, transmission can be suppressed during instants when the user is listening or pausing, thus a voice activity factor of roughly 40% may be used to increase system capacity [14], and
- very important for a PCS environment, multipath mitigation and interference suppression is inherent to the wideband signal [9].

However, nothing is for free; the overriding minus for a DS/SSMA system is the need for power control, the subject of many papers in the literature i.e. [18]. On average, all signals should arrive at the receiver with the same average power in order to get a reasonable throughput. Without power control, a user near the base station would overwhelm the others. Also, the capacity of a DS/SSMA system depends on several factors among which the performance of the power control technique itself [8].

As a point of note, DS/SSMA is normally suggested because of the unconditional applicability of coherent demodulation, while for Frequency Hop SSMA (FH/SSMA) systems, coherent demodulation is a severe challenge because of the random phase of the received signal as the carrier hops from one frequency to another [19].

Since spread spectrum as a technology is still new, it is crucially important to have theoretical performance results under frequently encountered conditions available. To evaluate a spread spectrum system, and in fact any digital communication system, certain assumptions have to be made and/or certain standard techniques can be used. One of the most common assumptions in performance evaluation of a SSMA system is to assume that the Interuser Interference (IUI) has a Gaussian distribution. To obtain accurate results, however, this assumption is not necessarily valid.

The question therefore arises, how can a SSMA system be evaluated accurately? One of the most straightforward methods is most certainly by computer simulation. The problem, however, is that simulations are very time consuming when a SSMA is to be evaluated - to calculate one point on an error rate curve with a moderate number of users and a moderate spreading factor can take up to five hours! It is clear that other methods has to be investigated.

With the above as background, this thesis sets out to accurately evaluate the performance and capacity of a indoor wireless communication, direct sequence spread spectrum system. To accurately assess the inter user interference, the Maximum Entropy method is investigated as a means to accomplish this.

1.1 Literature Survey

An overview of current papers available in the open literature on SSMA and the evaluation of digital communication performance, that is the calculation of error statistics such as the average error rate, is presented.

1.1.1 Spread Spectrum Multiple Access

This section outlines the significant recent studies of asynchronous SSMA systems. A very large body of literature exists on the analysis of SSMA systems, among which are [20, 21, 22, 23, 24, 18] and [25]. Much of this literature, such as the initial work by Cooper and Nettleton [26], considers FH/SSMA. Here is a brief discussion on some of the existing literature on the analysis of DS/SSMA systems.

Most analysis of DS/SSMA have resulted in Gaussian approximations, and various upper and lower bounds on the bit error probability for AWGN channels [20, 21, 22, 23]. For specular multipath-fading channels, Geraniotis and Pursley have approximated the bit error probability of single user DS systems that use coherent [27] and non-coherent [28] detection. This analysis has been extended to DS/SSMA for a multipath rejection receiver [29]. A few attempts have been made to evaluate the performance of a multipath combining receiver. Lehnert and Pursley [30] have concluded that a multipath combining receiver can overcome the increased effect of multiple-access interference due to multipath, provided that the receiver has knowledge of the amplitudes, delays and phases of the multiple received signal replicas.

Lam and Steel [31] have evaluated the performance of multipath receivers by simulation. For their purpose they used the frequency-selective, slowly fading, multipath channel model developed by Hashemi [1]. Despite channel sounding, multipath diversity and antenna diversity, it was reported

that a processing gain of 31 could only support three simultaneous transmissions at a bit error rate less than 10^{-2}. In contrast, the same system could support twelve transmissions on an AWGN channel. Turin [23] has also estimated the maximum number of allowable users for a DS/SSMA system that uses differentially coherent multipath combining receivers. For an AWGN channel, it was reported that the maximum number of allowable users is about 10-20% of the processing gain for a bit error rate of $10^{-5} - 10^{-3}$. However, for an urban multipath-fading channel without power control, this figure drops to 1-5% even with ideal multipath combining receivers. Xiang [25] also observed the same effect. If the channels consist of a single faded link then DS/SSMA may be unusable, a conclusion also reached by Gardner and Orr [32]. Power control will only partially recover the reduction in capacity due to multipath-fading, because power control cannot compensate for rapid signal fluctuations caused by multipath-fading [23]. For a multiple-cell DS/SSMA system, it is possible that power control can improve the downlink performance. The reason is the corner effect, where a mobile in a cell corner is equidistant from three base stations and will experience an increase in multiple-access interference. Nettleton and Alavi [33], [34] and Lee [9] have shown that downlink power control can be quite effective for channels without multipath fading.

Kavehrad and McLane [35] analyzed the performance of low-complexity channel coding and space diversity for the IWC channel, and showed that a combination of space diversity and coding are most effective in a multipath-fading environment. Boudreau et al [36] considered trellis and convolutional coding under AWGN conditions. Their conclusion was that convolutional coding performs better than trellis codes because of the larger minimum distance properties of convolutional codes.

All of the above mentioned literature, except Xiang [25], assumed either Rayleigh or Rician fading statistics. It has been shown, however, that the Nakagami-m distribution assumes the signals are received with random moduli and phases, leading to more flexibility in matching experimental data than that of Rayleigh or Rice models [18, 37, 38] and [39] to mention a few. This is especially true for the indoor wireless and densely built urban channels.

With this as background it is possible to illustrate where this work fits into the global SSMA picture. Instead of using Rayleigh fading with its fixed parameters, the average error rate of a SSMA system with Nakagami-m fading is presented. Further, most of the above mentioned literature use the Gaussian Assumption when calculating error statistics. It could therefore be argued that the Gaussian Assumption is indeed valid, but it has been shown by numerous authors [35, 40] that the Gaussian Assumption leads to an overly optimistic estimate of the SSMA capacity. To investigate this statement various techniques are implemented to give a quantative feel for the validity of the Gaussian Assumption. It is found that the assumption is not very accurate under certain conditions and therefore the MaxEnt formulism is implemented to accurately calculate the SSMA error statistics.

Therefore, this work extends the literature in numerous ways when the performance and capacity of a SSMA system is evaluated - calculating the average error rate using the exact correlation

parameters of the spreading codes via the MaxEnt method for a Nakagami-m faded channel. In addition to this, the system is evaluated with various forms of diversity - in the downlink of the cellular system the performance is evaluated using RAKE reception and error control coding while the uplink is evaluated with MRC diversity and error control coding. This evaluation is new and allows for a more flexible and accurate indication of the performance and capacity of a cellular SSMA system.

In certain respects the system model considered in this work addresses some of the same issues as the above literature, but with a different approach and emphasis. The basic approach is to evaluate the uplink and the downlink of the cellular system as a non-coherent and coherent link respectively. For non- coherent and coherent reception DPSK and PSK are respectively employed as modulation schemes. The reason for this is that the downlink can transmit a pilot tone to coherently lock all the mobiles, while this is not feasible for the uplink. This has interesting consequences, one of which is unequal capacity between the uplink and downlink and will be quantified.

1.1.2 Calculation of Error Statistics in Digital Communication Systems

As mentioned earlier, the IUI random variable is accurately estimated and therefore the calculation of error statistics are accurate. This section gives a background to numerical techniques, like MaxEnt and Gauss Quadrature Rule (GQR) principles, to calculate accurate error statistics.

A usual problem in digital communications is to mathematically estimate the probability density function (pdf), $p(x)$, which is generally unknown, to calculate average error probabilities. It is, however, possible in many instances to easily calculate a finite number of moments of the unknown pdf, from which there are a variety of techniques available, to estimate the density function accurately.

One possibility is to expand $p(x)$ in a set of orthogonal polynomials. The resulting series is truncated after $N_m + 1$ terms, and the coefficients or weights in the expansion of the unknown pdf. This requires solution of a system of $N_m + 1$ linear equations. Proper choice of weighted orthogonal polynomials leads to fast convergence as N_m grows. An improper choice, however, can lead to oscillating approximations of $p(x)$, and there is further inaccuracy from lack of positivity at each stage of iterations. A popular choice for orthogonal polynomials are Hermite polynomials [41, 42]. It should be noted that Murphy [43] and Nakhla [44], respectively, used Legendre and Chebyshev polynomials. Nakhla's [44] result is related to Murphy's by the way of an approximation in evaluating the coefficients in the series expansion. For a large number of problems, both results exhibit good convergence properties with respect to the number of moments required.

Powerful alternatives have been developed [45] over many years. For example, Gauss Quadrature Rules (GQR) [46] were applied to evaluation of error probability due to ISI in digital communication

by Benedetto et al [47, 48]. Here the unknown density is defined by the quadrature rule $\{w_j, \delta_j\}_{j=1}^{N_c}$, a set of weights and nodes. Using N_m known moments, $N_m = 2N_c + 1$, entails the solution to a set of nonlinear equations by diagonalization of a tridiagonal Jacobi matrix [46]. The corresponding numerical results are stable and accurate if enough moments are available.

Probably the most powerful technique available to estimate an unknown density function from its moments is the Maximum Entropy (MaxEnt) method. Shore and Johnson [49] have proven that the MaxEnt method [50, 51, 52, 53] is the only method for inferring from incomplete information that does not lead to logical inconsistencies. This proof has put the MaxEnt principle on a very solid foundation. Kavehrad et al [54, 55] have extended the application of MaxEnt to evaluation of average error rates in digital communication systems. They have shown that the MaxEnt method achieves results with typically a few moments, while the GQR method required many more moments to obtain the same, as accurately. The method requires about the same number of moments as techniques based on orthogonal expansions, and, in addition, provides an estimate of the pdf of the target variable.

Of these three methods described, the most powerful and most often used techniques are the GQR formulation and the MaxEnt method. A tradeoff between these two techniques is conducted when the interuser interference (IUI) pdf and average error probability of a SSMA system is to be calculated.

To try and quantify the accuracy of the Gaussian Assumption, the Minimum Relative Entropy (MRE) principle, related to the MaxEnt principle, is further implemented.

In essence the comparison between the different numerical techniques and the accuracy of the Gaussian Assumption is the subject of only one chapter, but of such importance that its lays the basis of all the chapters that follow.

1.2 Thesis Contributions

In order to fulfil the main goal of this thesis, to accurately evaluate an IWC system employing DS/SSMA as multiple access scheme and assuming Nakagami fading statistics, many new results are obtained and reported in e.g. [56, 57, 58, 59, 60, 61, 62, 63, 64, 65, 66, 67]. Consequently, the major contributions of this work can be summarized as follows:

- New results are obtained when GQR and MaxEnt techniques are compared when average error rates are calculated for digital communication systems,
- the validity of assuming the IUI random variable as being Gaussian distributed is investigated and accurately estimated via the MaxEnt method, with closed form expression for the IUI pdf

presented. In addition, using the Minimum Relative Entropy (MRE) principle, a quantative indication of the validity of the Gaussian Assumption is presented,

- a simple cellular DS/SSMA system is accurately evaluated using the MaxEnt principle,
- the above mentioned system is evaluated under Nakagami fading conditions with various forms of diversity and error control coding,
- not only performance evaluations are considered, but actual capacity estimates are presented,
- although the Gaussian Assumption is found to be inaccurate, closed form expressions for Nakagami fading with diversity (RAKE reception and MRC) are presented. This enables a comparison to the validity of the Gaussian Assumption under Nakagami fading with diversity,
- a comparison between the performance of convolutional- and block coding in a SSMA environment is performed,
- the influence of low rate coding on the performance and capacity of a SSMA system under faded and unfaded conditions are also investigated.

1.3 Thesis Organization

The general background and topic of this study, as well as an overview of the relevant papers in the open literature, have been presented in this introduction.

Chapter 2 is aimed towards describing an appropriate cellular system model to analyze the performance of a DS/SSMA system under multipath fading and additive noise conditions for the indoor wireless PCS. It also describes the major attributes to be gained from the described SSMA cellular system, and further strengthens the argument to use SSMA as a technology. Further, a method is proposed that allows for very uncomplicated capacity assessments of the cellular SSMA system, and an appropriate channel model is described together with the notation to analyze the SSMA system.

The system described in Chapter 2 is analyzed in detail for the uplink and downlink of the relatively simple, although realistic, cellular system derived. By relatively simple it is meant that binary modulation schemes, such as PSK and DPSK, are considered, with many new results, i.e. [65, 61]. General performance expressions is also derived for the downlink, when Coherent Phase Shift Keying (CPSK) with RAKE reception is assumed, and the uplink, when DPSK with diversity and Maximum Ratio Combining (MRC) is assumed. These closed form expressions are only valid when the Gaussian Assumption is used, and is therefore only for comparative purposes.

The Inter User Interference (IUI) in a DS/SSMA system is often assumed to have a Gaussian probability distribution function (pdf) [20], and is probably the most frequently debated issue in SSMA communications. It has many times been shown as an underestimate of the interuser interference (IUI), i.e. [35], under certain conditions. By investigating the accuracy of two methods, the GQR [24] and MaxEnt methods [54], and by estimating a pdf from its moments, it is possible to quantify how close the IUI random variable is to a Gaussian variable. It is shown that the tail probability of the IUI does not follow the Gaussian pdf very accurately and hence, under certain conditions, is not reliable when average error rates are calculated. The investigation also delivers some supplementary results on the accuracy of GQR formulas when compared to the MaxEnt method. Results and discussions on the above are found in Chapter 4.

When fading is neglected in the model described in Chapter 2, or the Nakagami fading parameter m is assumed infinitely big, a special case of the mobile system of Chapter 2 results; a stationary SSMA system, with performance results presented in Chapter 5 for benchmark purposes. These results can be used quite productively to predict the capacity of a stationary IWC system (under certain conditions) or a stationary rural communication system. Viterbi [68, 69] has shown that low rate coding can improve the capacity of a SSMA system tremendously; this statement is verified and quantified for a few specific convolutional and block codes with hard decision decoding. It is shown that only under specific practical conditions the statement by Viterbi is correct, but in general, coding is a very powerful means to increase the capacity of a SSMA system.

Chapters 6 and 7, respectively, describe the downlink and uplink performance and capacity of an IWC system under Multipath Fading, Noisy Channel (MFNC) conditions. The performance for different Nakagami fading parameters are investigated with a maximum of five diversity branches. The influence of low rate convolutional and block coding is also investigated, and it is shown that error control coding, combined with diversity, is the most effective way to improve system capacity under MFNC conditions.

The study is concluded in Chapter 8 with general conclusions and suggestions for future research.

Appendix B and C respectively describe the spreading sequences and error control codes used in the performance and capacity calculations. Appendix E and D provide relevant moment information, whereas Appendix A describes some of the important features of the Nakagami distribution. Finally Appendix F, G and H provide derivations relevant to determine closed form expression for CPSK and DPSK using the Gaussian Assumption.

CHAPTER 2

SYSTEM MODEL

This chapter describes a generic digital cellular DS/SSMA system together with an appropriate multipath channel model that characterizes the IWC channel.

Instead of assuming a conventional cellular model where the average error rate is calculated at a specific distance from the basestation, the *average* error rate of the cellular system is calculated. The advantage of assuming such a system model is that the capacity of a single or multiple cell cellular system can easily be assessed. The cellular system is described in Section 2.1.

Further, the features of the proposed system are described in Section 2.2. The system description includes a discussion on how the system will handle power control, cell-to-cell handoff, frequency reuse, voice activity monitoring etc. Some of the unique features of the system, which will also be discussed, are multiple forms of diversity, privacy, enhanced capacity (relative to other multiple access schemes), "soft" capacity and relatively low transmit power.

The system described will be analyzed and its performance evaluated in subsequent chapters.

2.1 Cellular System Architecture

2.1.1 Equivalent System Model

The cellular layout is described by a uniform planar grid of J hexagonal cells, as described in Figure 2.1. Each cell contains a centrally located base station. The cells can be divided into 120^0 sectors, where each sector employs the same carrier frequency. The mobiles are uniformly distributed throughout the system area with a density of K' mobiles/cell, using DS/SSMA to establish a full-duplex channel with the base station. All cells are assumed to be equally loaded, with the up- and downlink transmission on two different frequencies.

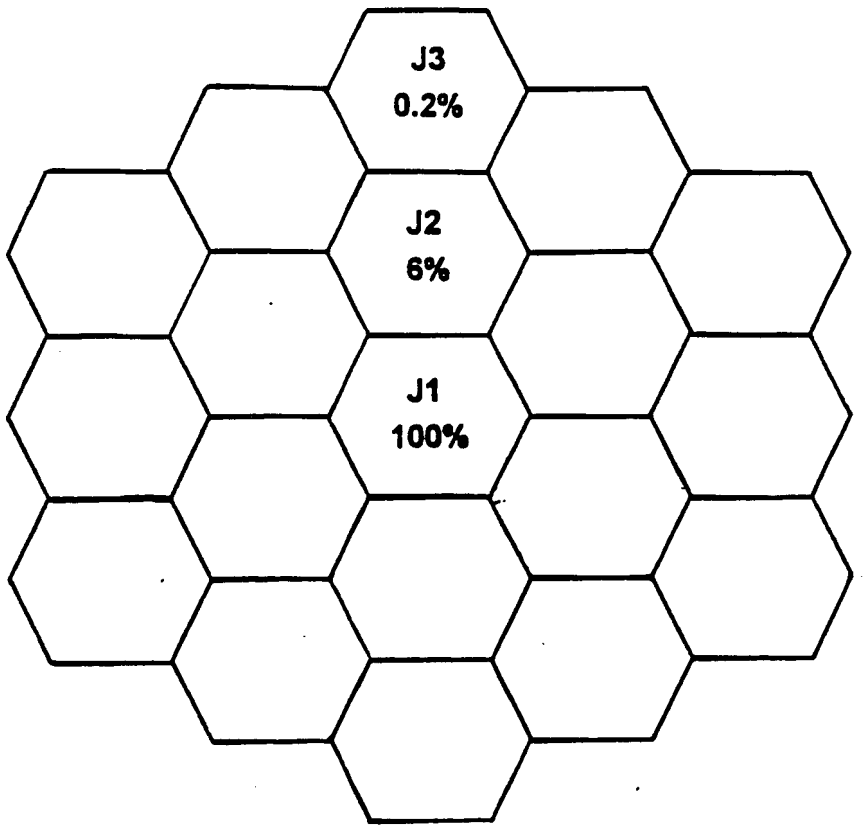

Figure 2.1: Cellular system model

Since the wideband SSMA signal is reused in every cell, the total interference at the cell site, to a given inbound mobile station, is comprised of interference from other mobile stations in the same cell plus interference from mobile stations in neighbouring cells. Also indicated in Figure 2.1, is the percentage of **average** interference contributions from neighbouring cells when a fourth order propagation path loss exponent is assumed [8].

Our cellular system analysis differ from previous multiple cell analysis; a simple, yet effective, method is proposed to determine the cellular capacity. A maximum interference parameter, K, is defined that includes the interference from all mobiles in all cells (adjacent plus reference cells). In other words, the maximum interference, K, can be written as

$$K = K' \frac{V_{on}}{N_{sect}} \{J_1 + 0.06 \times J_2 + 0.002 \times J_3 + \cdots\}, \tag{2.1}$$

where K' is the total number of mobiles/cell, V_{on} the voice activity factor, N_{sect} the cell splitting factor and $\{J_i\}, i \neq 1$ the interfering cells in the first to ith tier surrounding the reference cell (J_1). Experimental measurements [8] indicate that the total interference from all surrounding tiers contribute approximately 50% of the total interference. Therefore, (2.1) can be written as

$$K = K' \frac{N_{sect}}{V_{on}} 1.5 \tag{2.2}$$

Using (2.2), it is possible to analyze the **average** performance of a cellular SSMA system. In our calculations K will be calculated and K' (the number of users/cell) can then be determined using (2.2). When only one cell without voice activity monitoring or cell splitting is considered, (2.1) simplifies to $K = K'$. However, it is evident that many of the inherent advantages of SSMA are lost when a non-cellular system is considered.

The equivalent cellular star architecture is as indicated in Figure 2.2, which has been used frequently in previous studies of single cell asynchronous SSMA systems [24, 70, 71]. The system consists of K users transmitting over a MFNC which is further corrupted by IUI, and K is as defined in (2.2). The three sections which a communication system consists of are indicated in Figure 2.2; that is the transmitter, channel and receiver. The transmitter consists of a FEC encoder whose output is spread and up converted to an RF frequency. The modulated signal is transmitted through a channel and despread, demodulated and decoded by either a CPSK or DPSK receiver for the down- and uplink respectively. The following sections describe each component in more detail.

2.1.2 Notation

The following notation is based on that developed by Pursley [71] and utilized by Kavehrad in his analysis of SSMA for indoor wireless radio [24]. Each user transmits using a different spreading code and the signal transmitted by the kth user, $s_k(t)$, is assumed to be delayed randomly by a delay of τ_k. Therefore, if the receiver of the ith user is attempting to receive the signal transmitted by the jth user, the demodulated signal will consist of the desired signal, effects of the channel fading statistics and interference due to a combination of AWGN and the cross-correlation from the signals transmitted by the other users in the system with random phase ψ_k.

The kth user's information signal, $b_k(t)$, is a sequence of rectangular pulses taking on values from the set $\{\pm 1\}$ over a T-second interval, represented as

$$b_k(t) = \sum_{j=-\infty}^{\infty} b_j^k P_T(t - jT), \tag{2.3}$$

where b_j^k represents the kth users's data at the jth timing interval and $P_T(\cdot)$ is a rectangular waveform of T-seconds duration. The kth user is assigned a code waveform $a_k(t)$ that consists of a periodic sequence of rectangular chips taking on values from the set $\{\pm 1\}$ each of duration T_c seconds. If a_i^k represents the ith chip value of the kth user, then,

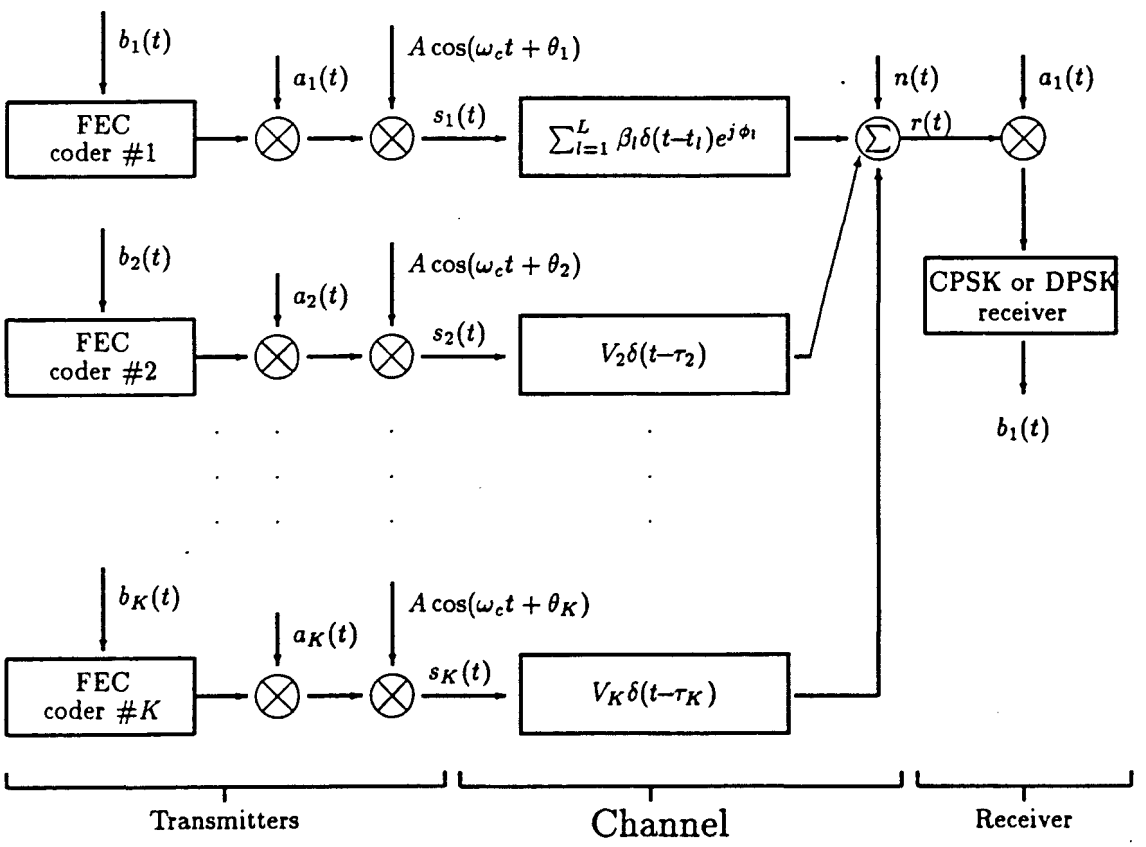

Figure 2.2: System model

$$a_k(t) = \sum_{j=-\infty}^{\infty} a_j^k P_T(t - jT). \tag{2.4}$$

We assume that each user's code sequence has a period of $N = T/T_c$. That is, there is one period of code sequence per data bit and is generally known as the processing gain of a spread spectrum system.

After spreading the information bandwidth to N times its original value, by modula-2 adding the direct sequence code to the data signal, bi-phase modulating the result onto the carrier signal, $A\cos(\omega_c t + \theta_k)$, where A is the carrier level, ω_c is the nominal carrier frequency and θ_k is the carrier phase that is assumed to be uniformly distributed between [0,2π), the transmitted signal of the kth user, becomes

$$s_k(t) \;=\; Aa_k(t)b_k(t)\cos(\omega_c t + \theta_k) \qquad \forall \qquad k = 1, 2, \cdots, K. \tag{2.5}$$

In the downlink transmission, that is from basestation to outstation, all K users can easily be synchronized and therefore the wideband signal will have better correlation properties than for the uplink, where each user's signal adds asynchronously in the air. Therefore, the downlink capacity and performance analysis will be more conservative than the uplink performance since it is assumed that all codes add with random carrier and code phase.

Two types of error control coding schemes are investigated to enhance the performance of the system indicated in Figure 2.2; these are convolutional and block codes. When coding is considered, the performance comparison has to be performed on an equatable base, therefore N, the spreading sequence length has to be reduced by the code rate, R_{cd} of the FEC code.

2.1.3 Transmission Channel Model

In spread spectrum transmission over multipath-fading channels, like IWC channels, the spread bandwidth of the transmitted signal exceeds the coherence bandwidth of the channel, the multipath components can be resolved into a discrete number of faded paths. The number of resolved paths depends on the channel multipath spread and the spreading bandwidth of the signal, as discussed by Proakis [72] and Lee [9].

As an example; for a typical IWC channel, the mean delay spread Δ, is typically 60-100 ns [35]. The transmission rate, R, should be based on the maximum delay spread, which can be about 2Δ. If a low bit error rate performance and little intersymbol interference is required then

$$R \leq \frac{1}{2\Delta}. \tag{2.6}$$

For an IWC channel the chip rate should therefore be 5-8.3 MHz. For example, if we choose to transmit speech at a rate of 16 kbps the maximum allowable processing gain is 27 dB (for $\Delta = 60$ ns) when Nyquist filtering is assumed. This translates to a maximum of $N \approx 511$, to adhere to the low error rate and negligible intersymbol interference criteria.

We assume that the IWC channel for the desired transmitter and receiver, depicted in Figure 2.2, can be represented by an L-paths fading model where a single transmitted pulse is received via L-paths at the random instants $t_l, l = 1, \cdots, L$. We assume that t_l is uniformly distributed over one bit period, that is over $(0, T]$. This is ensured by signalling at baseband at a rate less than the channel coherence bandwidth. Hence, intersymbol interference is negligible here.

To keep the analysis tractable we will assume that the kth interfering user, $k \neq 1$, of the multiple-access system is linked to the receiver of Figure 2.2 via a single Nakagami fading path with a uniformly distributed random delay τ_k ranging from zero to one bit T. This will result in a worst case scenario, rendering our results conservative, i.e. more elaborate models, incorporating more noise sources can only strengthen our conclusions.

When matched filter reception is considered, the time-invariant low-pass equivalent impulse response of the passband channel, $h(t)$, can be represented by

$$h(t) = \sum_{l=1}^{L} \beta_l \delta(t - t_l) e^{j\phi_l}, \tag{2.7}$$

where $\delta(\cdot)$ is the Kronecker delta, β_l is a Nakagami distributed random path gain and ϕ_l is the random path phase, uniformly distributed between $(0, 2\pi]$ (See Appendix A for a description of the Nakagami distribution). It is further assumed that all the parameters of all paths are identically distributed over their specified range. These assumptions are related to Turin's [23] description of a discrete multipath fading environment. As stated earlier, the L-paths model stems from the fact that spread spectrum signalling with a transmitted signal bandwidth much wider than the coherence bandwidth of the multipath fading channel enables components to be resolved. Therefore, the IWC channel can be characterised as frequency selective, slowly fading, i.e. [24, 9, 25, 18].

Since our signal bandwidth is much greater than the coherence bandwidth of the channel, B_c, we can use this inherent property of SSMA to resolve the multipath conditions by providing the receiver with several independent fading signal paths. Consequently, there are ΔB resolvable signal components, where B is the signal bandwidth. Since $\Delta \approx 1/B_c$, the number of resolvable signal components may also be expressed as B/B_c. Thus the use of a wideband signal may be viewed as

just another method for obtaining frequency diversity of order $P \approx B/B_c$. The optimum receiver for processing the wideband signal is called a RAKE receiver and will be compared to matched filter reception for the CPSK downlink. For the DPSK uplink space diversity with MRC combing diversity is assumed and is also compared with a matched filter receiver.

For analysis of the RAKE receiver and MRC combining diversity, the IWC channel is a continuum of multipath components, with low- pass impulse response of the channel $c(\tau;t)$. It is commonly modelled as a tapped delay line with a tap spacing equal to the chipping rate, T_c, i.e.

$$c(\tau;t) = \sum_{n=-\infty}^{\infty} c_n(t)\delta(\tau - nT_c), \tag{2.8}$$

where the tap gains $\{c_n(t)\}$ are complex Gaussian random processes. For a wide-sense stationary channel with uncorrelated scattering, the $c_n(t)$ are uncorrelated and, since they are Gaussian, independent. For a total multipath spread T_m, the tapped delay line can be truncated at $P = \lfloor T_m/T_c \rfloor + 1$ taps, where $\lfloor x \rfloor$ is the largest integer contained in x. For a slowly varying channel, $c_n(t) = c_n$ for the duration of several tens of bits.

Assuming the above tapped delay line model, the total **instantaneous** received signal-to-noise ratio is given by

$$\gamma_b = \sum_{i=0}^{P-1} \gamma_i, \tag{2.9}$$

where $\gamma_i = |\beta_i|^2 E_b/N_0$ and E_b/N_0 is the received signal-to-noise ratio per bit in the absence of multipath fading.

From Figure 2.2, the interuser and multipath delays, τ_k and t_l respectively, are received independent and asynchronous compared to the desired user sequence. The distribution of the interfering users and multiple path amplitudes is further assumed to be Nakagami distributed, with path gain specified by $V_k, k = 1, 2, \cdots, K$ and $\beta_l, l = 1, 2, \cdots, L$, respectively. Therefore, as depicted in Figure 2.2, the received signal for the faded model, is given by

$$\begin{aligned} r(t) &= A\sum_{l=1}^{L} \beta_l a_1(t - t_l) b_1(t - t_l) \cos(\omega_c t - \omega_c t_l + \phi_l + \theta_1) \\ &+ A\sum_{k=2}^{K} V_k a_k(t - \tau_k) b_k(t - \tau_k) \cos(\omega_c t - \omega_c \tau_k + \theta_k) \\ &+ n(t), \end{aligned} \tag{2.10}$$

where $n(t)$ is white Gaussian noise with double-sided spectral density of level $N_0/2$ and θ_1 can be assumed zero with no loss in generality.

In Chapter 4 the signal in (2.10) will be used as input to CPSK and DPSK receivers to respectively analyze the down- and uplink performance of the system described in Figure 2.2.

2.2 System Features

This section is aimed to describe the major attributes and characteristics of the proposed cellular system model and to suggestions how to accomplish power control, cell handoffs etc. The description is not strictly limited to the IWC channel and can also be applied to an urban cellular mobile system. Some of the system concepts stem from the Qualcomm SSMA cellular system [8, 9, 73], but differs in the respect that the Qualcomm system is inherently narrowband system, while the proposed system is inherently wideband.

Since differential PSK and coherent PSK are respectively assumed for the uplink and the downlink of the cellular system, the capacity in the two directions is not equal. Therefore, more efficient coding or more diversity branches is needed in the uplink for the system to ensure an even capacity. The discrepancy in capacity between the two directions is quantified in chapters to follow.

2.2.1 Multiple Forms of Diversity

In relatively narrowband modulation schemes such as analog FM modulation, employed by the first generation cellular phone systems, the existence of multipath causes severe fading. With wideband SSMA modulation, however, the different paths may be independently received, greatly reducing the severity of the multipath fading. This is not completely eliminated because multipaths which cannot be independently processed by the demodulator occasionally occur. This will result in some fading behaviour.

Diversity is the favoured approach to mitigate fading [72]. There are three major types of diversity; time, frequency and space. Time diversity can best be obtained by the use of interleaving and error correction coding. Wideband SSMA offers a form of frequency diversity by spreading the signal energy over a wide bandwidth; frequency selective fading usually affects only a 200-300 kHz portion of the signal bandwidth [72]. Space or path diversity is obtained in three different ways, by providing the following:

- Multiple signal paths through simultaneous links from the mobile station to two or more cell sites (soft handoff),

- exploiting of the multipath environment through spread spectrum processing (RAKE reception and MRC combining diversity), allowing signals arriving with different propagation delays to be received separately and then combined,
- multiple antennas at the cell site.

Antenna diversity can easily be provided in FDMA and TDMA systems. Time diversity can be provided in all digital systems that can tolerate the required higher transmitted symbol rate needed to make the required error correction process effective. An interesting attribute of spread spectrum signalling is that coding can be achieved while maintaining a constant bandwidth and data throughput [68]. Another unique feature of DS/SSMA is the ability to provide extensive path diversity; the greater the order of diversity in a system, the better the performance in this difficult propagation environment.

Multipath processing can take on the form of parallel correlators for the spreading sequences waveform. The mobile and cell receivers may employ three or four parallel correlators. Receivers using parallel correlators (RAKE or MRC combining diversity receivers) allow individual path arrivals to be tracked independently and the sum of the received signal strengths is then used to demodulate the signal. While there is fading on each of the arrivals, the fades are independent. Demodulation based on the sum of the signals is then much more reliable. The multiplicity of correlators is also the basis for the simultaneous tracking of signals from two different cells and allows the subscriber unit to control the soft handoff.

2.2.2 Power Control

Very important in SSMA design is power control. To achieve high capacity and quality, our SSMA mobile system must employ forward (base-to-mobile) and reverse link (mobile-to-base) power control. The objective of the mobile station transmitter power control process is to produce a nominal received signal power from each mobile transmitter operating within the cell at the cell site receiver. Regardless of a mobile's position or propagation loss, each mobile's signal will be received at the cell with the same level. If all the mobile transmitters within a cell site's area coverage are so controlled, then the total signal power received at the cell site from all mobile stations is equal to the nominal received power times the number of mobiles.

Each SSMA receiver at the cell site operates by converting a selected SSMA signal from one of the mobile station transmitters into a signal that carries narrowband digital information. At the same time the other signals that are not selected remain wide bandwidth noise signals. The bandwidth reduction processing, commonly called processing gain, increases the signal-to- interference ratio (in dB) from a negative value to a level that allows operation with an acceptable bit error rate.

It is very desirable to maximise the capacity of the SSMA system in terms of the number of simultaneous callers that can be handled in a given system bandwidth. The system capacity is maximised if the transmit power of each mobile station is controlled so that its signal arrives at the cell site with the minimum required signal-to-interference ratio.

If a mobile station's signal arrives at the cell site with too low a value of received power, the bit error rate is too high to permit high quality communications. If the received power is too high, the performance of this mobile station is acceptable, but the interference to all the other mobile station transmitters that are sharing the same channel is increased and may result in unacceptable performance to other users unless the traffic is reduced.

Reverse link open loop power control, reverse link closed loop power control and forward link power control can be employed in the SSMA system. Reverse link open loop power control is primarily a function of the mobile stations. The goal of the open loop portion of the reverse link power control is for the mobile station to rapidly adjust transmit power according to changes in the received power from the cell. The mobile stations measure the received power level from the cell sites and adjust their transmitter power in an inverse proportional manner. Open loop power control attempts to have all mobile station's transmitted signals arrive at the cell site with the same nominal power level. The cell site supports the open loop control function by providing a calibration constant to the served mobile stations. The calibration constant is determined primarily by the cell site effective received power (ERP). Cells that transmit at a higher than nominal ERP must inform their subscribers so the mobile stations will not transmit lower than nominal required power and conversely for low ERP cell sites.

The cell site takes an active role in the reverse link closed loop power control functions. The goal of the closed loop portion is for the cell to provide rapid corrections to the mobile station's open loop estimate to maintain the optimum transmit power. The cell measures the relative received power level of each of the associated mobile station's signals and compares it to an adjustable threshold. As a typical example, the Qualcomm system determine every 1.25 ms to either transmit a power-up, or power-down command. It must be noted that the Qualcomm system is designed for urban mobile communications and therefore, in our generic IWC system the channel will vary slower and perhaps a longer adjustable time can be tolerated.

This closed loop correction to any variation required in the open loop estimate accommodates gain tolerances and unequal propagation losses between the forward and reverse links.

The cell supports forward link power control by adjusting the forward link power for each subscriber link signal in response to measurements provided by the mobile station. The purpose is to reduce power for the units that are either stationary, relatively close to the cell site, impacted little by multipath fading and shadowing effects, or experiencing minimal other cell interference. Thus, extra power can be given to units that are either in a more difficult environment or far away from

the cell and experiencing high error rates.

In our analysis we will assume that power control, as described above, is employed in an ideal way, that is, all mobiles and basestations will receive and transmit at the same power levels. In our stationary analysis (Chapter 5), ideal power control can almost practically be realised due to the undynamic changes in a stationary environment.

2.2.3 Low Transmit Power

Besides directly improving capacity, one of the more important results of reducing the required E_b/N_0 (signal-to- interference level), is the reduction of the transmitter power required to overcome noise and interference. This reduction means that mobile stations also have reduced transmitter output requirements which reduces cost and allows lower power units to operate at larger ranges than similarly powered analog and TDMA units. Furthermore, a reduced transmitter output requirement increases coverage and penetration and may also allow a reduction in cells required for coverage. Average traffic also influences this aspect.

An even greater gain is the reduction of average (rather than peak) transmitted power that is realised because of the power control used in SSMA. Most of the time propagation conditions are benign. Narrowband systems must always transmit with enough power to override the occasional fades. To summarise, SSMA uses power control to provide only the power required at the time, and thus reduces the average power by transmitting at high levels only during fades.

2.2.4 Vocoder and Variable Data Rates

The vocoder (voice encoder/decoder) in our SSMA system can be a variable rate design. The Qualcomm system uses a variable rate vocoder at nominally 8 kbps. Commercially there is Code Excited Linear Prediction (CELP) VLSI implementations available with selectable rates, corresponding to 9600, 4800, 2400 and 1200 bps frame rates. The rates can be automatically determined by the input data. Also available is a SSMA-specific algorithm termed QCELP [8].

A further important feature of the variable rate vocoder is the use of adaptive thresholds to determine the required data rate. The thresholds can be changed according to the background noise level activating the higher vocoder rates only on the local voice quality. The result is suppression of background noise and good voice transmission even in a noisy environment.

2.2.5 Privacy

The scrambled form of SSMA signals provides for a very high degree of privacy and makes our digital cellular system inherently more immune to cross-talk, inexpensive scanning receivers and air-time fraud. The digital voice channel is, of course, amendable to direct encryption using DES or other standard encryption techniques.

2.2.6 Mobile Station Assisted Soft Handoff

Soft handoff allows both the original cell and a new cell to temporarily serve the call during handoff transition. The transition is from the original cell to both cells and then to the new cell. Not only does this greatly minimise the probability of dropping a call, but it also makes the handoff virtually undetectable by the user. In this regard, analog and digital TDMA-based systems provide a break-before-make switching function whereas a SSMA-based soft handoff system provides a make-before-break switching function.

After a call is initiated, the mobile station continues to scan the neighbouring cells to determine if the signal from another cell becomes comparable to that of the original cell. When this happens, it indicates to the mobile station that the call has entered a new cell's coverage area and that a handoff can be initiated. The mobile station transmits a control message to the Mobile Telephone Switching Office (MTSO) which states that the new cell site is now strong and identifies the new cell site. The MTSO initiates the handoff by establishing a link to the mobile station through the new cell while maintaining the old link. While the mobile station is located in the transitional region between the two cell sites, the call is supported by communication through both cells; thereby eliminating the ping- ponging effect, or repeated requests to hand the call back and forth between two cell sites. The original cell site will only discontinue the call when the mobile station is firmly established in the new cell.

Soft handoff is one of the important features of the Qualcomm mobile system.

2.2.7 Capacity

In the cellular reuse concept, interference is accepted but controlled with the goal of increasing system capacity. SSMA does this effectively because it is inherently a better anti- interference waveform than FDMA or TDMA. Indeed, its genesis was in military anti-jamming systems. Narrowband modulations are limited in frequency reuse efficiency by the requirement to achieve a carrier-to-interference (C/I) ratio of about 18 dB [9]. This requires that a channel used in one cell is not reused in a nearby cell. In SSMA, the wideband channel is reused in every cell.

In SSMA, frequency reuse is determined by the signal-to- interference ratio that results from all the system users within range, instead of the users in any given cell. Since the total capacity becomes quite large, the statistics of all the users are more important than those of a single user. The so called "law of large numbers" can be said to apply. This means that the net interference to any given signal is the average of all the users' received power times the number of users. As long as the ratio of received signal power to the average noise power density is greater than a threshold value, the channel will provide an acceptable signal quality. With FDMA and TDMA, interference is governed by a "law of small numbers" in which "worst-case" situations determine the percentage of time in which the desired quality will not be achieved.

The primary parameters that determine SSMA digital cellular system capacity are processing gain, E_b/N_0 (with the required fading margin), voice duty cycle, frequency reuse efficiency and the number of sectors in the cell site antenna.

In our analysis and subsequent performance evaluations, all these features will be exploited and quantified.

2.2.8 Voice Activity Detection

In a typical full duplex conversation, the duty cycle of each voice is less than 35% or approximately the fraction $V_{on} = 3/8$. It is difficult to exploit the voice activity in either FDMA and TDMA systems because of the time delay associated with reassigning the channel resource during the speech pauses [12]. With SSMA, it is possible to reduce the transmission rate when there is no speech and thereby substantially reduce interference to the other users. Since the level of other user interference directly determines capacity, the capacity is increased by approximately a factor of 8/3. This also reduces average mobile station transmit power requirements by approximately a factor of 8/3.

2.2.9 Frequency Reuse and Sectorisation

In SSMA, the wideband channel is reused in every cell. The total interference at the cell site to a given inbound mobile station signal is comprised of interference from other mobile stations in the same cell plus interference from mobile stations in neighbouring cells. In other words, each mobile station's signal competes with all other mobile station signals. The contribution of all the neighbouring cells is equal to approximately half the interference due to the mobile stations within the same cell. The frequency reuse efficiency of omnidirectional cells is the ratio of interference from mobile stations within a cell to the total interference from all the cells, or about 65%. Figure 2.1 shows the percentage of interference contributions from neighbouring cells. Each cell in the first tier contributes about 6% of the total interference, so the entire first tier contributes an average of

6 time 6% or 36%; cells in the second and greater tiers contribute less than 14%.

When directional cell site antennas are used (i.e. typical 120° sector antennas) the interference is simply divided by three because, on the average, each antenna receives only in the direction of one-third of the mobile stations. The capacity supportable by the total system is therefore increased by nearly a factor $N_{sect} = 3$.

2.2.10 Low E_b/N_0 and Error Protection

E_b/N_0 is the ratio of energy per bit to noise power spectral density and is the standard figure-of-merit by which digital modulation and coding schemes are compared. It is directly analogous to carrier-to-noise (C/N) for analog FM modulation. Due to the wide channel bandwidth employed in SSMA systems, it is possible to use extremely powerful, high redundancy error correction coding techniques when the coding and spreading sequences are combined. With narrowband digital modulation techniques, a much higher E_b/N_0 is required compared to SSMA because less powerful low redundancy error correction codes must be used to conserve channel bandwidth. The lower E_b/N_0 increases capacity and decreases transmitter output power requirements.

2.2.11 Soft Capacity

To illustrate the advantage of SSMA "soft capacity" consider the following: in the present U.S. cellular environment, the FCC has allocated 25 MHz of spectrum which is equally split between two system operators in each service area. The spectrum is further divided between cells, with a maximum of 57 analog FM channels in a three sector cell site. When demand for service is at a peak, the 58th caller in a given cell must be given a busy signal. There is no way to add even one more signal to a fully occupied system. This call blocking behaviour results in about 35% loss of capacity. With the SSMA system, however, there is a much softer relationship between the number of users and the grade of service. For example, the system operator could decide to allow a small degradation in the bit error rate and increase the number of available channels during peak hours.

This capability is especially important for avoiding dropped calls at handoff because of a lack of channels. In the analog systems and in digital TDMA, if a channel is not available, the call must be reassigned to a second candidate or it will be dropped at the handoff. With SSMA, however, the call can be accommodated if it is acceptable to slightly raise the users' bit error rates until another call is completed.

It is also possible to offer a higher grade of service (at a higher cost to the user) where the high-grade user would obtain a larger fraction of the available power (capacity) than the low- grade user. Handoffs for high-grade users can be given priority over those for other users.

CHAPTER 3

SYSTEM PERFORMANCE ANALYSIS

The chief purpose of this thesis is to assess the communication performance and capacity of the DS/SSMA system described in the previous chapter for IWC. In our system evaluation, the criterion of merit is average probability of error as a function of signal-to-noise ratio.

This chapter analyses and derives the necessary equations to calculate the average error probability for CPSK and DPSK in Sections 3.1 and 3.2 respectively. These equations enable us to accurately determine the average error probability using MaxEnt principles and to investigate the Gaussian Assumption (GA) for the up- and downlink of the system described in Chapter 2.

3.1 CPSK Performance Analysis

In the subsequent analysis, the reference user is arbitrarily assumed as $k = 1$, with the received signal as expressed in (2.10). A typical coherent RAKE receiver for DS/SSMA is as indicated in Figure 3.1. Following the standard procedure, as described in Proakis [72], the average error rate is first derived for a non-diversity, matched filter system and then the diversity statistics are included.

Since coherent demodulation is assumed, the receiver coherently recovers the carrier phase and delay lock to the first arriving desired signal. Therefore, after correlation and demodulation, a signal sample at the receiver low-pass filter output can be expressed as

$$\zeta = \int_0^T r(t) a_1(t) \cos\omega_c t dt, \tag{3.1}$$

or, substituting (2.10) in (3.1) we have

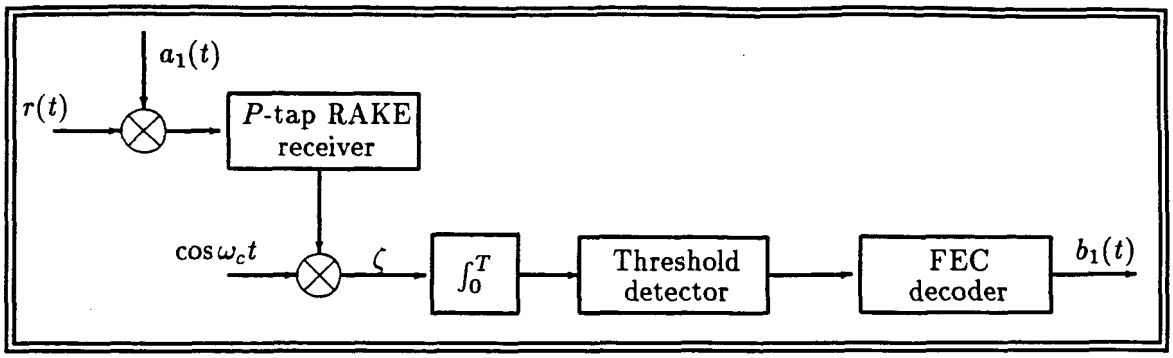

Figure 3.1: CPSK receiver

$$\begin{aligned}\zeta &= \frac{A}{2}\sum_{l=1}^{L}\beta_l\int_0^T a_1(t-t_l)b_1(t-t_l)a_1(t)\cos\Psi_l dt \\ &+ \frac{A}{2}\sum_{k=2}^{K}V_k\int_0^T a_k(t-\tau_k)b_k(t-\tau_k)a_1(t)\cos\Theta_k dt \\ &+ \eta,\end{aligned} \tag{3.2}$$

where η is a sample of the Gaussian noise with zero mean and $(N_0T)/4$ variance, $\Psi_l = \phi_l - \omega_c t_l$ and $\Theta_k = \theta_k - \omega_c\tau_k$.

By the assumption of phase delay locking of the receiver to the desired received signal and by examining (3.1), one can express (3.2) as

$$\begin{aligned}\zeta &= \beta_1\frac{AT}{2}b_0^1 \\ &+ \frac{A}{2}\sum_{l=2}^{L}\beta_l\left\{b_{-1}^1R_{1,1}(t_l) + b_0^1\hat{R}_{1,1}(t_l)\right\}\cos\Psi_l \\ &+ \frac{A}{2}\sum_{k=2}^{K}V_k\left\{b_{-1}^kR_{k,1}(\tau_k) + b_0^k\hat{R}_{k,1}(\tau_k)\right\}\cos\Theta_k \\ &+ \eta,\end{aligned} \tag{3.3}$$

where b_0^1 represents the information bit detected and b_{-1}^1 is the preceding bit, which due to the channel delay spread, affects the detection of b_0^1 received on the first path between the desired transmitter and receiver.

In (3.3)

$$R_{1,1}(t_l) = \int_0^{t_l} a_1(t - t_l)a_1(t)dt \tag{3.4}$$

and

$$\hat{R}_{1,1}(t_l) = \int_{t_l}^{T} a_1(t - t_l)a_1(t)dt \tag{3.5}$$

are partial autocorrelation functions of the regenerated desired code at the receiver, that is, $a_1(t)$ with its delayed version received via the lth Nakagami faded path, namely, $a_1(t - t_l)$. We note that the coded sequence received via the first path between the transmitter and receiver of Figures 2.2 and 3.1 is fully correlated with the regenerated sequence $a_1(t)$, owing to the delay locking operation introduced at the receiver.

Also, due to the asynchronous arrival of the interfering user's code, (3.3) contains partial correlations of the regenerated sequence, $a_1(t)$ and a delayed version of the interfering codes defined by

$$R_{k,1}(\tau_k) = \int_0^{\tau_k} a_k(t - \tau_k)a_1(t)dt \tag{3.6}$$

and

$$\hat{R}_{k,1}(\tau_k) = \int_{\tau_k}^{T} a_k(t - \tau_k)a_1(t)dt. \tag{3.7}$$

The standard notation of Pursley can be used to evaluate the correlation functions of (3.4) to (3.7). This is accomplished by assuming rectangular chips and noting that, as shown by Pursley [70], for any $0 \leq nT_c \leq \tau \leq (n+1)T_c \leq T$

$$\begin{aligned} R_{k,1}(\tau) &= A_{n_{k,1}}T_c + B_{n_{k,1}}(\tau - nT_c) \\ \hat{R}_{k,1}(\tau) &= \hat{A}_{n_{k,1}}T_c + \hat{B}_{n_{k,1}}(\tau - nT_c) \end{aligned} \tag{3.8}$$

where

$$\begin{cases} A_{n_{k,1}} &= C_{k,1}(n-N) \\ B_{n_{k,1}} &= C_{k,1}(n+1-N) - C_{k,1}(n-N) \\ \hat{A}_{n_{k,1}} &= C_{k,1}(n) \\ \hat{B}_{n_{k,1}} &= C_{k,1}(n+1) - C_{k,1}(n) \end{cases} \tag{3.9}$$

which is valid for all $k = 1, 2, \cdots, K$. The discrete aperiodic cross-correlation term $C_{k,1}(\cdot)$ is related to the chip sequences a_j^k and a_j^1 via

$$C_{k,1}(n) = \begin{cases} \sum_{j=0}^{N-1-n} a_j^k a_{j+n}^1 & 0 \le n \le N-1 \\ \sum_{j=0}^{N-1+n} a_j^1 a_{j-n}^k & 1-N \le n \le 0 \\ 0 & |n| \ge N. \end{cases} \tag{3.10}$$

The assumption of rectangular pulses results in conservative results; Pursley [71] indicates that sine pulses instead of rectangular pulses result in a decrease in the multiple access interference by as much as 12%. To keep the analysis simple and trackable, rectangular pulses will nevertheless be assumed, rendering our results conservative.

The objective of the matched filter detector is to compare the received sample in (3.3) with a preset threshold in order to make a decision on the polarity of the data bit being detected, that is, b_0^1. The detector makes a wrong decision if ζ is negative while $b_0^1 = +1$, or if ζ is positive and $b_0^1 = -1$. We note that during the detection interval of b_0^1 the other three data bits in (3.3), namely, b_{-1}^1, b_{-1}^k and b_0^k, $k \neq 1$, can independently take on $\{\pm 1\}$. To calculate the probability of a bit error for a matched filter receiver, we can write

$$\begin{aligned} P_{e|\alpha,\beta_1} &= P(b_0^1 = +1) P_r \left\{ \frac{AT}{2}(\alpha + \beta_1) + \eta < 0 | b_0^1 = +1 \right\} \\ &+ P(b_0^1 = -1) P_r \left\{ \frac{AT}{2}(\alpha - \beta_1) + \eta > 0 | b_0^1 = -1 \right\} \end{aligned} \tag{3.11}$$

where

$$\alpha = x + y, \tag{3.12}$$

$$x = \sum_{k=2}^{K} \frac{V_k}{T} \left\{ b_{-1}^k R_{k,1}(\tau_k) + b_0^k \hat{R}_{k,1}(\tau_k) \right\} \cos \Theta_k,$$

$$y = \sum_{l=2}^{L} \frac{\beta_l}{T} \left\{ b_{-1}^1 R_{1,1}(t_l) + b_0^1 \hat{R}_{1,1}(t_l) \right\} \cos \Psi_l.$$

For the case when the a priori probabilities are equal, that is, $P(b_0^1 = -1) = P(b_0^1 = +1) = \frac{1}{2}$, and using the fact that the Gaussian pdf is symmetrical, we can write

$$P_{e|\alpha,\beta_1} = P_r \left\{ \frac{AT}{2}(\alpha + \beta_1) + \eta < 0 | b_0^1 = +1 \right\}. \tag{3.13}$$

We know that the probability of a bit error is numerically equal to the area under the "tail" of the Gaussian pdf that falls on the "incorrect" side of the threshold [74]. We can therefore compute the average error rate by integrating between the limits γ_m and ∞, where γ_m is the mean of the Gaussian pdf. Performing the integration and realising that η is Gaussian with mean $\gamma_m = \frac{AT}{2}(\alpha + \beta_1)$ and variance σ^2, we can calculate (3.13) as

$$P_{e|\alpha,\beta_1} = \frac{1}{2} \text{erfc} \left\{ \frac{AT(\alpha + \beta_1)}{2\sqrt{2}\sigma} \right\} \tag{3.14}$$

where

$$\text{erfc}(\mu) = \frac{2}{\sqrt{\pi}} \int_{\mu}^{\infty} e^{-y^2} dy. \tag{3.15}$$

Further, we can recall that

$$\sigma = \frac{\sqrt{N_0 T}}{2} \tag{3.16}$$

and observing the bit energy

$$E_b = \frac{A^2 T}{2}, \tag{3.17}$$

(3.14) can be expressed as

$$P_{e|\alpha,\beta_1} = \frac{1}{2}\text{erfc}\left\{\sqrt{\frac{E_b}{N_0}}(\alpha+\beta_1)\right\}. \tag{3.18}$$

Now, having a generalised expression for the conditional error probability, it is possible to remove the conditioning in α and β_1 using various techniques and assumptions.

3.1.1 Exact Calculation of Error Probability

By calculating the moments of α (see Appendix D) and making use of the MaxEnt formulation, it is possible to calculate the exact error probabilities for specific spreading code parameters. (The next chapter considers the use of MaxEnt and GQR to calculate averages based on formulas such as (3.18).)

Using the channel model described earlier, where the channel is modelled as a P tap delay line, it is possible to derive the performance of an optimum RAKE receiver. By definition β_1 is Nakagami distributed with actual received signal-to-noise ratio

$$\begin{aligned}\gamma_b &= \frac{E_b}{N_0}\sum_{i=1}^{P}\beta_i^2 \\ &= \sum_{i=1}^{P}\gamma_i,\end{aligned} \tag{3.19}$$

with average

$$\overline{\gamma}_b = E\{\beta_i^2\}\frac{E_b}{N_0}, \tag{3.20}$$

where $E\{\cdot\}$ denotes expected value. Each of the $\{\gamma_i\}$ is distributed according to

$$p(\gamma_b) = \left(\frac{m}{\overline{\gamma}_b}\right)^m \frac{{\gamma_b}^{m-1}}{\Gamma(m)}\exp\left(-\frac{m\gamma_b}{\overline{\gamma}_b}\right), \tag{3.21}$$

as discussed in Appendix A. Using the characteristic function of (3.21) and the fact that the P channels are mutually statistically independent, the probability distribution function of $p(\gamma_b)$ is (see Appendix A)

$$p(\gamma_b) = \left(\frac{m}{\overline{\gamma}_b}\right)^{\epsilon} \frac{\gamma_b^{\epsilon-1}}{\Gamma(\epsilon)} \exp\left(-\frac{m\gamma_b}{\overline{\gamma}_b}\right) \qquad \forall \qquad \gamma_b \geq 0, \tag{3.22}$$

$\epsilon = mP$, m the Nakagami fading parameter, and P the number of taps in the RAKE receiver. Since all P channels are assumed to be identical and independent, the mean-square values $E\{\beta_i^2\}$ will be equal, and therefore, (3.19) can be written as

$$\gamma_b = P\beta_1^2 \frac{E_b}{N_0}. \tag{3.23}$$

The average signal-to-noise per bit γ_0, is related to the average signal-to-noise ratio per channel $\overline{\gamma}_b$ by the formula

$$\gamma_0 = P\overline{\gamma}_b. \tag{3.24}$$

Therefore, to calculate the average error probability we have to solve

$$P_e = \int_{-\infty}^{\infty} \int_0^{\infty} P_{e|\alpha,\gamma_b} p(\gamma_b) p(\alpha) d\gamma_b d\alpha \tag{3.25}$$

numerically.

As explained earlier, the distribution of $p(\alpha)$ is the unknown IUI distribution. Using MaxEnt, moments as derived in Appendix D and Gold spreading sequences indicated in Appendix B, it is possible to accurately determine the IUI distribution, and therefore to calculate exact error probabilities. In Chapter 4 the accuracy of assuming $p(\alpha)$ to be Gaussian distributed, is investigated using equations derived in the next section.

3.1.2 Error Probability using the Gaussian Assumption

When the Gaussian Assumption is invoked the IUI random variable, α, is assumed to be a zero mean Gaussian random variable with variance $\sigma_{m\alpha}^2$. To calculate $\sigma_{m\alpha}^2$ expressions derived for the moments of α by Kavehrad [24] is used and, for the sake of continuity, summarised in Appendix D, with actual values for $\sigma_{m\alpha}^2$ tabulated in Appendix E. (The $\sigma_{m\alpha}^2$ values presented are calculated

for Gold codes with generator polynomials as given in Appendix B.)

The conditioning in α is removed analytically by realising that

$$P_{e|\beta_1} = \int_{-\infty}^{\infty} P_{e|\alpha,\beta_1} p(\alpha) d\alpha, \tag{3.26}$$

where

$$p(\alpha) = \frac{1}{\sqrt{2\pi}\sigma_{ma}} \exp\left(-\frac{\alpha^2}{2\sigma_{ma}^2}\right). \tag{3.27}$$

Integrating by parts, using integration tables by Ng et al [75] and some manipulations, (3.26) results in

$$P_{e|\beta_1} = \frac{1}{2}\text{erfc}\left\{\sqrt{\Lambda\beta_1^2 \frac{E_b}{N_0}}\right\}, \tag{3.28}$$

with

$$\frac{1}{\Lambda} = 1 + 2\frac{E_b}{N_0}\sigma_{ma}^2. \tag{3.29}$$

Next the conditioning in β_1 has to be removed. Substituting (3.23) into (3.28), the average error rate can be determined by

$$P_e = \int_0^{\infty} P_{e|\gamma_b} p(\gamma_b) d\gamma_b. \tag{3.30}$$

The result after integration by parts, using tables in [75] and Abramowitz et al [76], we derive at

$$P_e = \frac{1}{2}\left\{1 - \frac{2\Gamma\left(\epsilon + \frac{1}{2}\right)}{\sqrt{\pi}\Gamma(\epsilon)}\sqrt{\frac{\Lambda\overline{\gamma}_b}{m}}\,{}_2F_1\left(\frac{1}{2}; \epsilon + \frac{1}{2}; \frac{3}{2}; -\frac{\Lambda\overline{\gamma}_b}{m}\right)\right\} \tag{3.31}$$

where ${}_2F_1(\cdot)$ is the Gauss hypergeometric function [76]. (A detailed derivation of P_e is included in Appendix F.)

We note that for $m = 1$ and $P = 1$, which is single path Rayleigh fading, ${}_2F_1(\cdot)$ reduces to [76]

$$ {}_2F_1\left(\frac{1}{2};\frac{3}{2};\frac{3}{2};-q\right) = (1+q)^{-\frac{1}{2}}. \tag{3.32} $$

Substituting (3.32) in (3.31), realising that $\Lambda = 1$ in the absence of IUI and some manipulations, (3.31) reduces to

$$ P_e = \frac{1}{2}\left\{1 - \sqrt{\frac{\gamma_0}{1+\gamma_0}}\right\} \tag{3.33} $$

which is the ideal performance of a single-path Rayleigh fading channel [72].

Also, in the absence of any multiple-access and fading (3.28) becomes

$$ P_e = \frac{1}{2}\text{erfc}\left\{\sqrt{\frac{E_b}{N_0}}\right\}, \tag{3.34} $$

which is the well-known performance of a coherently demodulated BPSK signal, i.e. [72].

As described in Appendix A, the Nakagami pdf tends to an impulse function as $m \to \infty$. This is the case when the system is stationary and no fading is present. It is shown in Appendix G that the limit as $m \to \infty$ and letting $\beta_1 = 1$ in (3.31) we have

$$ P_e = \frac{1}{2}\text{erfc}\left\{\left(\frac{N_0}{E_b} + 2\sigma_{ma}^2\right)^{-\frac{1}{2}}\right\}, \tag{3.35} $$

which is similar to an expression by Pursley [70] and Turin [23]. In essence it is the same except that Pursley gives the multiple access variance as $\sigma_{ma}^2 = \frac{K-1}{3N}$ which was derived for random code sequences. Our estimate of the multiple access interference is more accurate and aimed at specific code parameters, i.e. Gold sequences. Turin's result for the multiple access variance is $\frac{K-1}{4N}$. The result in (12) of Turin is incorrect; the lower integration limit, over the variable z should be from $-y$ and not y. When this is rectified Turin has the same result as Pursley for the multiple access variance.

When fading is neglected, that is using (3.18) and (3.35), it is possible to investigate the GA and to calculate the average error rate under non-fading conditions. Using equations (3.25) and (3.31) it is possible to do the same under fading conditions with and without diversity.

Using these equations the GA is investigated in Chapter 4, while average error rates under non-fading and fading conditions are accurately calculated in Chapters 5 and 6 respectively using the

MaxEnt approach.

3.2 DPSK Analysis

Since DPSK concerns non-coherent detection of the received signal the analysis and performance is slightly different from that derived for coherent detection. However, the notation and procedure followed in the previous section is maintained; first the error rate for matched filter detection is derived and then the statistics of a MRC diversity system is included.

The analysis presented here is based on a DPSK system studied by Kavehrad and Ramamurthi [77] and modified to investigate the effects of MRC diversity (in their study Kavehrad et al investigate the effects of selection and predetection combining diversity). The model proposed by Kavehrad et al is further modified to be consistent with the CPSK system, that is, multipath is only considered to effect the reference user, rendering our results conservative since, on average, multipath degrades the signal-to-noise ratio.

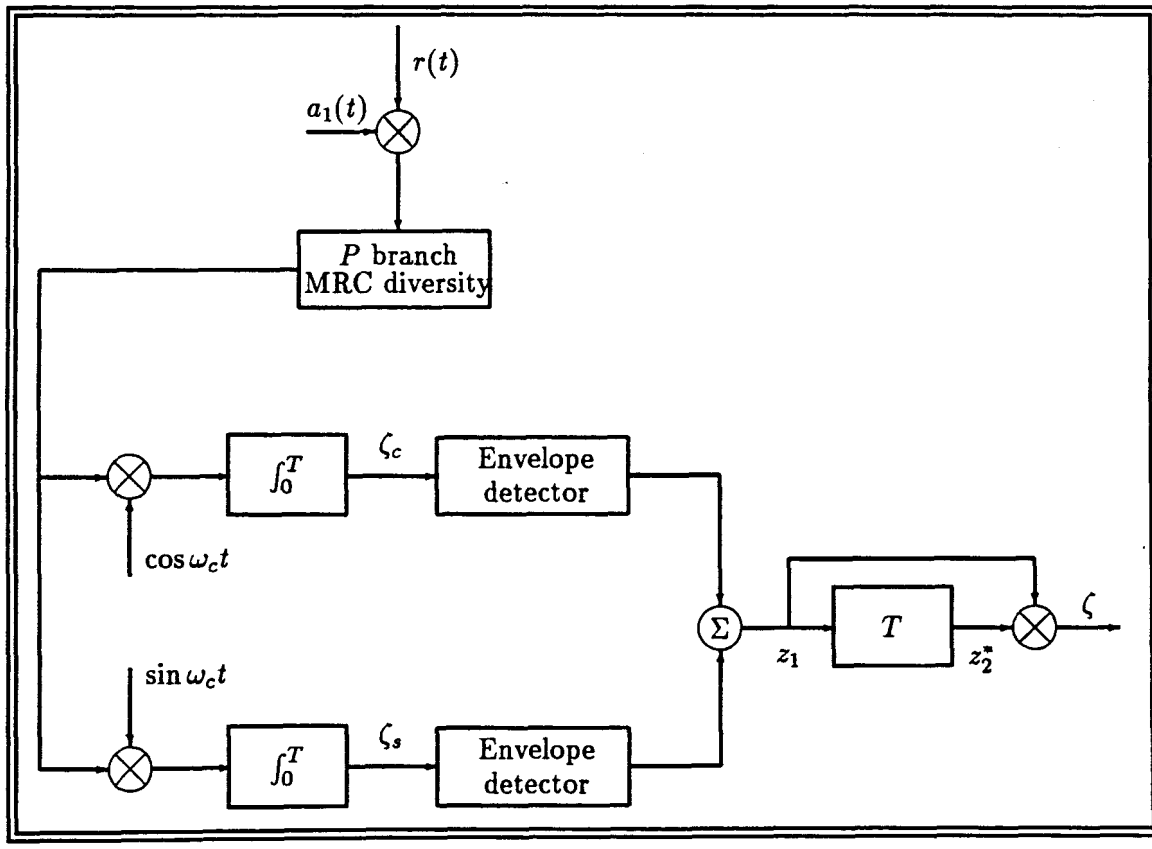

Figure 3.2: DPSK receiver

The DPSK receiver is as indicated in Figure 3.2 and the received signal, $r(t)$, at the input to the matched filter is given by

$$\begin{aligned} r(t) &= A\sum_{l=1}^{L}\beta_l a_1(t-t_l)b_1(t-t_l)\cos(\omega_c t+\phi_l) \\ &+ A\sum_{k=2}^{K}V_k a_k(t-\tau_k)b_k(t-\tau_k)\cos(\omega_c t+\phi_k) \\ &+ n_c(t)\cos\omega_c t + n_s(t)\sin\omega_c t, \end{aligned} \tag{3.36}$$

where $n(t)$ has been expressed in terms of its lowpass equivalent components $n_s(t)$ and $n_c(t)$ [78]. The carrier phases θ_k and θ_1 has been absorbed in the random phases ϕ_k and ϕ_l respectively.

As before we arbitrarily choose user $k = 1$ as the reference user and calculate the probability of error of the data symbol b_0^1. At time $t = T$, the nominal sampling point for matched filter detection, we have [77]

$$\begin{aligned} \zeta_c(T) &= A\sum_{l=1}^{L}\beta_l\left\{b_{-1}^1 R_{1,1}(t_l)+b_0^1\hat{R}_{1,1}(t_l)\right\}\cos\phi_l \\ &+ A\sum_{k=2}^{K}V_k\left\{b_{-1}^k R_{k,1}(\tau_k)+b_0^k\hat{R}_{k,1}(\tau_k)\right\}\cos\phi_k \\ &+ \eta, \end{aligned} \tag{3.37}$$

and

$$\begin{aligned} \zeta_s(T) &= A\sum_{l=1}^{L}\beta_l\left\{b_{-1}^1 R_{1,1}(t_l)+b_0^1\hat{R}_{1,1}(t_l)\right\}\sin\phi_l \\ &+ A\sum_{k=2}^{K}V_k\left\{b_{-1}^k R_{k,1}(\tau_k)+b_0^k\hat{R}_{k,1}(\tau_k)\right\}\sin\phi_k \\ &+ \nu, \end{aligned} \tag{3.38}$$

with the definitions of b_0^k, b_{-1}^k, $R_k(\tau)$ and $\hat{R}_k(\tau)$ are as defined in (3.6) and (3.7), and

$$\eta = \int_0^T a_1(s) n_c(s) ds, \tag{3.39}$$

and

$$\nu = \int_0^T a_1(s) n_s(s) ds. \tag{3.40}$$

The noise samples η and ν are independent zero-mean Gaussian random variables with equal variance $\sigma_n^2 = N_0 T$ [74]. Notice that, as in the coherent case, the intersymbol interference here is due to partial correlation and involves only the previous bit. For most indoor channels, the delay spread is considerably less than the bit intervals of practical interest and the partial correlation intersymbol interference is the only type present.

Now, let us assume without loss of generality that $t_1 = 0$ and $\phi_1 = 0$. That is, we assume that the first path ($L = 1$) between the transmitter of user 1 and the corresponding receiver is the reference path and all other paths constitute interference. Let z_1 denote the complex envelope of the matched filter output at the sampling instant, i.e. $z_1 = \zeta_c(T) + j\zeta_s(T)$. Since the fading is slow compared to the data rate, we may assume that the corresponding complex envelope at the previous sampling instant, denoted z_2, differs from z_1 only in the data bits involved and in the additive Gaussian noise samples. It is therefore easily shown that

$$\begin{aligned} z_1 &= \beta_1 A T b_0^1 \\ &+ AT \left\{ \sum_{l=2}^{L} \beta_l X_l \cos\phi_l + \sum_{k=2}^{K} V_k X_k \cos\phi_k \right\} \\ &+ jAT \left\{ \sum_{l=2}^{L} \beta_l X_l \sin\phi_l + \sum_{k=2}^{K} V_k X_k \sin\phi_k \right\} \\ &+ (\eta_1 + j\nu_1), \end{aligned} \tag{3.41}$$

and

$$z_2 = \beta_1 A T b_{-1}^1 \tag{3.42}$$

$$
\begin{aligned}
&+ \quad AT\left\{\sum_{l=2}^{L}\beta_l Y_l\cos\phi_l + \sum_{k=2}^{K} V_k Y_k\cos\phi_k\right\} \\
&+ \quad jAT\left\{\sum_{l=2}^{L}\beta_l Y_l\sin\phi_l + \sum_{k=2}^{K} V_k Y_k\sin\phi_k\right\} \\
&+ \quad (\eta_2 + j\nu_2),
\end{aligned}
$$

with

$$
\begin{aligned}
X_l &= b^1_{-1}R_{1,1}(t_l) + b^1_0\hat{R}_{1,1}(t_l) \\
X_k &= b^k_{-1}R_{k,1}(\tau_k) + b^k_0\hat{R}_{k,1}(\tau_k) \\
Y_l &= b^1_{-2}R_{1,1}(t_l) + b^1_{-1}\hat{R}_{1,1}(t_l) \\
Y_k &= b^k_{-2}R_{k,1}(\tau_k) + b^k_{-1}\hat{R}_{k,1}(\tau_k).
\end{aligned}
\tag{3.43}
$$

In (3.42), the data bit b^k_{-2} of the kth user is transmitted two-bit intervals prior to b^k_0. The noise variables η_1, η_2, ν_1 and ν_2 are independent of one another, and the binary data bits are equal to $+1$ or -1 with equal probability. The output of the DPSK demodulator at the sampling instant is given by

$$
\zeta = \mathrm{Re}[z_1 z_2^*], \tag{3.44}
$$

where * denotes complex conjugate.

Before we continue, we must note the following facts. If the delays $\{\tau_k\}$ are given, the random variables R_k and $\hat{R}_k$, for all k, are zero-mean Gaussian. This follows from the fact that $\beta_k\cos\phi_k$ and $\beta_k\sin\phi_k$ are zero-mean Gaussian. Since these two random variables are also independent, all the noise and interference terms in z_1 and z_2 are independent for all k, because the path gains and phases are independent of each other. Finally, if x is a zero-mean Gaussian random variable, and b is a random variable which takes on $+1$ or -1 with equal probability, the random variable bx is also zero-mean Gaussian with the same variance as x. This can be shown easily using the standard formula for the density of the product of two random variables [53]. For the subsequent analysis this information has to be used to calculate the error probability for DPSK signalling. In the next chapter the validity of this assumption is investigated by means of simulations.

Let us indicate the transmitted DPSK signals as $s_1(t)$ and $s_2(t)$. In relation to the received signal,

z_1 and z_2, the following binary signal pair is transmitted

$$\begin{aligned} s_1(t) &= (z_1, z_1) \quad \text{or} \quad (z_2, z_2) \qquad 0 \leq t \leq 2T \\ s_2(t) &= (z_1, z_2) \quad \text{or} \quad (z_2, z_1) \qquad 0 \leq t \leq 2T. \end{aligned} \tag{3.45}$$

As explained before, the first T seconds of each waveform are actually the last T seconds of the previous waveform. Note that $s_1(t)$ and $s_2(t)$ can each have either of two possible forms and that z_1 and z_2 are antipodal signals. Therefore, pairs of DPSK signals can be represented as orthogonal signals $2T$ long. Detection could correspond to noncoherent envelope detection with four channels matched to each of the possible envelope outputs. Since the two envelope detectors representing each symbol are negatives of each other, the envelope of each will be the same. Hence the detectors can be implemented as a single channel matched to $s_1(t)$ or $s_2(t)$.

The probability of error can now be calculated by realizing that

$$P_e = P(\zeta > s_2 | z_2). \tag{3.46}$$

For the case where z_2 is sent, the output of z_1 will be only Gaussian noise, and therefore the output of the envelope detector is noise having a Rayleigh distribution, given by

$$p_{z_1|s_2} = \frac{z_1}{\sigma_n^2} \exp\left\{-\frac{z_1^2}{2\sigma_n^2}\right\} \qquad \forall \qquad z_1 \geq 0, \tag{3.47}$$

where σ_n^2 is the noise at the filter output.

On the other hand z_2 has a Rice distribution (see derivation in Appendix H) since the input to the envelope detector is Gaussian noise plus a signal component. The pdf is written as

$$p_(z_2|s_2) = \frac{z_2}{\sigma_n^2} \exp\left\{-\frac{z_2^2 + m_2^2}{2\sigma_n^2}\right\} I_o\left(\frac{z_2 m_2}{\sigma_n^2}\right) \qquad \forall \qquad z_2 \geq 0, \tag{3.48}$$

with [74]

$$m_2 = \frac{AT(\beta_1 + \alpha)}{2}, \tag{3.49}$$

which is the average of the Gaussian decision variable.

Now, when $s_2(t)$ is transmitted, the receiver makes an error whenever the envelope sample z_1 exceeds the envelope sample z_2. Thus the probability of this error can be obtained by integrating $p(z_1|s_2)$ with respect to z_1 from z_2 to infinity, and then averaging over all possible values of z_2. That is,

$$\begin{aligned} P_e &= \int_0^\infty p(z_2|s_2)\left\{\int_{z_2}^\infty p(z_1|s_2)dz_1\right\}dz_2 \\ &= \int_0^\infty \frac{z_2}{\sigma_n^2}\exp\left\{-\frac{z_2^2+m_2^2}{2\sigma_n^2}\right\} I_o\left(\frac{z_2 m_2}{\sigma_n^2}\right)\left\{\int_{z_2}^\infty \frac{z_1}{\sigma_n^2}\exp\left\{-\frac{z_1^2}{2\sigma_n^2}\right\}dz_1\right\}dz_2. \end{aligned} \tag{3.50}$$

Using integration tables by [76], the integral in (3.50) is evaluated analytically as

$$P_e = \frac{1}{2}\exp\left\{-\frac{m_2^2}{2\sigma_n^2}\right\} \tag{3.51}$$

After substituting (3.49) in (3.50) we have an expression for the conditional error rate for DPSK signalling

$$P_{e|\beta_1,\alpha} = \frac{1}{2}\exp\left\{-(\beta_1+\alpha)^2\frac{E_b}{N_0}\right\}. \tag{3.52}$$

Equation (3.52) can now be averaged using MaxEnt or the Gaussian assumption.

3.2.1 Exact Calculation of Error Probability

To calculate the error probability using MaxEnt, we have to solve

$$P_e = \int_{-\infty}^{\infty} \int_{0}^{\infty} P_{e|\gamma_b,\alpha} p(\alpha) p(\gamma_b) d\gamma_b d\alpha \tag{3.53}$$

where $p(\alpha)$ and $p(\gamma_b)$ are respectively the unknown IUI distribution and the Nakagami squared pdf given by (3.22), and $P_{e|\gamma_b,\alpha}$ is derived at by substituting (3.23) into (3.52).

Using (3.53) and the MaxEnt principle, it is possible to accurately calculate the average error rate for DPSK signalling.

3.2.2 Error Probability using the Gaussian Assumption

As in the CPSK case, the conditioning in α can be removed by the integration

$$P_{e|\beta_1} = \int_{-\infty}^{\infty} P_{e|\beta_1,\alpha} p(\alpha) d\alpha \tag{3.54}$$

where $p(\alpha)$ is a zero mean Gaussian variable given by (3.27). The result after integration is

$$P_{e|\beta_1} = \frac{1}{2} \exp\left(-\Lambda \beta_1^2 \frac{E_b}{N_0}\right) \tag{3.55}$$

with Λ as defined in (3.29).

Using (3.20) and (3.22) the conditioning in β_1 of (3.55) can be removed as in (3.30). The result after integration by parts is

$$P_e = \frac{1}{2}\left(1 + \frac{\gamma_0 \Lambda}{m}\right)^{-\epsilon} \tag{3.56}$$

which is the result for DPSK SSMA signalling under Nakagami fading and ϵ as defined in (3.22).

Without IUI and $m = 1$, (3.56) reduces to

$$P_e = \frac{1}{2}\left\{\frac{1}{1+\gamma_0}\right\} \tag{3.57}$$

which is the well known performance of a single-path Rayleigh fading channel, i.e. [72].

As $m \to \infty$ and $P = 1$, that is no fading, and using the identity [76]

$$\lim_{m\to\infty} \left(1 + \frac{z}{m}\right)^{-m} = \exp(-z) \tag{3.58}$$

it is easily shown that

$$\lim_{m\to\infty} P_e = \lim_{m\to\infty} \frac{1}{2}\left(1 + \frac{\gamma_0 \Lambda}{m}\right)^{-m} = \frac{1}{2}\exp\left\{-\left(\frac{N_0}{E_b} + 2\dot{\sigma}^2_{ma}\right)^{-1}\right\}, \tag{3.59}$$

which is similar to an expression by Turin [23] under non- fading conditions.

3.3 Concluding Remarks

By using equation (3.25) it is possible to calculate accurate error probabilities for specific spreading sequences when CPSK is used as modulation scheme. Further, the validity of the GA under faded and unfaded conditions can be investigated using (3.31) and (3.35).

Equation (3.53) permits us to calculate average error probabilities for specific spreading codes when DPSK is assumed as modulation scheme. However, certain assumptions were made and there accuracy is verified in the following chapter. Also, the legitimacy of the GA for DPSK signalling is verified using (3.56) and (3.59).

CHAPTER 4

THE VALIDITY OF THE GAUSSIAN ASSUMPTION

A question frequently debated in DS/SSMA communications is, how close is the IUI random variable to a Gaussian random variable? There are two ways to answer this question. The first of which is to determine the actual pdf of the IUI and to compare it to a Gaussian distribution with the same variance. The problem, however, is to obtain the IUI pdf. In general it can be obtained by computer simulations or inferred via GQR [48, 46] or MaxEnt [54, 55] methods.

A second way to determine the validity of the GA is to determine the average error rate using the Gaussian Assumption (GA) and to compare it to theoretical performance bounds, results obtained by computer simulations or average error rates determined via some exact method, like Gauss Quadrature Rules (GQR) or MaxEnt.

Computer simulations, especially SSMA simulations, are very time consuming, both when the IUI pdf and average error rates are determined, while bounds on the average error rate have only a very limited application because of the complexity involved. Since GQR and MaxEnt can both deliver quick and accurate results it was decided to investigate and compare these two methods in our investigation of the GA.

As input to the GQR and MaxEnt formulisms, the easiest and most accessible information are the moments of the IUI random variable. However, since a Nakagami fading channel model is considered, the moments will also be a function of the Nakagami fading parameter m. As $m \rightarrow \infty$ the moments, and therefore the IUI distribution, change. Consequently the validity of the GA for a range of m values is investigated.

In the section to follow a general description and formulation of the GQR and MaxEnt methods are presented, together with a description of the Minimum Relative Entropy (MRE) formulism, closely related to the MaxEnt principle. The MRE method can be used effectively to quantify the

relative missing information between two distributions and is applied successfully to quantify the validity of the GA.

Section 4.2 investigates the efficiency and accuracy of inferring a pdf via the GQR and MaxEnt methods when only the moments of a random variable are known. By first confirming the validity of the techniques by duplicating known results, it is possible to assess the applicability of the two techniques and to recommend one of them for investigation of the GA.

In Section 4.3 the accuracies of the GQR and MaxEnt techniques are compared when average error probabilities are investigated. The same philosophy as in the previous section is applied - first known results are duplicated to establish the validity of the two techniques, choosing one of the techniques and then comparing the average error rate of the GA with the chosen technique.

The chapter is concluded by commenting on the validity of the GA.

4.1 Formulation of GQR and MaxEnt

To calculate the average error rate, P_e, in digital communication systems, integrals, i.e. averages, such as

$$I = \int_a^b g(x)dF(x) \tag{4.1}$$

are often encountered, where $g(x)$ is a known function of a random variable X defined on the interval $[a, b]$ and $F(x)$ is the unknown probability density distribution function of X. A number of papers have been devoted to obtaining the average error probabilities in forms like (4.1) for several digital communication problems, i.e. [79, 80, 81, 82].

To determine $F(x)$, suitable algorithms [46, 83, 84, 85] for evaluating the power moments

$$\mu_i = \int_a^b x^i dF(x) = E[X^i] \qquad \forall \qquad i \geq 0 \tag{4.2}$$

can be used which usually represent the input data to the computation of (4.1). Using GQR or MaxEnt techniques, together with the moments as defined in (4.2), it is possible to numerically solve (4.1), and, in addition, derive closed form expressions of the distribution function.

The next sections will briefly describe the background to each of the GQR and MaxEnt techniques.

4.1.1 Formulation and Numerical Procedure for GQR

Using procedures outlined in e.g. [48, 46] it is possible to determine a well known set of orthogonal polynomials $\{p_j(x)\}_{j=1}^{N_c}$ that satisfy a three term recurrence relationship. From these polynomials the first N_c weights and nodes of the quadrature rule can be determined by computing $N_m = 2N_c+1$ moments. The procedure briefly incorporate the calculation of the power moments as defined in (4.2) or the modified moments using e.g. orthogonal Chebycheff polynomials [48]. A Cholesky decomposition is next performed on a Gram matrix constructed from the moments, forming a tri-diagonal matrix as described in [48, 24] and finally determining the eigenvectors and eigenvalues of the tri-diagonal matrix, it is possible to respectively arrive at the weights, A_i, and nodes, t_i of the quadrature rule.

It is also well known, i.e. [86, 83, 46], that the calculation of the quadrature rule using moments as described in (4.2) may be numerically unstable. Sack and Donovan [83] suggested the use of modified moments, which uses linear combinations of the power moments in (4.2), and is less sensitive to computer roundoff errors. A refined Cholesky decomposition, described by Meyers [48], further reduces the numerical stability problem by requiring square roots to be computed at the end of the decomposition and not at each step as in the standard Cholesky decomposition.

Using GQR techniques, (4.1) can be expressed in terms of the weights and nodes as

$$I = \int_a^b g(x)dF(x) = \lim_{N_c\to\infty} \sum_{i=1}^{N_c} A_i g(t_i). \tag{4.3}$$

Also, given a finite number of moments, an estimator as described by Meyers [48], can be used to determine the density function of $F(x)$. Briefly the GQR method to determine a pdf is given by

$$W^*_{N_c}(t_i) = \hat{W}_{N_c}(t_i) - \frac{A_i}{2}, \tag{4.4}$$

where

$$\hat{W}_{N_c}(t_i) = \sum_{S^a_{N_c}} A_i \tag{4.5}$$

and

$$S_{N_c}^{\alpha} = \{i | t_i \leq \alpha\} \tag{4.6}$$

is the set of indices for which $t_i \leq \alpha$. The estimator $W_{N_c}^*(t_i)$ gives a staircase approximation to the true cumulative distribution that becomes increasingly fine as N_c increases. Equivalently, each (A_i, t_i) can be considered a point mass of a discrete approximation to the true probability density function. To obtain a closed form expression of the estimated pdf obtained with the GQR formulation, a curve fit to the numerical data is needed.

The code to determine the weights and nodes of the quadrature rule, the evaluation of integrals as indicated in (4.1) and pdf estimation was realised in Turbo *C* with double precision arithmetic.

4.1.2 Formulation and Numerical Procedure for MaxEnt

Shore and Johnson [49] have proven that MaxEnt [50] is the only method for inferring from incomplete information that does not lead to logical inconsistencies.

In the MaxEnt formulation the missing information (the information entropy) [87]

$$I(x) = -\int_a^b p(x) \ln p(x) dx \tag{4.7}$$

is maximized subject to the constraints of the normalization of the pdf and subject to the available information. In our case the moments must be equal to the measured or calculated moments, i.e. the pdf must satisfy equations (4.2). This is a standard maximum entropy moment problem (the MaxEnt moment problem has been studied in detail by Tagliani [88]). The constraints are introduced via Lagrange multipliers and the resulting expression for the inferred pdf is

$$p(x) = \frac{1}{Z} \exp\left\{-\sum_{m=1}^{M} \lambda_m x^m\right\} \tag{4.8}$$

where the information about the normalization is contained in the partition function

$$Z = \int_a^b \exp\left\{-\sum_{m=1}^{M} \lambda_m x^m\right\} dx \tag{4.9}$$

and the Lagrange multipliers are determined by requiring that

$$\langle x^m \rangle = \mu_m = \int x^m p(x) dx \quad ; \quad m = 1, \ldots, M. \tag{4.10}$$

Agmon et al [89] have noted that defining

$$F(\{\lambda_m\}) = \ln Z + \sum_{m=1}^{M} \lambda_m \mu_m \tag{4.11}$$

yields

$$\frac{\partial F}{\partial \lambda_m} = \mu_m - \langle x^m \rangle. \tag{4.12}$$

Hence minimizing F is equivalent to solving the set of coupled nonlinear equations of (4.10). Furthermore, the authors [89] have shown that the Hessian matrix $\mathbf{H}$ with

$$H_{mm'} = \frac{\partial^2 F}{\partial \lambda_m \partial \lambda_{m'}} = \langle x^{m+m'} \rangle - \langle x^m \rangle \langle x^{m'} \rangle \tag{4.13}$$

is positive definite and thus that F is a strictly convex function of the Lagrange multipliers $\{\lambda_m\}$. Consequently F has a unique minimum (i.e. (4.10) has a unique solution) and a Newton-Raphson minimization procedure [52] is guaranteed to converge. Define an error vector

$$\overline{\epsilon} = (\epsilon_1, \ldots, \epsilon_M)^T \quad : \quad \epsilon_m \equiv \mu_m - \langle x^m \rangle \tag{4.14}$$

and let $\overline{\lambda} = (\lambda_1, \ldots, \lambda_M)$. Then the new guess after a Newton Raphson step is

$$\overline{\lambda}' \;=\; \overline{\lambda} - \mathbf{H}^{-1} \cdot \overline{\epsilon}. \tag{4.15}$$

During each iteration a set of coupled linear equations is solved for the Newton step $\overline{\delta} = \overline{\lambda} - \overline{\lambda}'$

$$\mathbf{H} \cdot \overline{\delta} = \overline{\epsilon}. \tag{4.16}$$

Since **H** is positive definite it is also non-singular. Equation (4.16) is solved with a standard LU-decomposition with a back-substitution algorithm coded in C^{++}.

Also included in the code to combat spurious divergence due to computer round-off errors, the "globally convergent" Newton- Raphson method found in *Numerical Recipes in C* [90] was translated into C^{++} using vector and matrix classes, resulting in an increase of the number of Lagrange multipliers to about 24.

Integrals as expressed in (4.1) can now be solved numerically since we have a closed form expression for the distribution function. It is interesting to note that with the GQR formulation, we can solve integrals, such as (4.1), without actually calculating the distribution function.

4.1.3 The Minimum Relative Entropy Method

The MRE method allows one to include a prior estimation $q(x)$ of the pdf. In the case where the prior distribution is uniform the MRE method reduces to the MaxEnt method. The fundamental concept of MRE is to minimizes the relative entropy or Kulback Leibler distance

$$\mathcal{I} = -\int_a^b p(x) \ln \frac{p(x)}{q(x)} dx, \tag{4.17}$$

subject to the boundary conditions of the available data. Following the same approach as in the previous section, the following expression for the inferred pdf, $p(x)$, can be obtained in terms of the Lagrange multipliers $\{\lambda_m, m = 1, \ldots, M\}$

$$p(x) = \frac{q(x)}{Z} \exp\left(-\sum_{m=1}^{M} \lambda_m x^m\right) \tag{4.18}$$

with partition function

$$Z = \int_a^b q(x) \exp\left(-\sum_{m=1}^{M} \lambda_m x^m\right) dx. \tag{4.19}$$

The algorithm used to solve for the Lagrange multipliers is essentially identical to that developed for MaxEnt.

It is seen from (4.17) that if $p(x)$ and $q(x)$ are the same, the missing information is zero. Equation (4.17) is therefore used to quantify how close the IUI distribution is to a Gaussian distribution with variance equal to the second moment of the IUI random variable.

4.2 Estimated pdf via GQR and MaxEnt

The main aim of this section is to investigate the distribution function of the IUI of a SSMA system and to comment on the accuracy of the Gaussian Assumption (GA), often used to simplify calculations of SSMA systems.

The two methods, described above, are available to accomplish this. However, it is not known which of the two methods will yield the most accurate and reliable distribution estimates, and therefore the investigation is started by inferring known distribution functions from moments. From these results, it is then possible to recommend a reliable and accurate method to be used in the investigation of the IUI random variable.

A few commonly encountered pdf's in digital communications are investigated. Kavehrad et al [54] have shown that the MaxEnt approach estimates an elementary monomial very well. To ensure that the MaxEnt algorithm was operating properly, and to compare it with the GQR estimator, a result presented in [54] is repeated.

Figure 4.1 shows

$$p(x) = 2x \qquad \forall \qquad 0 \leq x \leq 1 \tag{4.20}$$

with moments

$$\mu_i = \frac{2}{2+i} \qquad \forall \qquad i \geq 0 \tag{4.21}$$

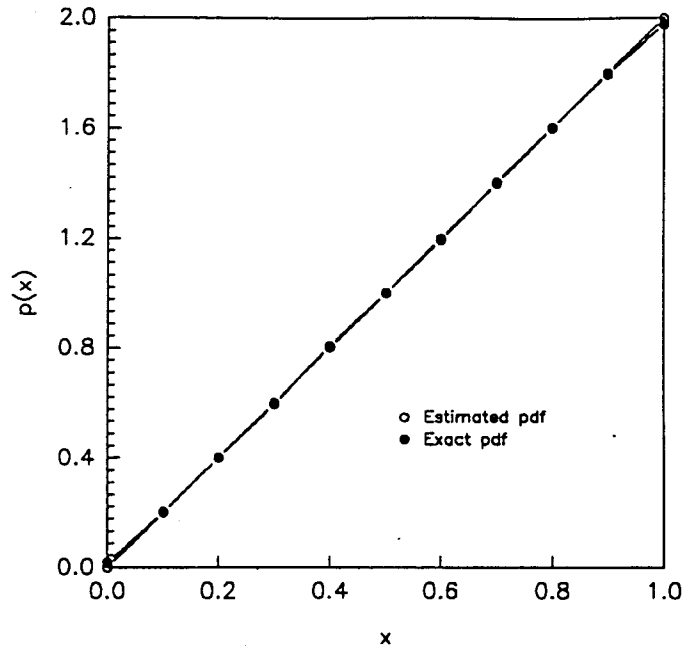

Figure 4.1: Exact and estimated distribution of a monomial

and the estimated density function when the MaxEnt formulation, (4.8), is used. With as few as eight moments a very good estimate is obtained, which is similar to results of [54].

Figure 4.2 indicates the exact value and GQR estimator, equations (4.4) to (4.6), of the pdf in (4.20). After $N_m = 25$ and $N_m = 45$ moments the standard and modified Cholesky decomposition respectively become numerically unstable. It is clear that even with high order moments this estimator is not accurate.

Also, to verify the GQR algorithm a result by Meyers [48] is repeated and the results compared to the MaxEnt formulation.

Assuming a zero-mean, unit variance Gaussian random variable X (as in Meyers [48]), the GQR estimator for various values of N_m is computed in Figure 4.3, with moments given by

$$\mu_i = \begin{cases} \frac{\sigma^i 2^{\frac{i}{2}}}{\sqrt{\pi}} \Gamma\{\frac{i+1}{2}\} & \forall \ i \ \text{ even} \\ 0 & \forall \ i \ \text{ odd} \end{cases} .$$

Also indicated in the figure is the exact pdf. As suggested in [48] the GQR algorithm converges to the true pdf if enough moments are available. However, the algorithm becomes numerical unstable

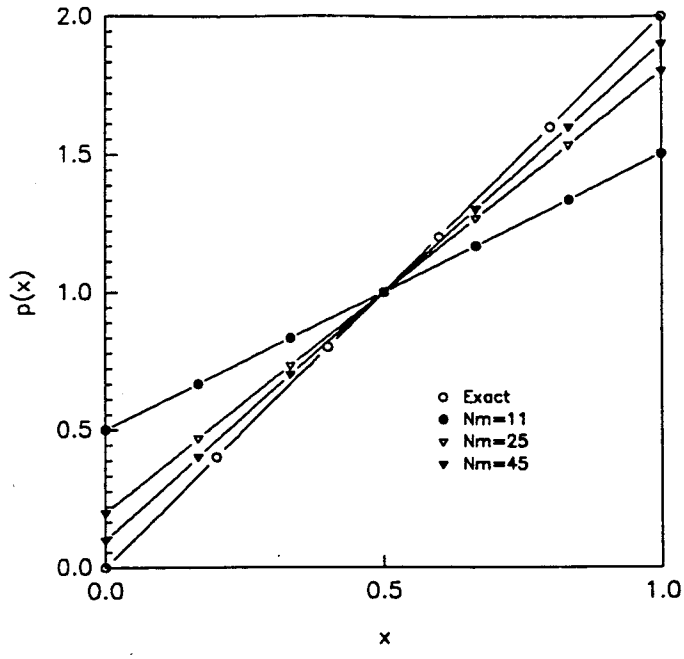

Figure 4.2: Convergence of GQR estimator for monomial

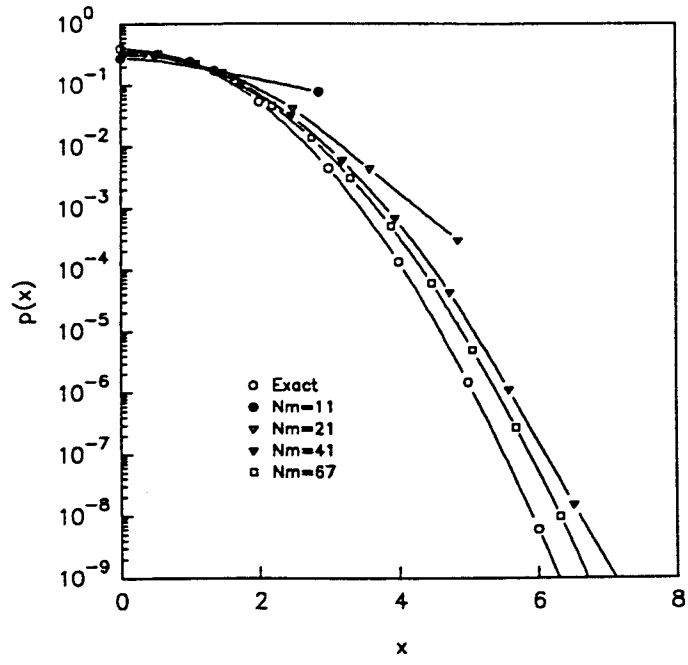

Figure 4.3: Convergence of GQR estimator for Gaussian distribution

at $N_m = 67$ moments when the standard Cholesky decomposition is used. When the modified Cholesky decomposition, as described by Meyers [48, pp 2257-2261], is used, $N_m = 141$ moments deliver accurate results, following the tail probabilities very well. If any moments less that 141 are used the approximation is not sufficiently accurate.

Figure 4.3 is similar to Figure 1 of Meyers [48, pp 2251]. Meyers is of the opinion that "reasonable accurate results are obtained at 10^{-6} for $N_c > 10$" [48, p 2251]. It is of course debateable what is meant by "reasonable accurate", but in general it is clear that not less than $N_m = 141$, that is $N_c = 70$, moments are necessary to follow the tail accurately. As mentioned before, a curve fit has to be performed on the numerical data to obtain a closed form expression of the estimated distribution.

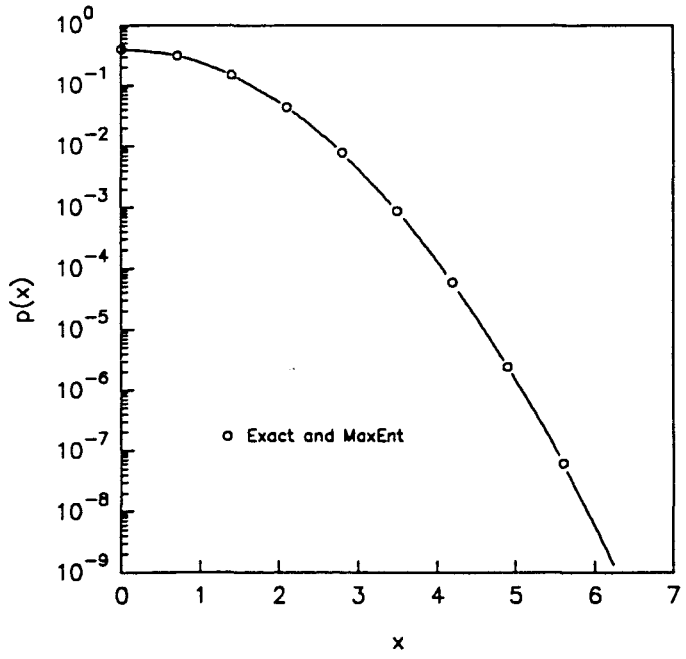

Figure 4.4: Estimated Gaussian distribution obtained with MaxEnt

Using again a unit variance, zero mean Gaussian random variable, the estimated density function as well as the actual density function is indicated in Figure 4.4 when the MaxEnt formulation, equation (4.8), is used. A total of three moments were used to obtain a result that is almost exact. Table 4.1 indicates the coefficients, λ_r, when higher order moments are used. It is evident that the estimated pdf approximates the actual distribution very well, including the tail probabilities with very few moments.

As another example, the Exponential distribution is investigated, given by

N_m	Z	λ_r			
3	2.506628	3.061006e-17	0.5	-	-
4	2.506628	2.258665e-16	0.5	-5.379226e-17	-
5	2.506628	7.119094e-17	0.5	-2.203197e-17	-2.057082e-13
Exact	2.506628	0	0.5	0	0

Table 4.1: Estimated Gaussian distribution λ_r's, $\sigma^2 = 1$

$$p(\gamma_b) = \frac{1}{\overline{\gamma}_b} \exp\left\{-\frac{\gamma_b}{\overline{\gamma}_b}\right\} \qquad \forall \qquad \gamma_b \geq 0 \tag{4.22}$$

with moments

$$\mu_i = \gamma_b^i i!. \tag{4.23}$$

It is clear from Figure 4.5 that the GQR algorithm fails again dismally, even for $N_m = 37$ moments, irrespective of the use of modified moments or the modified Cholesky decomposition.

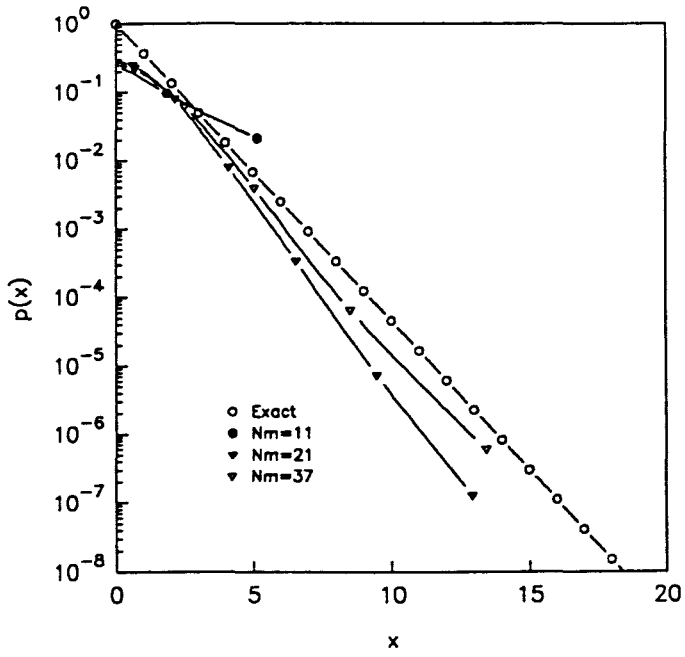

Figure 4.5: Convergence of GQR estimator for Exponential distribution

Figure 4.6 shows the pdf obtained with MaxEnt; again very accurate tail probabilities with only three moments. Table 4.2 indicates the coefficients λ_r when higher order moments are used.

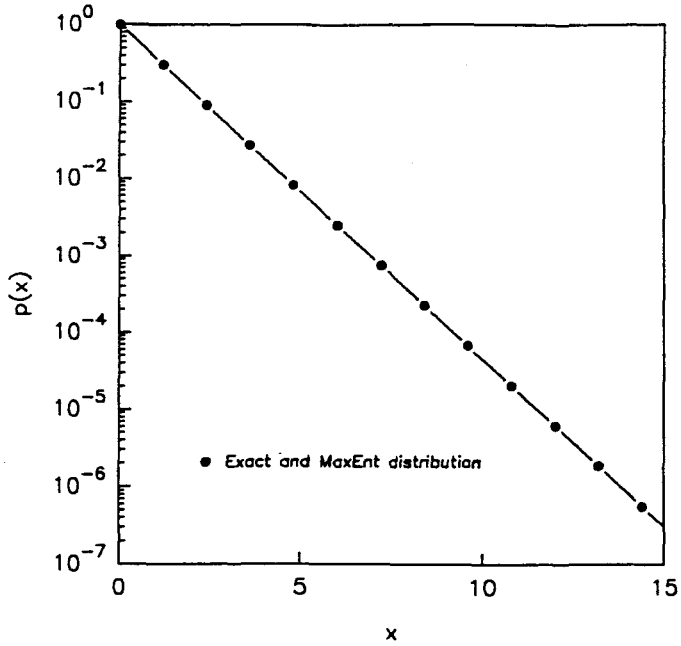

Figure 4.6: Estimated Exponential distribution obtained with MaxEnt

N_m	Z	λ_r			
3	1	1	-7.504413e-16	-	-
4	1	1	6.05662e-15	-5.415413e-16	-
5	1	1	1.35561e-19	-1.303146e-15	-1.154032e-17
Exact	1	1	0	0	0

Table 4.2: Estimated Exponential distribution λ_r's, $\overline{\gamma}_b = 1$

At this point it is concluded that the GQR estimator suggested by Meyers [48] and indicated in equations (4.4) to (4.6), only becomes accurate when a very large number of moments is available. However, as in the monomial pdf example (equation (4.20)), not even a large number of moments can ensure sufficient accuracy before the algorithm becomes numerically unstable.

Although the algorithm to determine a distribution via the GQR formulation is much simpler and computationaly quicker (roughly orders quicker) than that of the MaxEnt formulation, it is essentially worthless when accurate estimates of a desired pdf are needed. It is therefore suggested that a new estimator be investigated to determine the distribution via GQR methods. However, it is not proven here that GQR's can not deliver accurate estimates of a desired distribution, but it is merely suggested that the estimator, as described by Meyers, is not always sufficiently accurate.

From the examples investigated it is clear that MaxEnt produces more accurate results than GQR with less moments, and in fact, deliver accurate results under conditions where the GQR estimator fails.

Having a method available that can infer the actual distribution from a small number of moments has additional advantages in digital communication, specifically in SSMA communications. In the following section it is shown that in SSMA only a limited number of moments is available under certain conditions and in general, in a practical system, only a small number of moments can be measured effectively.

The MaxEnt approach can deliver accurate results under a wide variety of conditions. The advantages of MaxEnt relative to the GQR approach can be summarized as follows:

- A smaller number of moments is needed to estimate pdf from moments,
- information other than moments can be used to infer a pdf.

4.3 SSMA IUI Distribution

In the previous section it was shown that the MaxEnt approach produces credible estimates of the distribution of a random variable under a variety of conditions. It is hence possible to reliably infer the IUI distribution and to quantify the validity of the GA by calculating $\mathcal{I}$, the relative missing information. Also, the influence of the Nakagami fading parameter m on the validity of the GA is further investigated. (As explained in Appendix A, $m = \frac{1}{2}$ corresponds to the case where the signal suffers severest fading, while the condition $m = \infty$ indicates no fading.)

For the unfaded case ($m = \infty$), Table 4.3 signifies the moments, as derived in Appendix D, for $K = 2$ and $N = 127$. Only the even moments are indicated since the IUI is a symmetric, zero mean random variable [70, 91] and hence all odd moments are zero. These moments were generated with Gold sequences as indicated in Appendix B. Also tabulated are the moments of a Gaussian distribution with variance equal to the second moment of the IUI variable.

For $K = 2$ only the first 18 moments are meaningful. Numerical inaccuracies cause the higher order moments (greater than 18) to become inaccurate. This strengthens the suggestion earlier that a method is needed that converge quickly when the IUI distribution is inferred since only a small, finite number of moments are available under certain conditions. Also indicated in this table are moments for $K = 25$. It is clear that the moments for this condition is closer to a Gaussian distribution than for $K = 2$.

Although the pdf of the IUI is not of much significance other than to calculate $\mathcal{I}$ and the average probability of error, let us nevertheless briefly examine the pdf for $K = \{2, 25\}$, $N = 127$ and

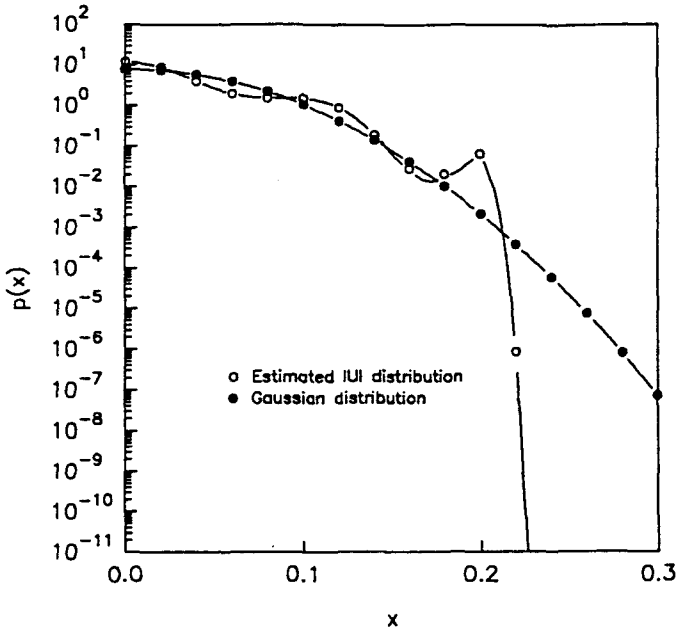

Figure 4.7: IUI distribution for $K = 2, N = 127, N_m = 10$ and $m = \infty$

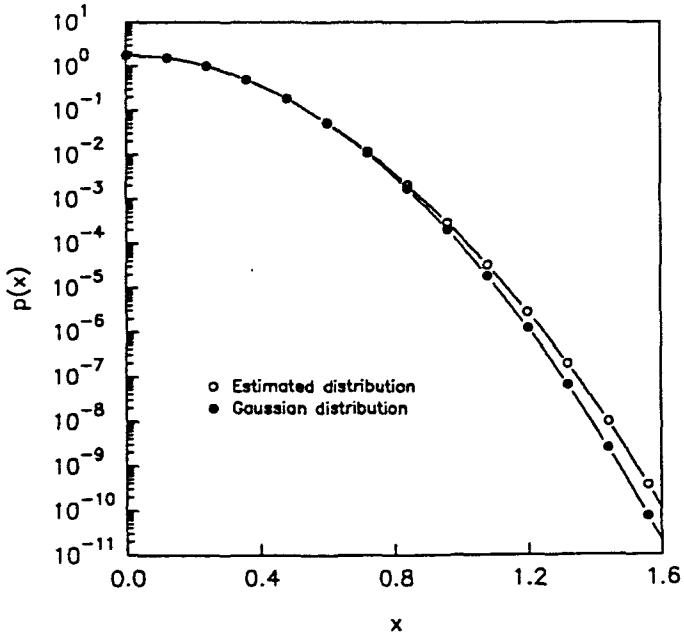

Figure 4.8: IUI distribution for $K = 25, N = 127, N_m = 10$ and $m = \infty$

N_m	$N = 127$ $K = 2$	Gaussian moments	$N = 127$ $K = 25$	Gaussian moments
2	0.00242647	0.00242647	0.063177	0.063177
4	2.45809e-05	1.76633e-05	0.0121269	0.011974
6	4.08285e-07	2.14297e-07	0.00392591	0.00378241
8	9.56568e-09	3.6399e-09	0.00179922	0.00167273
10	2.86238e-10	7.94889e-11	0.00107131	0.000951101
12	1.00233e-11	2.12165e-12	0.000787382	0.000660965
14	3.86378e-13	6.69256e-14	0.000690347	0.000542851
16	1.58152e-14	2.43589e-15	0.000704616	0.000514436
18	6.73614e-16	1.00481e-16	0.000821985	0.000552509
20	8.34723e2	4.63245e-18	0.000872412	0.000663211

Table 4.3: Moments of the IUI random variable for $K = \{2, 25\}$, $N = 127$ and $m = \infty$

$m = \infty$ as indicated in Figures 4.7 and 4.8 respectively. These distributions were generated using 10 moments of the IUI random variable.

For $K = 2$ (Figure 4.7) it is apparent that the distribution of the IUI is not very close to a Gaussian distribution. The IUI distribution has a lot more structure and does not follow the Gaussian tail at all. However, as intuitively expected from the central limit theorem, the IUI random variable approaches the Gaussian distribution much better as K increases - as indicated in Figure 4.8 for $K = 25$ only the tail distribution of the IUI random variable does not follow the Gaussian distribution exactly.

By looking at the moments, as in Table 4.3, or the actual distribution, as in Figures 4.7 and 4.8, of the IUI random variable, it is apparent that as K increases the GA becomes more valid. However, these measures do not give a generalised or quantative indication of the validity of the GA. By calculating $\mathcal{I}$, as defined in (4.17), we have a dimensionless quantity that fulfil the criteria of a generalized parameter with $0 \leq \mathcal{I} \leq \frac{1}{2}$. If $\mathcal{I} = 0$ the two random variables are 100% identically distributed. On the other hand, when $\mathcal{I} = \frac{1}{2}$ the missing information is a maximum.

Figure 4.9 shows $\mathcal{I}$ as defined in 4.17, between the "exact" IUI-pdf and a Gaussian distribution with the same variance σ^2_{ma} for $m = \{\frac{1}{2}, 5, \infty\}$. Irrespective of m, the missing information between the two distributions decreases exponentially as K increases. As m decreases, in other words as the channel becomes more faded, the IUI distribution is less Gaussian.

Further, for the Gold sequences adopted in this work, the maximum family size is 65 for $N = 127$. From Figure 4.9 it is clear that the missing information, $\mathcal{I}$, saturates at roughly 10^{-5} for $m = \infty$ and 10^{-3} for $m = \frac{1}{2}$. This observation is quite significant since an increase in the number of users, that is an increase in K, does not imply a more Gaussian nature of the IUI random variable. The saturation of $\mathcal{I}$ suggest that the GA is only valid at high signal-to-noise ratios or high average error rates, especially under faded conditions. This statement is investigated in the next section.

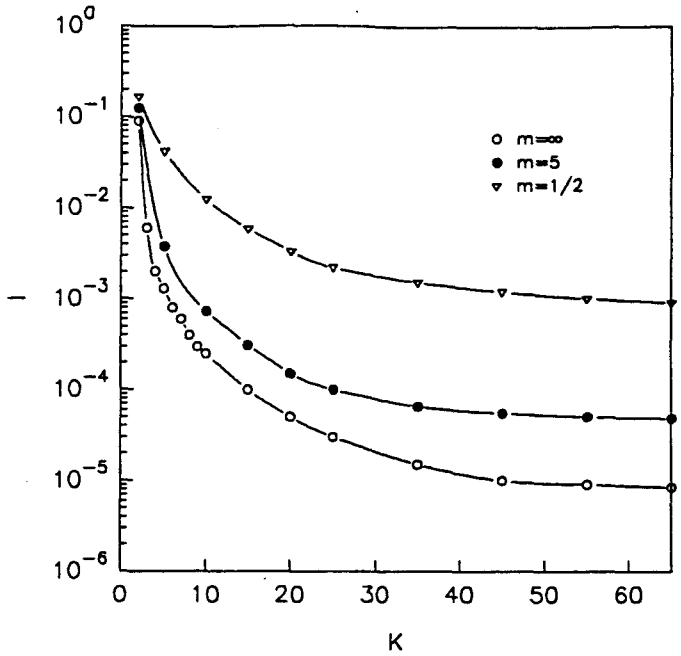

Figure 4.9: Relative Entropy, $\mathcal{I}$, of the IUI distribution, $m = \{\frac{1}{2}, 5, \infty\}$

Table 4.4 gives an indication of the influence of the chipping sequence length N for $m = \{\frac{1}{2}, 5, \infty\}$. To investigate the influence of N the ratio $\frac{K}{N}$ has to be constant for different values of N. As N increases, $\mathcal{I}$ decreases, indicating that the IUI random variable becomes more Gaussian as N increases. As for an increase in K, $\mathcal{I}$ also saturates at a specific value, indicating that not even an infinite increase in N will not result in a perfect Gaussian distribution. When fading is added to the signal, that is low values of m, the distribution is even less Gaussian.

It can be concluded that for the Gold spreading sequences used in this study, the GA is inaccurate, especially when a fading channel is considered.

A final measure of the validity of the GA is to calculate the average error rate using the GA

		$\mathcal{I}$		
K	N	$m = 1/2$	$m = 5$	$m = \infty$
2	31	0.12616	0.11971	0.01190
3	63	0.03171	0.02157	0.01154
5	127	0.01929	0.00613	0.00141
9	255	0.01348	0.00281	0.00049
17	511	0.00974	0.00128	0.00021

Table 4.4: Relative entropy, $\mathcal{I}$, for $m = \{\frac{1}{2}, 5, \infty\}$ and $\frac{K}{N}$ constant

and GQR or MaxEnt. In the following section the applicability of GQR and MaxEnt is briefly investigated before a final verdict on the GA is reached.

4.4 Digital Communication Performance Results

The applicability of GQR and MaxEnt in the calculation of average error rates in digital communication systems is briefly investigated by an appropriate example. Further, to comment on the validity of the GA, average error rates are calculated using the GA and MaxEnt and compared with bounds available in the open literature and computer simulations for CPSK and DPSK as modulation scheme.

Consider the following integral

$$P_e = \int_{-\infty}^{\infty} P_b(\gamma_b) p(\gamma_b) d\gamma_b \tag{4.24}$$

$$= \sum_{i=1}^{N_c} A_i P_b(t_i), \tag{4.25}$$

where

$$P_b(\gamma_b) = \frac{1}{2}\text{erfc}\left\{\sqrt{\gamma_b}\right\}, \tag{4.26}$$

and $p(\gamma_b)$ the exponential density function as indicated in (4.22) with moments as in (4.23). This integral can be evaluated in a closed form as

$$P_e = \frac{1}{2}\left\{1 - \sqrt{\frac{\overline{\gamma}_b}{1+\overline{\gamma}_b}}\right\}, \tag{4.27}$$

and represents the well known performance of BPSK signalling under Rayleigh fading conditions [72].

Using the quadrature rule as indicated in (4.25) and the estimated Exponential distribution, as tabulated in Table 4.2 GQR and MaxEnt can respectively be implemented to calculate (4.24).

Figure 4.10 indicates the performance results obtained with GQR integration, MaxEnt and the

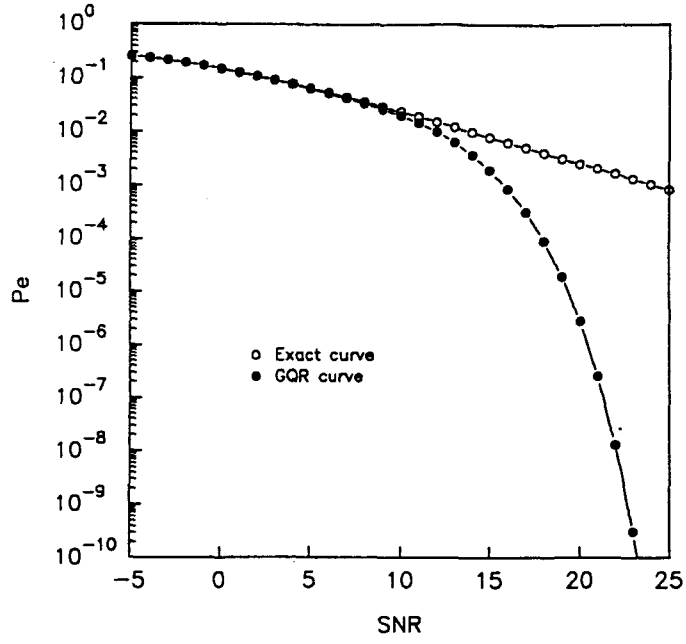

Figure 4.10: Comparison of exact error rate with GQR and MaxEnt techniques

exact results. GQR and MaxEnt integration are performed with 31 moments (more moments resulted in numerical instability) and 3 moments respectively. GQR integration is accurate only at low SNR ($\overline{\gamma}_b$) values, while the MaxEnt algorithm delivered excellent results for any value of $\overline{\gamma}_b$.

To investigate the accuracy of GQR and MaxEnt techniques for SSMA, Figure 4.11 indicates the CPSK performance when calculated with MaxEnt and GQR. The results are also compared with simulated values. It is clear that, as in the previous example, the GQR algorithm fails at high signal-to-noise ratios.

However, it has been shown in the literature that GQR can deliver accurate results [24, 82, 92] under certain conditions, but it has been shown that MaxEnt deliver accurate results under more general conditions. With the above results in mind MaxEnt has been selected as the method to accurately calculate average error probabilities and will be used throughout this thesis.

To investigate the accuracy of the GA together with CPSK and DPSK signalling, let us examine Figures 4.12 and 4.13 respectively.

We note that, as with most Gaussian approximations, that the GA results in less conservative performance results. As m grows, it is seen that the GA becomes less valid, which is also the case when no diversity is present. As P increases, the GA becomes less valid.

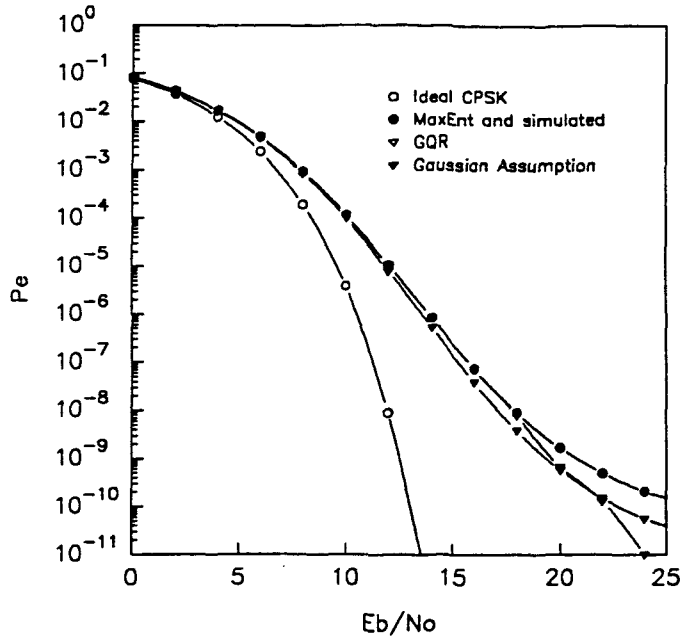

Figure 4.11: MaxEnt and GQR compared with computer simulations for CPSK; $m = \infty$, $K = 10$ and $N = 127$

In Figure 4.13 a computer simulation for $P = 3$ is presented to verify the assumption made in Section 3.2. It is clear that the MaxEnt result is closer to the simulated curve than the GA result. By making the assumption as described in Section 3.2 our results are inaccurate by approximately 5% and is within acceptable limits.

To further verify the accuracy of MaxEnt and to investigate the GA, consider Tables 4.5 and 4.6, calculated for an unfaded ($m = \infty$) CPSK channel. Tables 4.5 and 4.6 indicate results for $N = 31$ and $K = 2$ (generators 45 and 67 in octal) and $K = 3$ (generators 45, 67 and 75 in octal) respectively. The performance of the same systems has previously been evaluated by Pursley et al. [93] using bounding techniques. The generator polynomials of the 3 spreading sequences were chosen to have Auto Optimal Least Sidelobe Energy (AO/LSE) initial loadings of 63, 70 and 57 [94]. The performance results obtained with MaxEnt provide accurate results up to 2 and 3 decimal places (using 10 moments), which is more than sufficient when calculating probability of error.

The GA error probabilities are calculated using the second moment of the IUI random variable using (3.35). It is clear that the error rates calculated using the GA do not fall within the performance bounds. At high SNR values the GA is inaccurate by more than 5%.

Also, using (3.31), Table 4.7 tabulates performance results using MaxEnt and the GA for $m = \frac{1}{2}$ and $P = \{1,3\}$. For the faded, non diversity case, the GA is inaccurate by approximately 10%,

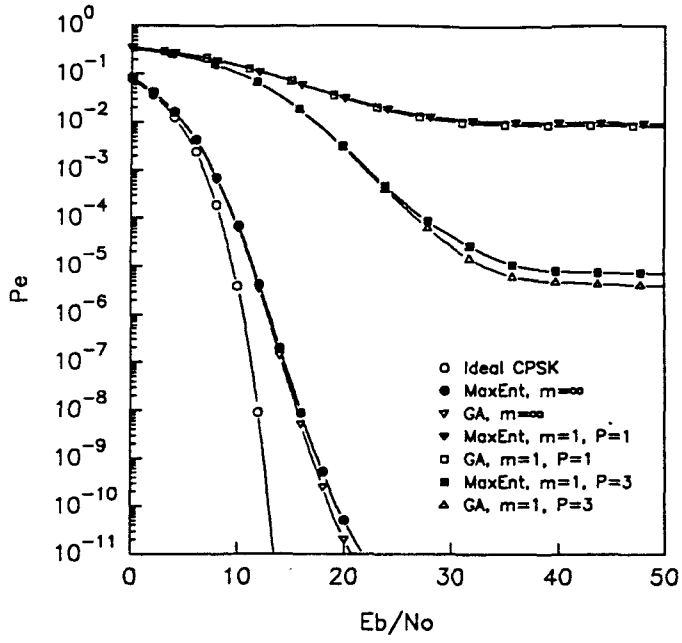

Figure 4.12: Accuracy of the GA with CPSK signalling; $m = \{\infty, 1\}$, $K = 30$, $N = 511$ and $P = \{1, 3\}$

while for the faded, diversity case ($P = 4$), the GA is inaccurate by as much as 20% at high signal to noise ratios.

4.5 Conclusions

Using the GA assumption as formulated and investigated by e.g. Pursley [70] and Turin [23], allows us to significantly simplify SSMA system analysis. Having a reliable alternative approach at hand

E_b/N_0	Probability of error, P_e			
	Lower Bound	Upper Bound	MaxEnt	GA
4	1.44×10^{-2}	1.45×10^{-2}	1.443×10^{-2}	1.452×10^{-2}
6	3.35×10^{-3}	3.36×10^{-3}	3.357×10^{-3}	3.382×10^{-3}
8	4.24×10^{-4}	4.42×10^{-4}	4.316×10^{-4}	4.289×10^{-4}
10	2.40×10^{-5}	2.42×10^{-5}	2.397×10^{-5}	2.484×10^{-5}
12	4.81×10^{-7}	4.89×10^{-7}	4.815×10^{-7}	5.806×10^{-7}
14	2.28×10^{-9}	2.34×10^{-9}	2.285×10^{-9}	5.608×10^{-9}

Table 4.5: CPSK performance of SSMA system; $K = 2$, $N = 31$ and $m = \infty$

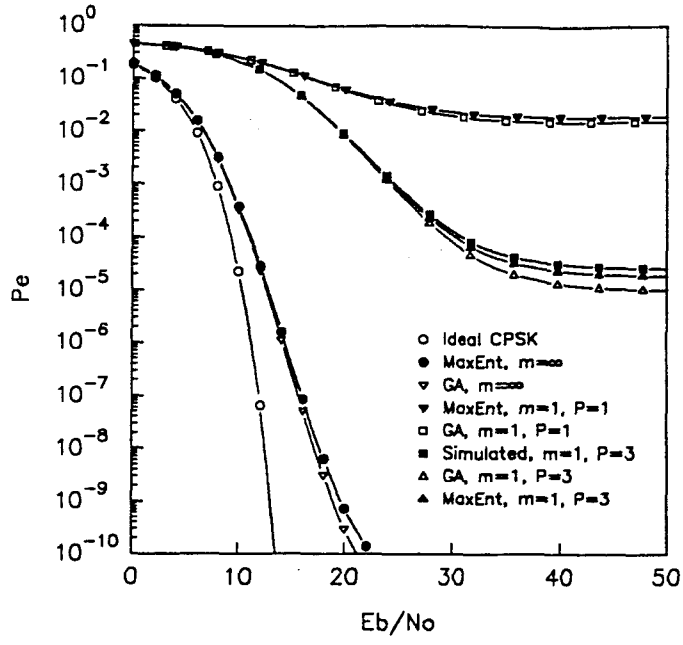

Figure 4.13: Accuracy of the GA with DPSK signalling; $m = \{\infty, 1\}$, $K = 30$, $N = 511$ and $P = \{1, 3\}$

to compare performance results and using exact aperiodic correlation parameters of the spreading codes (not random codes as in [70] and [23]), it is possible to reach a verdict on the validity of the GA, with and without coding.

It has been shown that the GQR pdf estimator as described by Meyers [48] is not very accurate when the distribution of a random variable is inferred from its moments. Although it is well known [46] that a N_c GQR formula is exact for a polynomial of degree $2N_c - 1$ or less, the estimator proposed by Meyers was not very accurate with $N_c = 11$ for a monomial. Therefore, it is suggested that the GQR estimator of Meyers be rejected and the MaxEnt approach used when an accurate

E_b/N_0	Probability of error, P_e			
	Lower Bound	Upper Bound	MaxEnt	GA
4	1.66×10^{-2}	1.69×10^{-2}	1.662×10^{-2}	1.661×10^{-2}
6	4.58×10^{-3}	4.77×10^{-3}	4.597×10^{-3}	4.562×10^{-3}
8	8.43×10^{-4}	9.11×10^{-4}	8.487×10^{-4}	8.149×10^{-4}
10	1.06×10^{-4}	1.21×10^{-4}	1.076×10^{-4}	9.213×10^{-5}
12	1.04×10^{-5}	1.29×10^{-5}	1.081×10^{-5}	7.074×10^{-6}
14	9.68×10^{-7}	1.33×10^{-6}	1.046×10^{-6}	4.459×10^{-7}

Table 4.6: CPSK performance of SSMA system; $K = 3$, $N = 31$ and $m = \infty$

E_b/N_0	Probability of error, P_e			
	MaxEnt: $P = 1$	GA: $P = 1$	MaxEnt: $P = 4$	GA: $P = 4$
5	2.861×10^{-1}	2.841×10^{-1}	2.355×10^{-1}	2.341×10^{-1}
10	1.960×10^{-1}	1.897×10^{-1}	1.151×10^{-1}	1.114×10^{-1}
15	1.207×10^{-1}	1.171×10^{-1}	3.290×10^{-2}	3.012×10^{-2}
20	7.047×10^{-2}	5.210×10^{-2}	5.560×10^{-3}	4.762×10^{-3}
25	4.064×10^{-2}	3.011×10^{-2}	6.907×10^{-4}	5.517×10^{-4}
30	2.392×10^{-2}	1.907×10^{-2}	7.741×10^{-5}	5.917×10^{-5}
35	1.508×10^{-2}	1.115×10^{-2}	9.063×10^{-6}	8.321×10^{-6}
40	1.087×10^{-2}	9.812×10^{-3}	1.329×10^{-6}	1.107×10^{-6}

Table 4.7: CPSK performance of SSMA system; $K = 2$, $N = 511$, $m = \frac{1}{2}$ and $P = \{1, 4\}$

estimate of a distribution is needed. The drawback of the MaxEnt approach is the relative large code complexity and long computational time. However, if accurate pdf estimates are needed, especially when only a limited number of moments is available, there is only one choice - MaxEnt.

When average error rates are considered MaxEnt is again the most general and accurate formulism, using the least number of moments.

The most important results of this chapter is the investigation of the IUI random variable. It has been shown, via the parameter $\mathcal{I}$ and by calculation of the average error rate, that the GA is not valid when accurate performance results are required. This is especially true under faded (m small), diversity conditions. Therefore, MaxEnt will be used in all the average error rate calculations to follow.

CHAPTER 5

PERFORMANCE RESULTS IN AN AWGN CHANNEL

As the parameter m of the Nakagami-m distribution converge to infinity, a special condition of the system as described in Chapter 2 is realised. This is when the IWC system is stationary, with negligible multipath effects. In the absence of multiple paths to be resolved in a stationary system, the only factors that degrade the wideband signal are the IUI and AWGN. Therefore, only coding can be used as a form of diversity to enhance system performance. The performance enhancement due to block- and convolutional coding, with hard decision decoding, is investigated.

To accomplish a comparison on an equal basis between a coded and uncoded system, two options are available. One option is to fix the length of the spreading code and calculate a bandwidth efficiency parameter for the coded system and compare it to the bandwidth efficiency of the uncoded system. The other option is to reduce the processing gain by the code rate R_{cd} (the effective processing gain is constant [69, 68]). In effect this means that shorter spreading sequences are needed to calculate the coded performance. The latter option is adopted in this chapter (and in Chapters 6 and 7) since it gives a direct indication of the coded system performance. Further, since actual Gold sequences are utilised, the results are more accurate than calculating a dimensionless bandwidth efficiency parameter.

As indicated in Chapter 4, very accurate results are obtained with the MaxEnt approach. Gold codes with generator polynomials and initial loading as indicated in Appendix B are used to obtain the results presented, with CPSK and DPSK as modulation schemes.

In the first two sections, Section 5.1 and 5.2, the maximum interference parameter, K, is calculated with and without coding for the cellular system described in Chapter 2. Section 5.3 will use these results to compare CPSK and DPSK capacity in a single- and multiple cell environment.

5.1 CPSK Performance

We will start by investigating the uncoded performance of a cellular SSMA system, followed by evaluations of convolutional- and block coding for similar conditions.

5.1.1 Uncoded CPSK

We begin our investigation by looking at the influence of processing gain, N, on the capacity of a SSMA system with CPSK as modulation scheme. Using MaxEnt and moments indicated in Appendix D, the average error rate is observed to increase with an increase in K and a decrease in N, which is as expected, and indicated in Figure 5.1, for a fixed multiple access interference, $K = 10$, and different values of N. We notice that, due to the finite cross correlation of the spreading sequences, the error rate saturates to an irreducible rate with increasingly unacceptable performance as N decreases. By increasing the processing gain from 15 dB ($N = 31$) to 21 dB ($N = 127$), a situation which is unacceptable for speech, can be improved dramatically. Also indicated in Figure 5.1 is the performance of ideal coherent PSK for reference purposes.

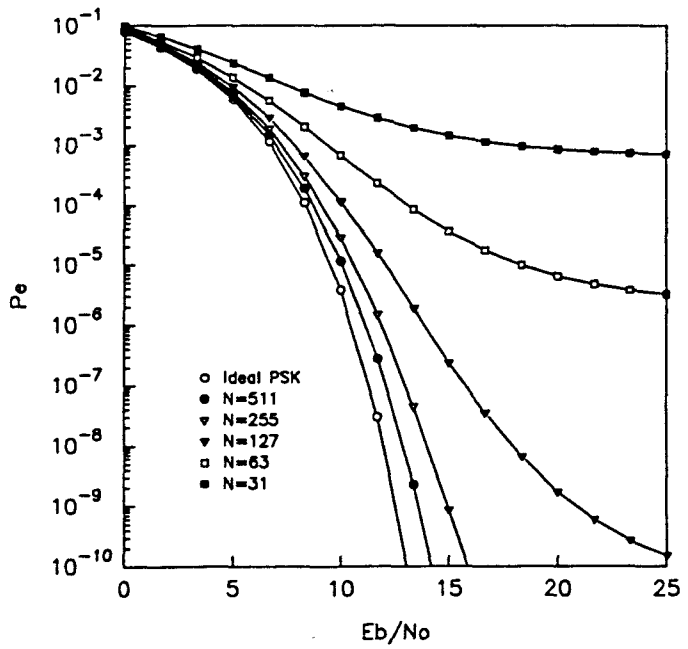

Figure 5.1: Uncoded CPSK performance, $K = 10$

Figure 5.2 depicts the system capacity in terms of average error probability as a function of K for a fixed, large value of $E_b/N_0 = 20$ dB. As intuitively expected the error rate increases monotonically

with increased K. Also, when the processing gain is low, i.e. $N = 31$, K is relatively small for an acceptable error rate. Table 5.1 quantifies and tabulates K for different error rates (also at $E_b/N_0 = 20$ dB). From this it is seen that K is exceedingly small for low values of N and P_e. Pickholtz et al [95] stated a rule of thumb for the capacity of a DS/SSMA system under AWGN conditions as being approximately 10% of the processing gain. At $P_e = 10^{-8}$ this would seem to be an accurate estimate.

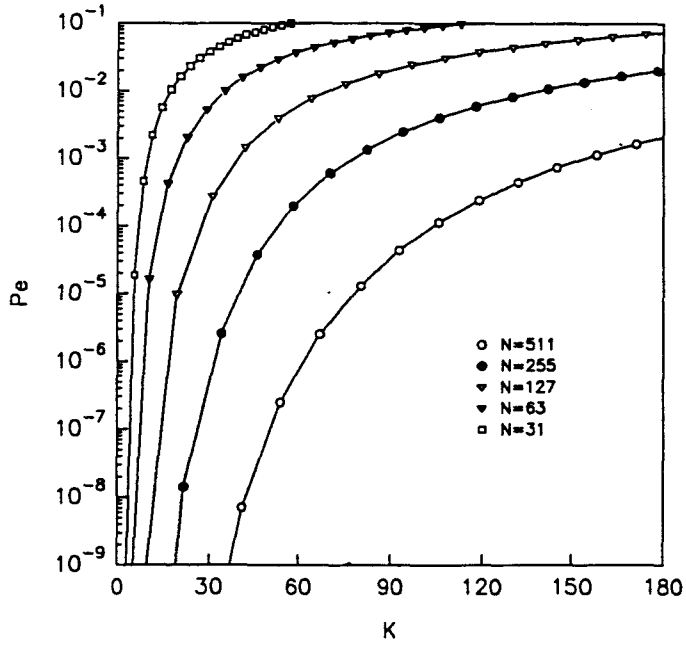

Figure 5.2: Uncoded CPSK capacity performance, $E_b/N_0 = 20$ dB

P_e	$N = 511$	$N = 255$	$N = 127$	$N = 63$	$N = 31$
10^{-3}	152	76	38	19	9
10^{-5}	77	39	19	9	4
10^{-8}	41	21	10	5	2

Table 5.1: K for uncoded CPSK, $E_b/N_0 = 20$ dB

An interesting point to note is that a change in processing gain results in a linear change in capacity. For example, by reducing the processing gain by 75% (i.e. from $N = 511$ to $N = 127$) the capacity is also reduced by 75%, in this case from 77 to 19 at 10^{-5}. This knowledge can be used quite productively when a capacity estimate is needed at a different processing gain, i.e. at $N = 1024$.

5.1.2 CPSK Convolutional Coding

The convolutional codes considered here have generator polynomials as listed in Appendix C with code rates $R_{cd} = 1/2$, $1/4$ and $1/8$. These rates were chosen to make comparisons on an equitable base. For example, the performance of an uncoded, $N = 511$ system will be compared to a rate $R_{cd} = 1/2$, $N = 255$ system. Both of these will result in the same data throughput and bandwidth.

The convolutional code constraint lengths are chosen to show how relatively simple codes ($\nu = 2, 3, 4$) perform. A rate $R = 1/2$, $\nu = 6$ encoder and decoder are commercially available and its performance is also presented.

Figure 5.3 indicates the average error performance as a function of the received signal-to-noise ratio for different coding rates, constraint length $\nu = 4$ and $K = 150$. The comparison is performed with approximately equal complexity. (Clark and Cain [96] indicate that convolutional codes with the same constrained length, irrespective of code rate have approximately equal complexity). The processing gain, N, of the coded signals is reduced by the code rate, R_{cd}, as explained earlier.

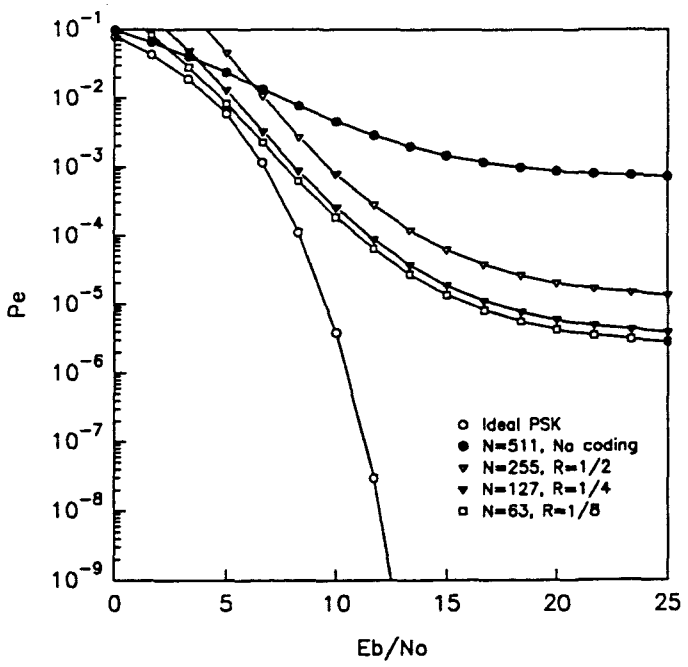

Figure 5.3: Convolutional coded CPSK performance, $\nu = 4$ and $K = 150$

We observe that low rate coding improves the average error rate considerably, and hence, will result in increased system capacity. An interesting point to note is that the rate $R_{cd} = 1/8$ code gives an error rate improvement at lower values of signal-to-noise ratio than higher rate codes when compared to the uncoded case. In this example (Figure 5.3) the improvement over the uncoded

case starts at approximately 3 dB for $R_{cd} = 1/8$, while the rate $R_{cd} = 1/2$ code only starts at 7 dB.

	$N = 511$ No Coding	$N = 255, R_{cd} = 1/2$				$N = 127, R_{cd} = 1/4$			$N = 63, R_{cd} = 1/8$		
		ν				ν			ν		
P_e		2	3	4	6	2	3	4	2	3	4
10^{-3}	152	190	208	226	263	183	228	256	203	226	270
10^{-5}	77	113	123	141	170	106	130	156	116	134	160
10^{-8}	41	66	69	86	110	60	75	95	68	80	98

Table 5.2: K for convolutional coded CPSK, $E_b/N_0 = 20$ dB

Table 5.2 quantifies the convolutional coded capacity. We note that low rate coding increases the capacity significantly. At an average error rate of 10^{-5} a rate $R_{cd} = 1/8$, constrained length $\nu = 4$ convolutional code increases K by 77% over the uncoded case.

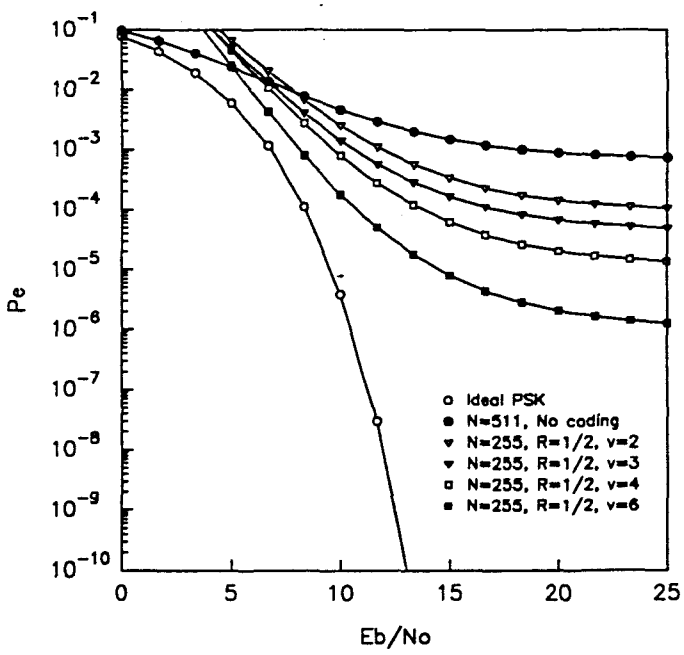

Figure 5.4: Convolutional coded CPSK performance, $K = 150$

Figures 5.4, 5.5 and 5.6 graphically illustrate the performance of rate $R_{cd} = 1/2, 1/4$ and $1/8$ convolutional codes, respectively, for different constraint lengths. The performance is indicated for $K = 150$ and compared to ideal CPSK and uncoded SSMA.

Of particular interest is the rate $R_{cd} = 1/2$, $\nu = 6$ code's performance since, as mentioned, these codecs are commercially available. Because of the code's long constrained length performance/capacity is improved over the low rate $R_{cd} = 1/8$, $\nu = 4$ code. Although it is not entirely

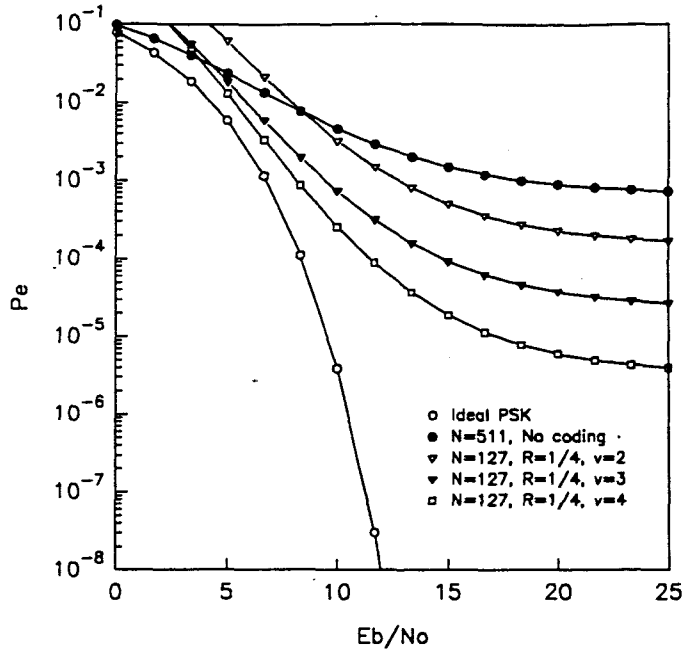

Figure 5.5: Convolutional coded CPSK performance, $K = 150$

fair to compare these codes to each other (different complexity) it is nevertheless instructive to know what is achievable in practice.

Tables 5.3, 5.4 and 5.5 summarise the capacity for a convolutional coded system, where K is tabulated and again compared under equitable conditions. Even for $N = 31$ low rate coding allows for the highest capacity.

	$N = 255$	$N = 127, R_{cd} = 1/2$				$N = 63, R_{cd} = 1/4$			$N = 31, R_{cd} = 1/8$		
	No Coding	ν				ν			ν		
P_e		2	3	4	6	2	3	4	2	3	4
10^{-3}	76	96	103	112	130	90	113	127	99	110	132
10^{-5}	40	56	61	70	96	52	64	78	57	66	79
10^{-8}	22	35	36	44	54	30	37	47	33	40	48

Table 5.3: K for convolutional coded CPSK, $E_b/N_0 = 20$ dB

To highlight the main results of this section; for **coherent PSK** low rate **convolutional** coding is very effective to increase system performance and capacity. In the following sections it is shown that this is not necessarily the case when block coding and/or DPSK as modulation scheme are considered.

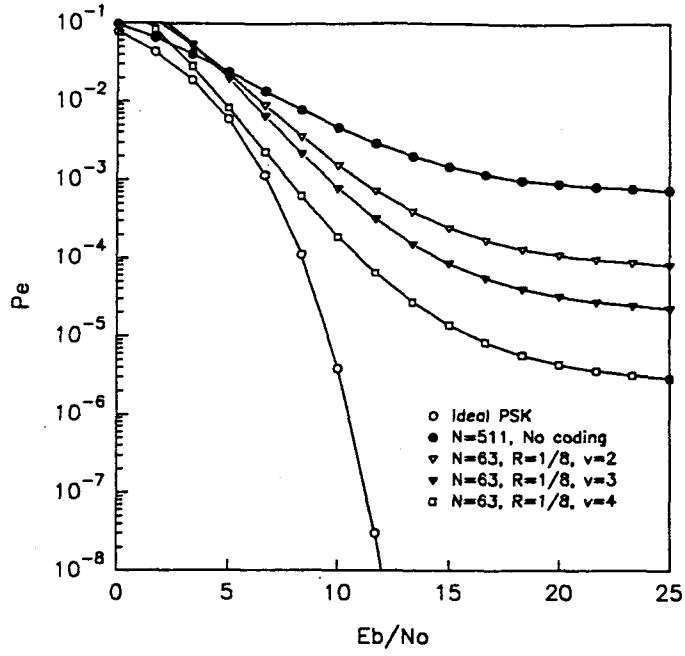

Figure 5.6: Convolutional coded CPSK performance, $K = 150$

	$N = 127$ No Coding	$N = 63, R_{cd} = 1/2$				$N = 31, R_{cd} = 1/4$		
		ν				ν		
P_e		2	3	4	6	2	3	4
10^{-3}	38	47	51	55	64	44	56	63
10^{-5}	19	28	30	35	41	26	32	38
10^{-8}	10	16	17	21	26	14	18	23

Table 5.4: K for convolutional coded CPSK, $E_b/N_0 = 20$ dB

5.1.3 CPSK BCH Block Coding

We will assume that a block code, with parameters (n, k, t), has code rate $R_{cd} = k/n$ and can correct t or fewer errors, with generator polynomials chosen from [97] and presented in Appendix C.

The block codes for performance evaluation are chosen in such a way as to have comparable minimum distance when compared to the convolutional codes in the previous section. Unfortunately it is not completely possible since there are no known block codes with exactly the same minimum distance parameters as convolutional codes, but the closest possible codes are chosen.

Further, the code rates of block codes are not exactly the same as convolutional codes. For example, the Hamming code considered has rate $R_{cd} = 4/7 \approx 1/2$. We will assume that the fractional

	$N = 63$ No Coding	$N = 31, R_{cd} = 1/2$			
		ν			
P_e		2	3	4	6
10^{-3}	19	17	25	27	31
10^{-5}	9	13	14	17	20
10^{-8}	5	7	8	10	12

Table 5.5: K for convolutional coded CPSK, $E_b/N_0 = 20$ dB

difference in rate is insignificant.

Again, as in the previous section, performance and capacity is compared on an equitable base.

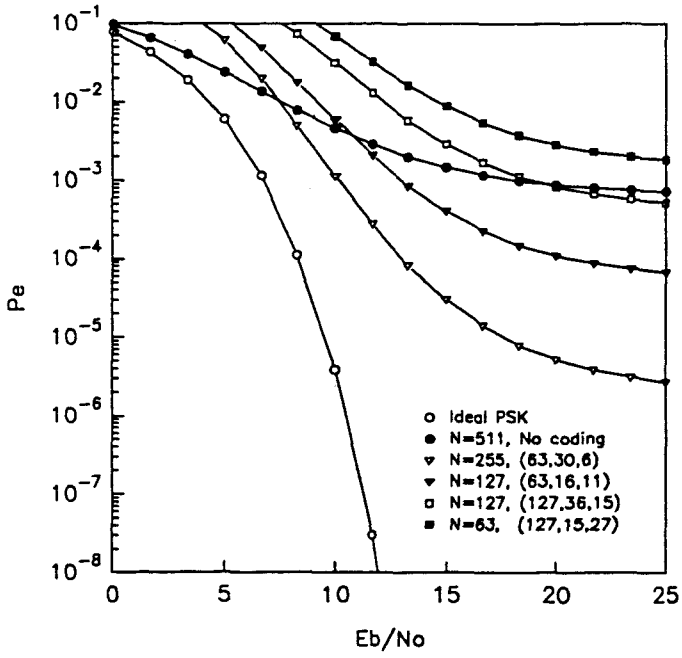

Figure 5.7: Block coded CPSK performance, $K = 150$

We begin our SSMA block code investigation by considering the performance of low rate coding. As before we investigate rate $R_{cd} \approx 1/2, 1/4$ and $1/8$ codes. Figure 5.7 depicts the error rate performance for low rate block codes with $K = 150$. Also indicated in the figure, for reference purposes, is ideal CPSK and the uncoded performance for $N = 511$. Here we note that low rate block coding **degrades** the overall system performance. Even for the BCH (127,15,27) code which can correct 27 or fewer errors; in fact the performance for this code is worse than the uncoded case (at relatively high error rates). It is evident that the rate $R_{cd} \approx 1/2$ code has the best overall performance. This observation is significantly different from low rate convolutional codes and is also consistent with non-spread spectrum systems [96]. It has been shown that a relatively broad

maximum of coding gain versus code rate for fixed n occurs roughly between $1/3 \leq R_{cd} \leq 3/4$ for BCH codes when non-spread spectrum systems are considered.

	$N = 511$	$N = 255$	$N = 127$		$N = 63$
	No Coding	$R_{cd} = 1/2$	$R_{cd} = 1/4$		$R_{cd} = 1/8$
P_e		$(63, 30, 6)$	$(63, 16, 11)$	$(127, 36, 15)$	$(127, 15, 27)$
10^{-3}	152	218	179	151	137
10^{-5}	77	155	127	116	103
10^{-8}	41	109	90	89	77

Table 5.6: K for block coded CPSK, $E_b/N_0 = 20$ dB

Table 5.6 quantifies the low rate coded capacity, again at $E_b/N_0 = 20$ dB. From this we see that a rate $R_{cd} \approx 1/8$ code manifests a capacity decrease, relative to the uncoded case, of approximately 10% at an error rate of 10^{-3}, while at 10^{-8} an increase of 46% is realised. Considering a moderate length, rate $R_{cd} \approx 1/2$ code, at 10^{-3} error rate the capacity increase is 30% and at an error rate of 10^{-8} the increase is 62%, which is substantially more than the low rate coded case.

Also interesting to note is that the less complex (63,16,11) code performs better than the (127,36,15) code (both rate $R_{cd} \approx 1/4$), but both perform worse than the rate $R_{cd} \approx 1/2$ code. We will now consider the performance and capacity of more complex rate $R_{cd} \approx 1/2$ codes.

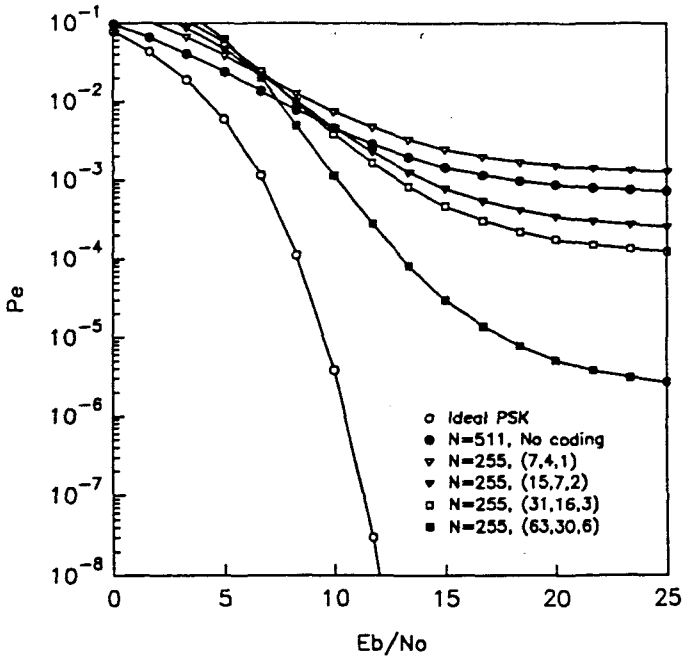

Figure 5.8: Block coded CPSK performance, $K = 150$

Figure 5.8 illustrates the performance of four half rate block codes of relatively low complexity

($K = 150$). An unacceptable situation for speech can be rescued by a (63,30,6) code. Also indicated in this figure is the bad performance of the (7,4,1) code relative to the uncoded case. This observation is consistent even at low error rates, as indicated in Tables 5.7, 5.8, 5.9 and 5.10. Also indicated in these tables are the capacity for the half rate block codes for different spreading sequence lengths.

	$N = 511$	$N = 255, R_{cd} = 1/2$			
P_e	No Coding	$(7,4,1)$	$(15,7,2)$	$(31,16,3)$	$(63,30,6)$
10^{-3}	152	136	172	179	218
10^{-5}	77	73	101	116	155
10^{-8}	41	41	60	74	109

Table 5.7: K for block coded CPSK, $E_b/N_0 = 20$ dB

	$N = 255$	$N = 127, R_{cd} = 1/2$			
P_e	No Coding	$(7,4,1)$	$(15,7,2)$	$(31,16,3)$	$(63,30,6)$
10^{-3}	76	69	86	90	109
10^{-5}	39	37	51	58	78
10^{-8}	21	21	30	37	55

Table 5.8: K for block coded CPSK, $E_b/N_0 = 20$ dB

	$N = 127$	$N = 63, R_{cd} = 1/2$			
P_e	No Coding	$(7,4,1)$	$(15,7,2)$	$(31,16,3)$	$(63,30,6)$
10^{-3}	38	35	43	45	55
10^{-5}	19	19	25	29	39
10^{-8}	10	11	15	19	27

Table 5.9: K for block coded CPSK, $E_b/N_0 = 20$ dB

5.2 DPSK Performance

As with coherent PSK modulation, we first investigate the uncoded DPSK performance, followed by convolutional- and block coded performance.

5.2.1 Uncoded DPSK

Figure 5.9 depicts the average error rate as function of signal-to-noise ratio for $K = 10$ and different values of N. As in the CPSK case, we note the saturating error rate, with increasingly unacceptable performance as N decreases. Naturally with noncoherent detection one has inherently less gain available, resulting in higher saturation of error rates. By comparison, for $N = 63$, DPSK signalling saturates at an average error rate of almost an order of magnitude higher than CPSK.

	$N = 63$	$N = 31, R_{cd} = 1/2$			
P_e	No Coding	$(7,4,1)$	$(15,7,2)$	$(31,16,3)$	$(63,30,6)$
10^{-3}	19	17	21	22	27
10^{-5}	9	9	12	15	19
10^{-8}	5	5	8	10	14

Table 5.10: K for block coded CPSK, $E_b/N_0 = 20$ dB

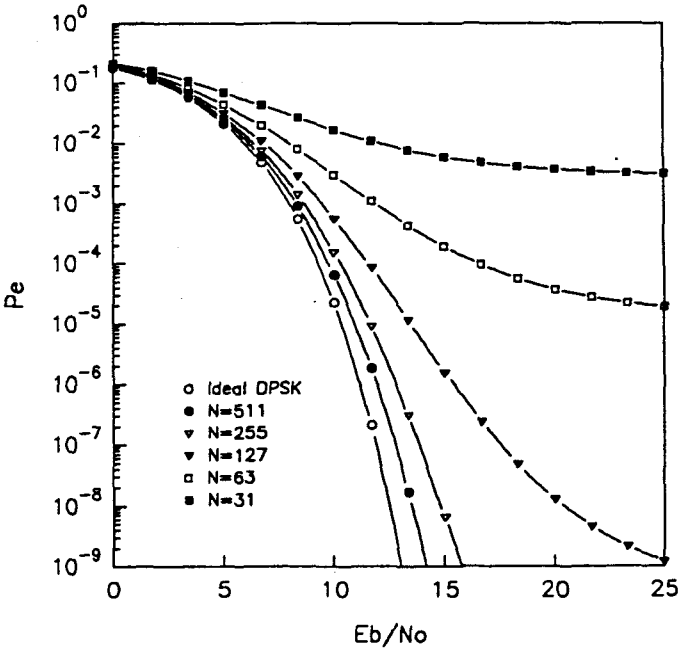

Figure 5.9: Uncoded DPSK performance, $K = 10$

Table 5.11 tabulates the capacity of an uncoded DPSK system for different values of average error rate ($E_b/N_0 = 20$ dB). Comparing Tables 5.11 and 5.1 we notice that at low error rates, i.e. 10^{-8}, the capacity for DPSK signalling is not significantly less than for CPSK. However, at high error rates, i.e. 10^{-3}, the capacity difference is in the order of 32% less with DPSK signalling.

It is thus evident that there is an interesting trade-off between CPSK and DPSK. Since systems are normally designed to operate at low error rates, DPSK as modulation scheme, due to its lower complexity, must definitely be considered. However, as mentioned earlier, the uncoded capacity of SSMA is very low when compared to other multiple access techniques. In the last section of this chapter it is shown that a multiple cell architecture can allow for acceptable uncoded SSMA performance, be that CPSK or DPSK.

P_e	$N = 511$	$N = 255$	$N = 127$	$N = 63$	$N = 31$
10^{-3}	115	57	28	14	6
10^{-5}	63	32	16	8	4
10^{-8}	36	18	9	4	2

Table 5.11: K for uncoded DPSK signalling, $E_b/N_0 = 20$ dB

5.2.2 DPSK Convolutional Coding

The same convolutional codes used in the CPSK case are considered, again under equal complexity and throughput conditions.

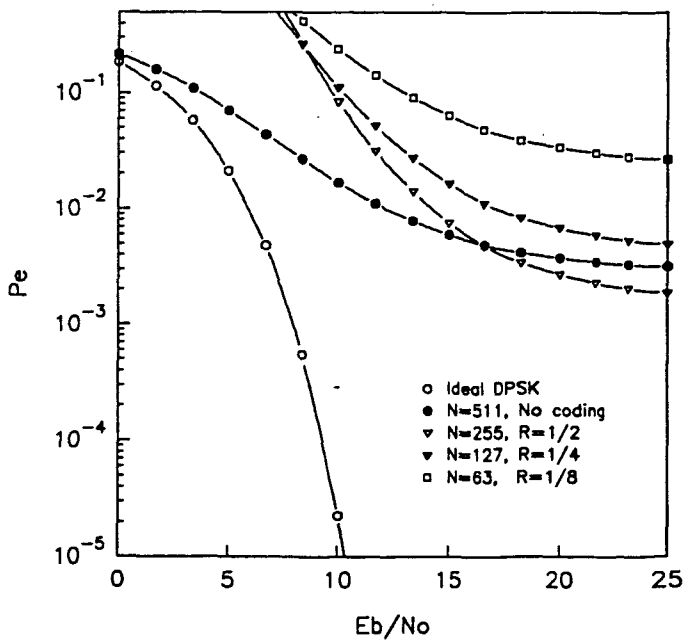

Figure 5.10: Convolutional coded DPSK performance, $K = 150$

Figures 5.10 and 5.11 indicate the performance of low rate convolutional coding when noncoherent detection is considered. In contrast to CPSK, half rate coding is optimum. Figure 5.10 indicates that at high error rates, low rate coding is even worse than the uncoded case. At low error rates, Figure 5.11, low rate coding performs better than the uncoded case, but the curves for $R_{cd} = 1/4$ and $1/8$ are uniformly worse than for the half rate code.

This behaviour is significantly different from that observed with CPSK because of the noncoherent combining loss which increases with the code free distance. A coherent modulator is able to utilise the additional code free distance more efficiently, and these characteristics is not observed. These

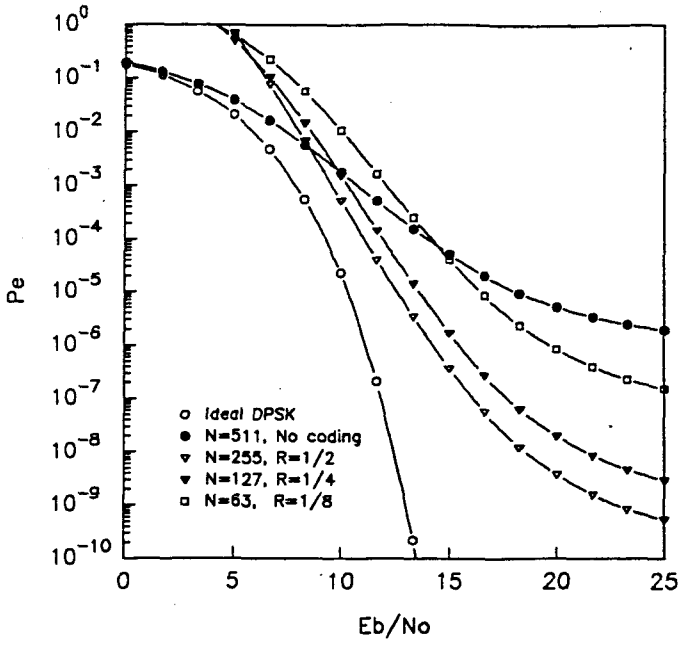

Figure 5.11: Convolutional coded DPSK performance, $K = 60$

observations are also consistent with non-spread spectrum systems [96, 97].

	$N = 511$	$N = 255, R_{cd} = 1/2$				$N = 127, R_{cd} = 1/4$			$N = 63, R_{cd} = 1/8$		
	No Coding	ν				ν			ν		
P_e		2	3	4	6	2	3	4	2	3	4
10^{-3}	115	120	128	135	152	95	112	122	81	87	98
10^{-5}	63	78	84	94	109	62	74	85	54	60	69
10^{-8}	36	49	52	62	75	39	47	57	36	41	48

Table 5.12: K for convolutional coded DPSK, $E_b/N_0 = 20$ dB

Table 5.12 quantifies the convolutional coded performance. At 10^{-5} the commercially available, half rate, $\nu = 6$ code delivers a capacity increase of 73%, while the lower rate codes deliver a constantly worse performance as the code rate is lowered.

Comparing the Tables 5.12 and 5.2 we recognise that coding accentuates the small capacity difference present in the uncoded case. For the half rate, $\nu = 6$ code the DPSK capacity is 56% worse than the corresponding CPSK case at 10^{-5}.

Figure 5.12 depicts convolutionally coded, half rate performance with constrained lengths $\nu = 2, 3, 4$ and 6. As intuitively expected the constrained length $\nu = 6$ code performs best. Table 5.13 quantifies the capacity for half rate convolutional coding for different values of N and ν.

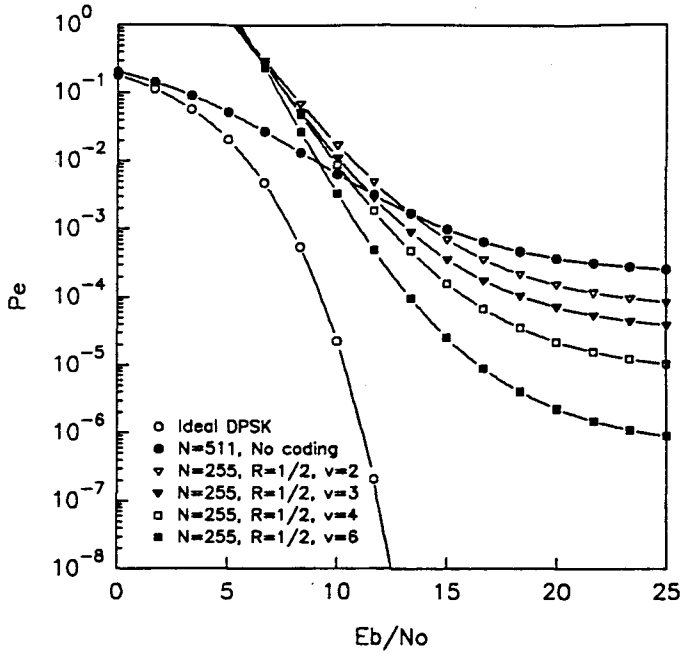

Figure 5.12: Convolutional coded DPSK performance, $K = 100$

	$N = 127, R_{cd} = 1/2$				$N = 63, R_{cd} = 1/2$				$N = 31, R_{cd} = 1/2$			
	ν				ν				ν			
P_e	2	3	4	6	2	3	4	6	2	3	4	6
10^{-3}	59	64	67	75	29	31	33	37	14	15	16	18
10^{-5}	39	42	47	54	19	21	23	27	9	10	11	13
10^{-8}	24	26	31	37	12	13	15	18	6	6	7	9

Table 5.13: K for block coded DPSK, $E_b/N_0 = 20$ dB

It is interesting to note that the linearity observed for the uncoded case is maintained under coded conditions. For example, from Table 5.13, changing N by 50% (i.e. $N = 127$ to $N = 63$) the capacity is also changed by 50%.

5.2.3 DPSK BCH Block Coding

The block codes evaluated in this section is the same as in Section 5.1.3. As in the CPSK case, low rate BCH codes perform uniformly worse than half rate codes, as illustrated in Figure 5.13 and Table 5.14. The low rate block coded performance is notably worse than even the uncoded case. To quantify, the $R_{cd} = 1/8$ code performance is 21% worse than the uncoded case, while the half rate (63,30,6) code realises a capacity increase of 62% at an error rate of 10^{-5}.

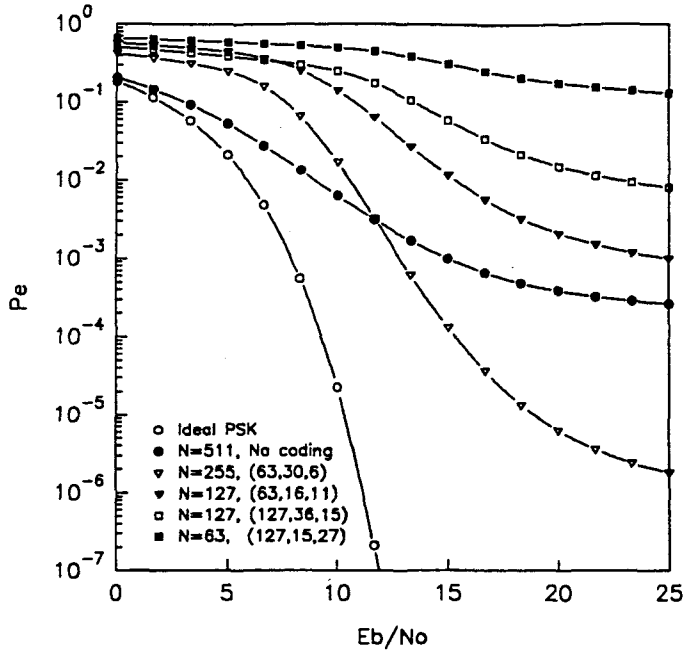

Figure 5.13: Block coded DPSK performance, $K = 100$

	$N = 511$	$N = 255$	$N = 127$		$N = 63$
	No Coding	$R_{cd} = 1/2$	$R_{cd} = 1/4$		$R_{cd} = 1/8$
P_e		$(63, 30, 6)$	$(63, 16, 11)$	$(127, 36, 15)$	$(127, 15, 27)$
10^{-3}	115	133	94	84	61
10^{-5}	63	102	73	69	50
10^{-8}	36	76	55	56	40

Table 5.14: K for block coded DPSK, $E_b/N_0 = 20$ dB

Table 5.14 summarises the performance of the low rate block codes. As in the CPSK case the (7,4,1) block code performs worse than the uncoded case (Figure 5.14 and Tables 5.15, 5.16, 5.17 and 5.18), and consequently block codes with more error correcting power has to be used to improve the SSMA capacity. Figure 5.14 and Table 5.15 also indicate the performance for other half rate block codes.

Comparing the DPSK and CPSK performance we realise that for a moderate complexity code, like the half rate (63,30,6) code, the capacity decrease due to noncoherent detection is approximately 34% at an error rate of 10^{-5}.

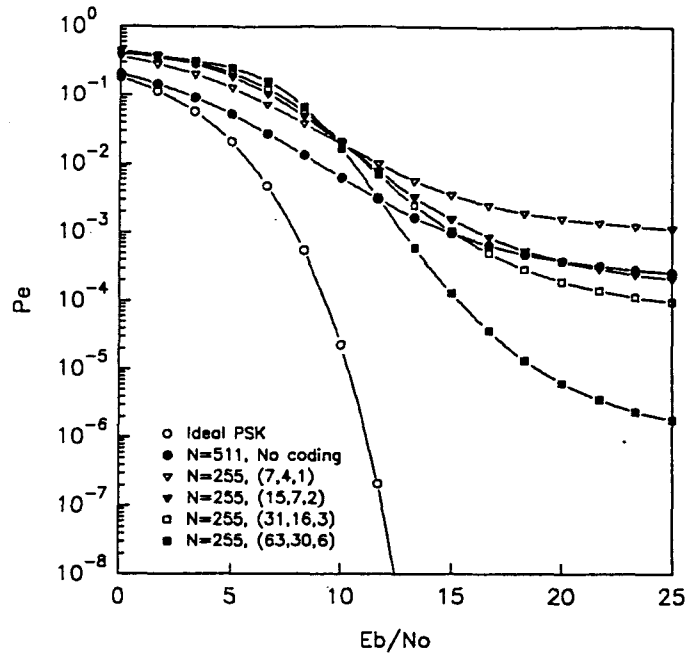

Figure 5.14: Block coded DPSK performance, $K = 100$

	$N = 511$	$N = 255, R_{cd} = 1/2$			
P_e	No Coding	$(7,4,1)$	$(15,7,2)$	$(31,16,3)$	$(63,30,6)$
10^{-3}	115	93	111	115	133
10^{-5}	63	56	72	81	102
10^{-8}	36	34	46	56	76

Table 5.15: K for block coded DPSK, $E_b/N_0 = 20$ dB

5.3 Conclusions

Results have been presented to determine the capacity of a SSMA system under AWGN conditions, that is when the Nakagami parameter $m \to \infty$. The results indicate that a SSMA system without coding is not very bandwidth efficient. The coded results verify and quantify the viewpoint by Viterbi on the subject of combined coding and SSMA [68, 69]. In these articles Viterbi makes the claim that very low rate coding and spread spectrum signalling provides optimum system capacity. It has been shown that with CPSK with convolutional coding this is indeed correct. However, when noncoherent detection, or block coding is used this statement is incorrect. It is now shown that by improved system architecture the SSMA capacity can be further enhanced.

As mentioned earlier, K is the maximum interference that the cellular system can tolerate. For the moment let us consider one cell with no cell splitting or voice activity factor, that is (2.2) reduces

P_e	$N = 255$ No Coding	$N = 127, R_{cd} = 1/2$ (7,4,1)	(15,7,2)	(31,16,3)	(63,30,6)
10^{-3}	57	47	55	58	67
10^{-5}	32	28	36	40	51
10^{-8}	18	17	23	28	38

Table 5.16: K for block coded DPSK, $E_b/N_0 = 20$ dB

P_e	$N = 127$ No Coding	$N = 63, R_{cd} = 1/2$ (7,4,1)	(15,7,2)	(31,16,3)	(63,30,6)
10^{-3}	28	23	28	29	33
10^{-5}	16	14	18	20	26
10^{-8}	9	9	12	14	19

Table 5.17: K for block coded DPSK, $E_b/N_0 = 20$ dB

to $K = K'$. In other words all the tables and figures presented are valid for a one cell system. Since no voice activity factor is included K also signifies the capacity for a data communication channel.

As a specific example, if data is transmitted at 64 kbps and $N = 511$ is assumed with CPSK as modulation scheme the system can support only 77 channels (Table 5.1) at $P_e = 10^{-5}$ with an RF bandwidth in excess of 32 MHz. If a half rate, constrained length $\nu = 6$ convolutional code is used the capacity is increased by 120% to 170 channels. Even when coding is considered, it is quite clear that the system capacity is relatively low.

Considering a cellular system with $N_{sect} = 3$, (2.2) can be written as $K' = \frac{3K}{1.5}$ users/cell. (Since **data** transmission is considered the voice activity factor $V_{on} = 1$.) It is clear that a cellular architecture almost doubles the SSMA capacity. Therefore, convolutional coding together with a cellular architecture can increase **data** communication system capacity by almost 340% - a substantial increase.

However, the most substantial increase is obtained when speech is transmitted. Consider again a cellular system, (2.2) can be written as $K' = \frac{8K}{1.5}$ users/cell which includes voice activity monitoring and cell splitting. We notice that a capacity increase of roughly five times can be gained by an enhanced system architecture. Returning to our previous example ($N = 511$ with convolutional coding), instead of 77 users the system can now support 906 users/cell - a massive increase of

P_e	$N = 63$ No Coding	$N = 31, R_{cd} = 1/2$ (7,4,1)	(15,7,2)	(31,16,3)	(63,30,6)
10^{-3}	14	12	14	14	17
10^{-5}	8	7	9	10	13
10^{-8}	4	4	6	7	9

Table 5.18: K for block coded DPSK, $E_b/N_0 = 20$ dB

1077%! It must be stressed that TDMA system capacity cannot be increased in this manner - this is a unique feature of SSMA.

An additional advantage to be gained from a SSMA system is that virtually a whole country can be covered by one frequency band, provided a large enough family of spreading codes is available.

Since actual spreading code cross-correlation parameters and realisable error control coders are considered, a practical system in a cellular set-up, will have capacity very close to the figures mentioned in the presented tables. A typical application of these results would be to predict the performance and/or capacity of a stationary cellular system, of which a stationary IWC network (under certain conditions), or a rural telephone system are typical examples.

It is apparent that the DPSK capacity is lower than CPSK capacity. To rectify this discrepancy in a cellular system, the uplink will need a more powerful error control code. Further, since DPSK errors often occur in pairs due to the differential encoding process, a two bit interleaver is also required in the uplink.

CHAPTER 6

CPSK PERFORMANCE RESULTS IN A NAKAGAMI FADING CHANNEL

This chapter presents performance results and capacity assessments of coherent PSK in the presence of impairments due to AWGN, IUI and Nakagami fading. The performance of a non- diversity matched filter receiver and diversity receiver structures are considered. Distinct forms of diversity, RAKE reception, error control coding and a combination of the two techniques are considered as means to enhance and increase system performance and capacity. Specifically, where error control coding is considered, convolutional- and block coding are investigated.

As explained in Section 2.1.3, length $N = 511$ spreading codes are assumed due to the channel delay spread of an IWC channel.

To set a potential scenario for our calculations, the following can be hypothesised: All the desired signals arriving at the mobile are received via Nakagami distributed random gains, with only the desired signal arriving via L-paths. This is a scenario in which the transmitter terminals are mobile and multipath gains are Nakagami with respect to geographical position of the terminals.

For the above scenario the maximum K for the parameters L, P and m are determined for $N = 511$, and it is therefore possible to determine the capacity for a fixed average error rate.

The average path strengths of the interfering users are arbitrarily adopted as $\Omega = -10$ dB. With $\Omega = 0.1$, the Nakagami pdf is reduced to a one-parameter distribution so that all of the results can be expressed in terms of the single parameter m. To investigate the influence of the Nakagami parameter m, five values are investigated $m = \{1/2, 1, 2, 3, 5\}$, with $m = 1$ being Rayleigh fading - the results for CPSK are as indicated in section 5.1.

Section 6.1 describes the performance under this conditions without any diversity, while Section

6.2 investigates the influence of RAKE reception on the performance and capacity of the proposed system. In Section 6.3 the performance of convolutional and block coding are investigated. It is shown in Section 6.4 that a combination of error control coding and RAKE reception is most effective in increasing system performance and capacity.

6.1 Non-diversity Performance

Figure 6.1 depicts the average probability of error as function of unfaded signal-to-noise ratio for different values of the Nakagami fading parameter, m, over a single path ($L = 1$) - the faded and unfaded signal-to-noise ratio is related by equation (3.20). Gold spreading sequences of length $N = 511$ chips are employed by the users for reasons explained in Chapter 2.

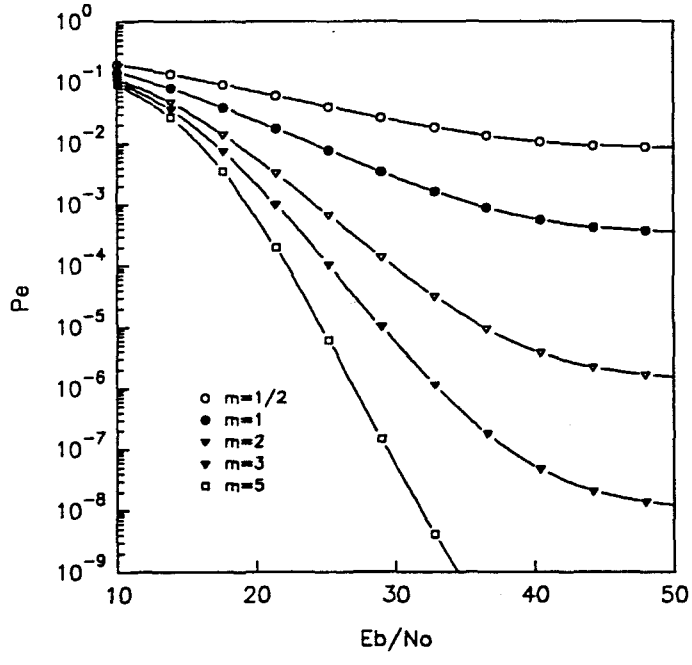

Figure 6.1: Nakagami faded CPSK performance: $K = 2$, $L = 1$ and $N = 511$

Performance curves are plotted for $m = \{\frac{1}{2}, 1, 2, 3, 5\}$ and $K = 2$. Since the $m = 1$ case corresponds to Rayleigh fading, it can be used for benchmark purposes and it is clear that for $K = 2$ the average error rate saturates at approximately 10^{-3}. This result is in agreement with that of Turin [23] in a non-cellular system. For $m = \frac{1}{2}$, severest fading, the performance for as little as two users is very poor and saturates at roughly 10^{-2}. As the amount of fading decreases, the error rate progressively improves.

The influence of an increase to $K = 5$ over a single path ($L = 1$) is depicted in Figure 6.2 - only $m > 1$ allows for an error rate of less than 10^{-3}. It is also clear that as m increases, the performance converge relatively fast to the non- faded ($m = \infty$) case described in Section 5.1.

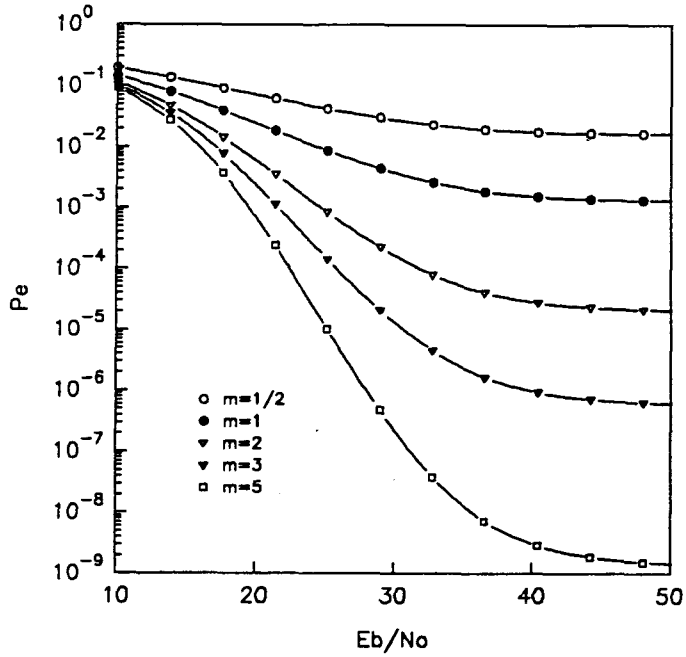

Figure 6.2: Nakagami faded CPSK performance: $K = 5$, $L = 1$ and $N = 511$

The influence of $L = 5$ is depicted in Figures 6.3 and 6.4 for $K = 2$ and $K = 5$ respectively. For low values of m, that is strong fading, the influence of an extra path does not have a great effect, while this effect is more pronounced as m decreases - for $m = \{3, 5\}$ the average error rate decreases roughly by two orders of magnitude.

From the preceding graphs, it is clear that the performance with $N = 511$ and low values of m is not very promising. In fact for $m = \frac{1}{2}$ the system fails as a multiple access system, while for $m = 1$ the system can support at most four users. To increase the processing gain is in general not a viable option in most applications because of bandwidth constraints and therefore processing gain can not readily be used to increase system capacity. However, as in the $m = \infty$ case, linearity is maintained - increasing, or decreasing the processing gain respectively increases or decreases the capacity proportionally.

Evidently, the finite cross correlation among codes, although small in magnitude, can cause co-channel interference limitation due to the Nakagami fading nature of the environment. Therefore, as the thermal noise tends to zero, the average error probability saturates to an unacceptable value, especially for low values of m.

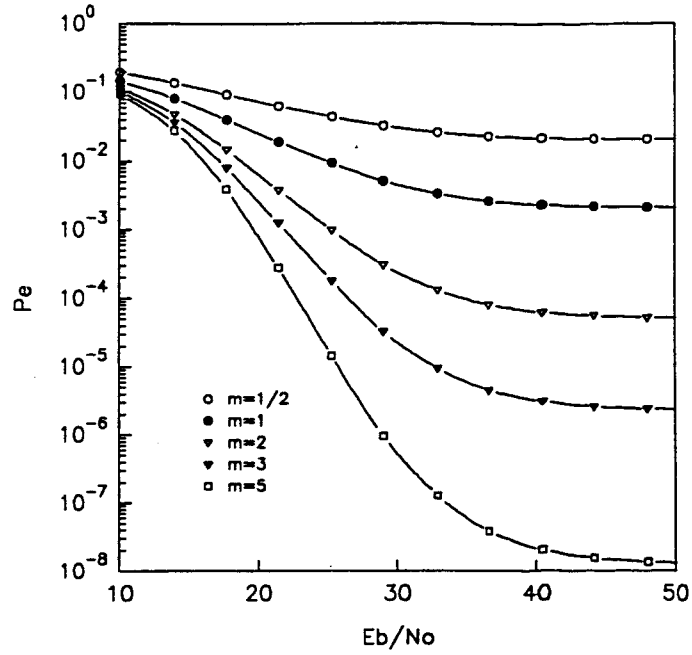

Figure 6.3: Nakagami faded CPSK performance: $K = 2$, $L = 5$ and $N = 511$

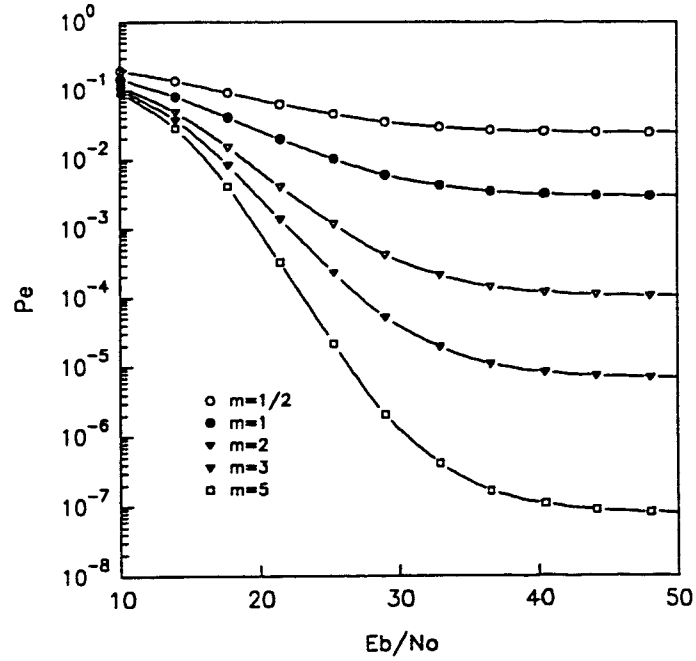

Figure 6.4: Nakagami faded CPSK performance: $K = 5$, $L = 5$ and $N = 511$

Table 6.1 quantifies the capacity for $m = \{\frac{1}{2}, 1, 2, 3, 5, \infty\}$. As mentioned earlier, for $m = \frac{1}{2}$, a SSMA system fails as a multiple access system at a reasonable error rate. This is also the case for $m = 1$ if the number of multiple paths is $L > 5$.

For the sake of clarity, the values of K for $m = \infty$ are replicated from Section 5.1. It is clear that the capacity converges fast to the $m = \infty$ case. For $m = 5$ the capacity is already 70% of the maximum value. Figure 6.5 indicates the convergence of K as a function of m graphically.

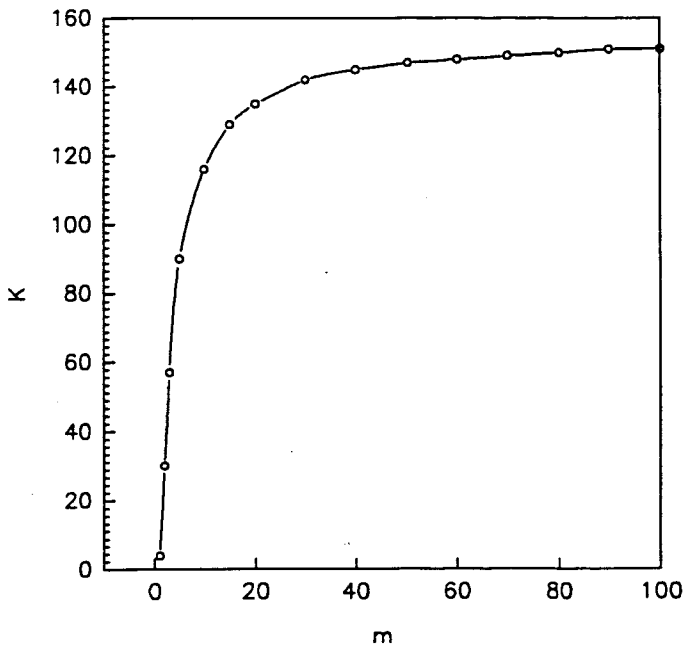

Figure 6.5: K as a function of the Nakagami fading parameter m: $P = 1$, $L = 1$ and $P_e = 10^{-3}$

As in Chapter 5 the values indicated in Table 6.1 are the maximum interference our SSMA system can support. Therefore, to calculate the capacity of the cellular system described in Chapter 2, equation (2.2) can be used. When voice activity monitoring and cell splitting are introduced, an increase by a factor of roughly five is possible.

From the preceding results, it can be observed that a simple correlation receiver that is not equipped with any diversity means (RAKE reception and/or error control coding) exhibits poor performance for the Gold sequences adopted in this work. Needless to say, the ideal performance of a receiver in the absence of any multiple access interference - but with a single Nakagami faded path - is poor to begin with [39]. Evidently, to increase the capacity some forms of diversity are needed, which is the subject of the following sections.

	P_e	$L=1$	$L=5$	$L=10$
$m=1/2$	10^{-3}	-	-	-
$m=1$	10^{-3}	4	-	-
$m=2$	10^{-3}	30	25	18
	10^{-5}	3	-	-
$m=3$	10^{-3}	57	52	45
	10^{-5}	11	6	-
$m=5$	10^{-3}	90	84	76
	10^{-5}	27	22	16
	10^{-8}	7	-	-
$m=\infty$	10^{-3}	152	-	-
	10^{-5}	77	-	-
	10^{-8}	41	-	-

Table 6.1: K for non-diversity CPSK: $E_b/N_0 = 60$ dB, $P = 1$ and $L = \{1, 5, 10\}$

6.2 RAKE Reception Performance

In a multiple access environment when a transmitter and a receiver are communicating, as soon as a second transmitted signal comes on the air, the Nakagami faded path between the interfering transmitter and the desired receiver can be stronger than the one between this receiver and the desired transmitter. This creates a near-far situation owing to the Nakagami fading channel model, resulting in a low capacity as indicated in the previous section. Using a RAKE receiver enables us to receive all channels at approximately equal strength and therefore increasing the performance substantially.

Figure 6.6 indicates the performance of a 3 path ($L = 3$) system, with $K = 30$ and $N = 511$ with a three tap, $P = 3$, RAKE receiver. It is evident that the performance improvement is quite significant. Even for $m = \frac{1}{2}$ the performance for $K = 30$ is acceptable.

Figures 6.7 to 6.11 depict the performance of the RAKE receiver as a function of the multipath parameter, L, and average error rate for different values of m. As expected, the performance is greatly improved by the number of taps in the RAKE receiver. Even a small amount of multipath diversity improves the performance significantly, provided that the channel has the right amount of dispersion. However, if the channel consists of a single faded path or is very dispersive, then the performance can be severely degraded because of the lack of diversity or the increased IUI , respectively.

An interesting point to note, is that an increase in the number of multipaths, that is an increase in L, results in a linear increase in average error rate. Intuitively, this is what can be expected, since receiving a spread spectrum signal through multiple paths, when the delay is larger than the chipping period, and due to the correlation process, a multipath ray can be viewed as an additional

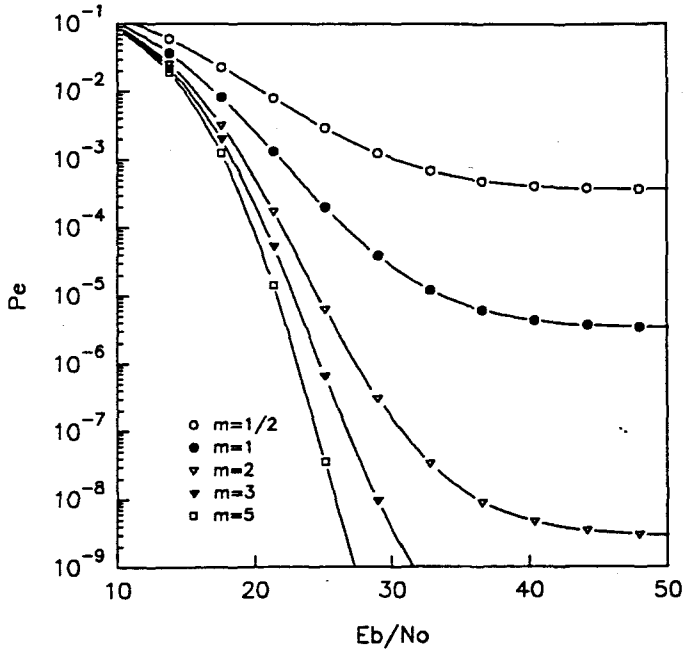

Figure 6.6: Nakagami faded CPSK performance: $K = 30$, $P = 3$, $L = 3$, and $N = 511$

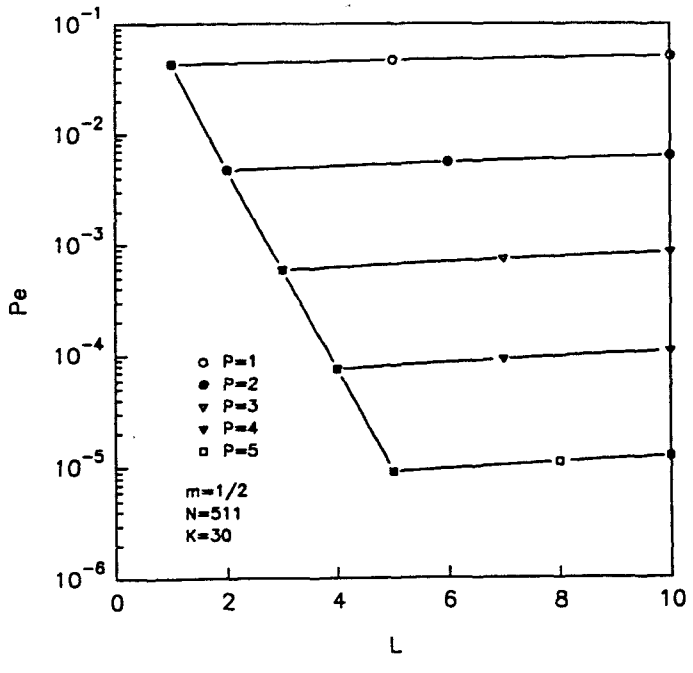

Figure 6.7: Average error rate as a function of the number of channel paths: $m = \frac{1}{2}$, $K = 30$ and $N = 511$

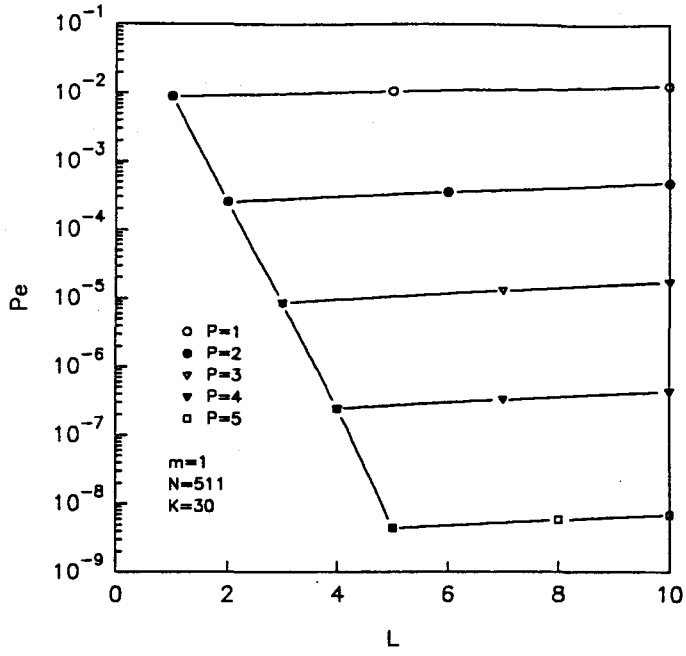

Figure 6.8: Average error rate as a function of the number of channel paths: $m = 1$, $K = 30$ and $N = 511$

user in the system. When adding users to the system the decrease in average error rate is linear, as indicated in the previous chapter and [11]. This is due to the approximate Gaussian nature of the IUI.

Table 6.2 tabulates the capacity of a RAKE received signal for various values of L, P and m. Comparing these results with Table 6.1, it is interesting to note that for relatively low values of P (and consequently low receiver complexity) and $m = \frac{1}{2}$ the system can operate as a multiple access scheme at an acceptable average error rate. Increasing P and m result in a massive increase in capacity. For example, at $m = 5$, $P = 5$ an increase of 840% over the $m = 5$, $P = 1$ case can be realised.

Figure 6.12 indicates the increase in K as P increases for different values of m. This graph, together with Table 6.2, can be used very productively. For instance, extrapolating the data can give a rough estimate of the capacity for higher values of P and m.

Figure 6.13 indicates K as a function of m and P at $\frac{E_b}{N_0} = 60$ dB. The increase in K as P and m increases is notable and tends to saturate at roughly 1000.

In this section it was shown that RAKE reception can be used with great success to increase the SSMA system capacity. In the next section the influence of error control coding as form of diversity

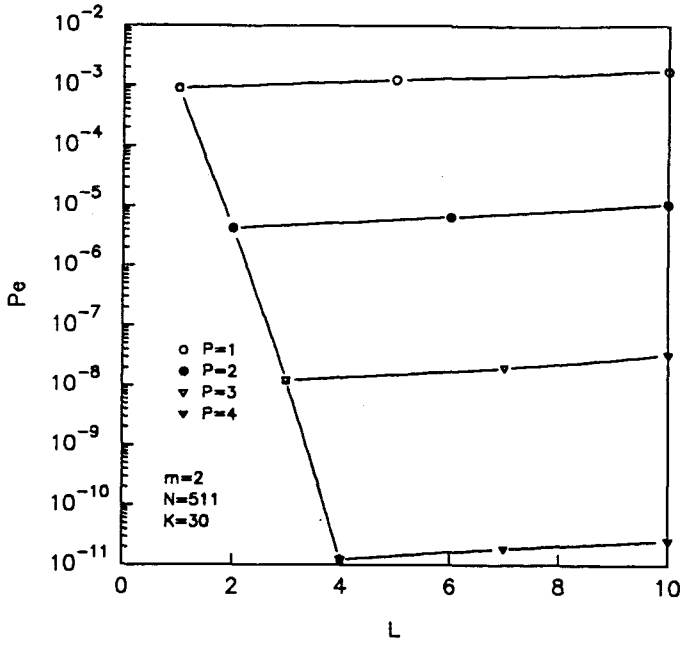

Figure 6.9: Average error rate as a function of the number of channel paths: $m = 2$, $K = 30$ and $N = 511$

	P_e	$P = 2$	$P = 3$	$P = 4$	$P = 5$
$m = 1/2$	10^{-3}	5	7	115	215
	10^{-5}	-	-	8	27
$m = 1$	10^{-3}	59	167	298	440
	10^{-5}	5	30	74	130
	10^{-8}	-	-	9	25
$m = 2$	10^{-3}	150	295	447	601
	10^{-5}	38	98	169	244
	10^{-8}	6	25	55	91
$m = 3$	10^{-3}	191	350	505	662
	10^{-5}	66	138	215	294
	10^{-8}	17	49	87	129
$m = 5$	10^{-3}	242	398	556	714
	10^{-5}	99	177	258	340
	10^{-8}	37	78	122	167

Table 6.2: K for RAKE received CPSK: $E_b/N_0 = 60$ dB, $P = \{2,3,4,5\}$ and $L = \{2,3,4,5\}$

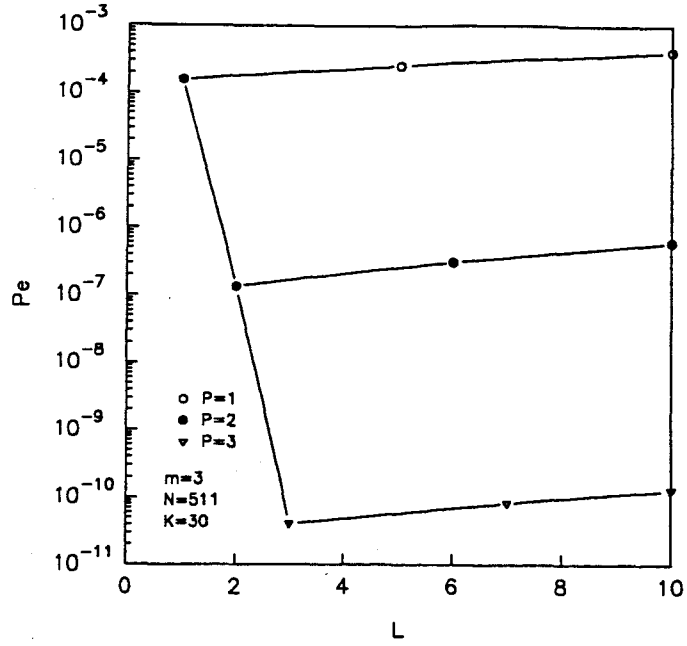

Figure 6.10: Average error rate as a function of the number of channel paths: $m = 3$, $K = 30$ and $N = 511$

is investigated.

6.3 Error Control Coded Performance

Up to this point it was shown that RAKE reception as form of diversity is very effective in overcoming the detrimental effects caused by the time-varying dispersive characteristics of the Nakagami channel. In general time and/or frequency diversity techniques may be viewed as a form of repetition coding of the information sequence. From this point of view, the combining technique in a RAKE receiver represents decoding of the repetition code. Since a repetition code is a trivial form of coding, let us consider the additional benefits derived from more efficient types of codes. In particular, it is demonstrated that coding provides an efficient means for obtaining diversity on a fading channel. With a SSMA system this additional advantage can be obtained with no additional penalty paid in bandwidth, therefore making it a very attractive and viable option. As intuitively expected the amount of diversity provided by a code is directly related to its minimum distance.

Frequency diversity is obtained by transmitting the signal components carrying the same information in multiple frequency slots mutually separated by an amount at least equal to the coherence bandwidth $(\Delta f)_c$ of the channel. Thus the signal components carrying the same information un-

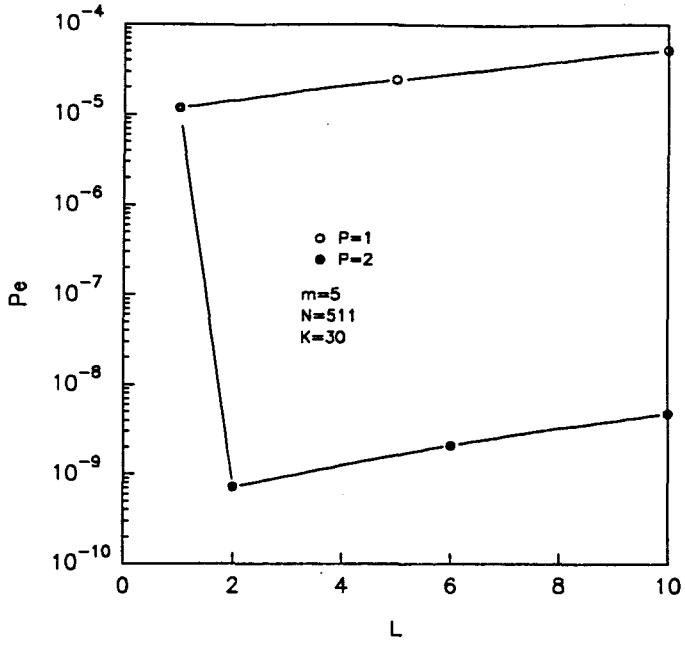

Figure 6.11: Average error rate as a function of the number of channel paths: $m = 5$, $K = 30$ and $N = 511$

dergo statistically independent fading.

To extend this notation to coded information sequences, it is simply required that the signal waveform corresponds to a particular code bit or code symbol fades independently from one signal waveform corresponding to any other code bit or code symbol. This requirement may result in inefficient utilization of the available time-frequency space, with the existence of large unused portions in this two dimensional signal space. To reduce the inefficiency, a number of code words may be interleaved either in time or in frequency or both, in such a manner that the waveforms corresponding to the bits or symbols of a given code word fade independently. Thus we assume that the time-frequency signalling space is partitioned into non- overlapping time-frequency cells. A signal waveform corresponding to a code bit or code symbol is transmitted within such a cell.

In addition to the assumption of statistically independent fading of the signal component of a given code word, it is also assumed that the additive noise components corrupting the received signals are white Gaussian noise processes together with the IUI which are statistically independent and identically distributed among the cells in the time-frequency space.

An important issue is the modulation technique that is used to transmit the coded information sequence. If the channel fades slowly enough to allow the establishment of a phase reference, CPSK may be employed.

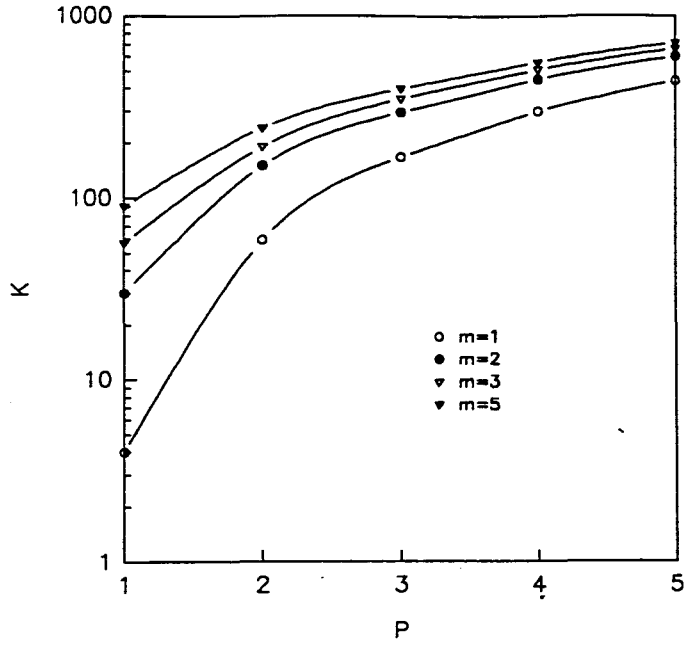

Figure 6.12: K for RAKE received CPSK: $E_b/N_0 = 60$ dB, $P = \{1,2,3,4,5\}$, $L = \{1,2,3,4,5\}$ and $m = \{\frac{1}{2},1,3,5\}$

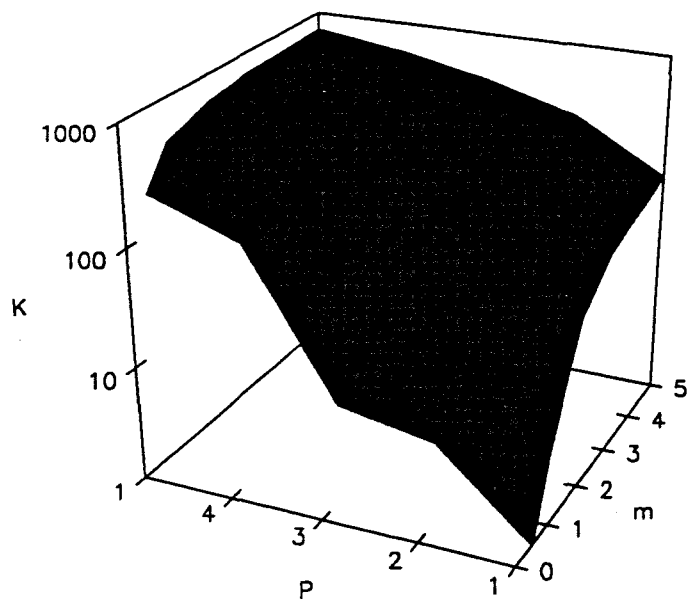

Figure 6.13: Surface plot of the capacity, K, as a function of P and m

In the following sections the performance and capacity improvements due to convolutional and block coding are investigated.

6.3.1 Convolutional Coding

As in Section 5.1.2 the performance of low rate convolutional coding is investigated. This is accomplished by the rate $R_{cd} = \{\frac{1}{2}, \frac{1}{4}, \frac{1}{8}\}$ codes with constraint lengths $\nu = \{2,3,4\}$ - the rate $R_{cd} = \frac{1}{2}$, $\nu = 6$ code is also investigated since it is commercially available.

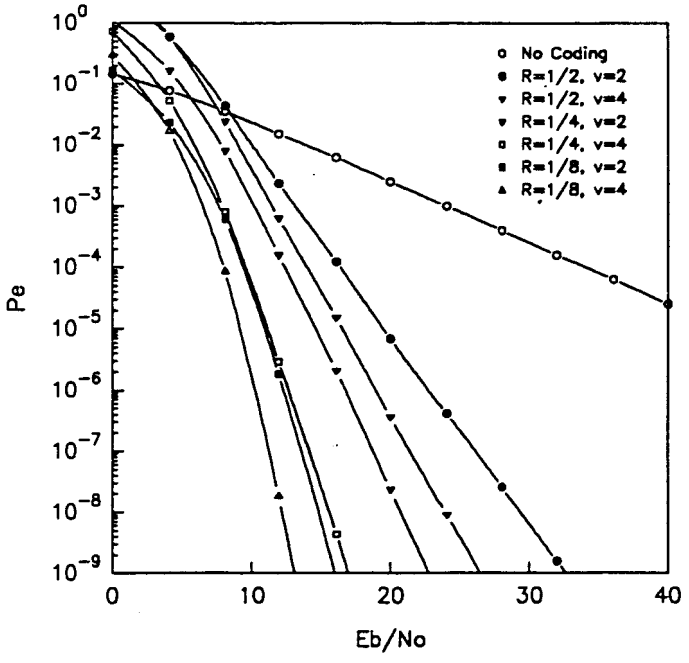

Figure 6.14: Convolutional coded Rayleigh faded performance in the absence of IUI

For reference purposes Figure 6.14 indicates the performance of a coded Rayleigh faded CPSK signal without any IUI. Clearly the low rate, $R_{cd} = \frac{1}{8}$ code enhances the performance significantly. The main disadvantage associated with low rate coding in a non-SSMA system is the bandwidth expansion, proportional to $\frac{1}{R_{cd}}$. However, Figure 6.15 indicates the performance for $m = 1$ and $K = 20$. As explained in Chapter 5, the chipping rate is reduced by the code rate R_{cd} to make comparisons on an equal bandwidth and throughput basis. Again, as in the non-SSMA case and the $m = \infty$ case the low rate $R_{cd} = \frac{1}{8}$, $\nu = 4$ code results in the best performance.

Tables 6.3, 6.4 and 6.5 indicate the capacity of the SSMA system with convolutional coding as a function of the Nakagami parameter m and constrained length ν. For comparative purposes the results for $m = \infty$ derived in Section 5.1.2 is also included.

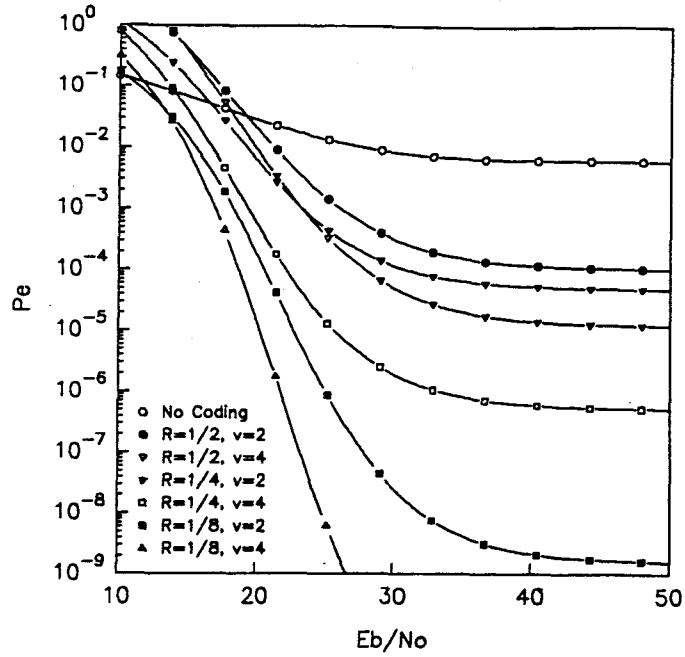

Figure 6.15: Convolutional coded CPSK performance: $K = 20$ and $m = 1$

	P_e	$\nu = 2$	$\nu = 3$	$\nu = 4$	$\nu = 6$
$m = 1/2$	10^{-3}	4	6	9	13
	10^{-5}	-	-	-	3
$m = 1$	10^{-3}	39	46	57	72
	10^{-5}	9	12	19	29
	10^{-8}	-	2	4	8
$m = 2$	10^{-3}	97	108	125	146
	10^{-5}	40	47	61	81
	10^{-8}	12	14	23	36
$m = 3$	10^{-3}	126	138	156	180
	10^{-5}	61	69	85	108
	10^{-8}	24	27	40	56
$m = 5$	10^{-3}	153	166	185	210
	10^{-5}	83	92	109	134
	10^{-8}	40	44	59	77
$m = \infty$	10^{-3}	190	208	226	263
	10^{-5}	113	123	141	170
	10^{-8}	66	69	86	110

Table 6.3: K for convolutional coded CPSK with $E_b/N_0 = 60$ dB, $P = 1$, $L = 1$, $R_{cd} = \frac{1}{2}$ and $N = 255$

	P_e	$\nu = 2$	$\nu = 3$	$\nu = 4$
$m = 1/2$	10^{-3}	12	19	27
	10^{-5}	2	5	8
	10^{-8}	-	-	2
$m = 1$	10^{-3}	38	52	65
	10^{-5}	14	21	30
	10^{-8}	4	6	11
$m = 2$	10^{-3}	62	79	94
	10^{-5}	30	40	52
	10^{-8}	13	18	26
$m = 3$	10^{-3}	72	90	106
	10^{-5}	38	49	61
	10^{-8}	18	24	34
$m = 5$	10^{-3}	80	99	116
	10^{-5}	45	56	69
	10^{-8}	24	31	40
$m = \infty$	10^{-3}	183	228	256
	10^{-5}	106	130	156
	10^{-8}	60	75	95

Table 6.4: K for convolutional coded CPSK with $E_b/N_0 = 60$ dB, $P = 1$, $L = 1$, $R_{cd} = \frac{1}{4}$ and $N = 127$

	P_e	$\nu = 2$	$\nu = 3$	$\nu = 4$
$m = 1/2$	10^{-3}	70	84	98
	10^{-5}	23	32	42
	10^{-8}	6	10	15
$m = 1$	10^{-3}	125	144	163
	10^{-5}	57	72	87
	10^{-8}	24	33	43
$m = 2$	10^{-3}	163	185	207
	10^{-5}	84	101	119
	10^{-8}	43	55	67
$m = 3$	10^{-3}	178	200	223
	10^{-5}	95	113	131
	10^{-8}	51	64	77
$m = 5$	10^{-3}	190	213	236
	10^{-5}	104	122	141
	10^{-8}	59	71	85
$m = \infty$	10^{-3}	203	226	270
	10^{-5}	116	134	160
	10^{-8}	68	80	98

Table 6.5: K for convolutional coded CPSK with $E_b/N_0 = 60$ dB, $P = 1$, $L = 1$, $R_{cd} = \frac{1}{8}$ and $N = 63$

As in the uncoded case, the capacity as a function of m converges relatively quickly to the $m = \infty$ case. The low rate $R_{cd} = \frac{1}{8}$ code has the best overall performance, and consequently results in the highest capacity.

As L increases the capacity reduces by roughly 9% for every increase in L by 5. Therefore, an increase to $L = 10$ reduces the capacity, as indicated in Tables 6.3, 6.4 and 6.5, by 18%. Again the linear multipath characteristics are maintained.

For CPSK modulation under Nakagami fading conditions low rate convolutional coding can be implemented with great success. However, the $R_{cd} = \frac{1}{4}$ code is not very effective for low values of m and constrained length $\nu = 2$. The unacceptable performance of $\nu = 2$ is due to the loss in processing gain which the minimum distance is not able to compensate for. Only as m converge to infinity the code becomes effective.

6.3.2 Block Coding

In this section we are interested in the performance and capacity improvement resulting of four simple block channel codes. The codes of interest are the half rate $(7, 4, 1)$, $(15, 7, 2)$, $(31, 16, 3)$ and the $(63, 30, 6)$ codes. The first of these codes is the Hamming code, while the rest are BCH codes. Such codes are discussed in introductory textbooks such as [97, 96].

Figures 6.16 and 6.17 respectively indicate the performance of block coding for Rayleigh fading without IUI and Rayleigh fading with $N = 255$ and $K = 20$. As in the $m = \infty$ case of Section 5.1.3, low rate block coding is not a viable option to increase system performance or capacity. Therefore, only half rate block codes are investigated.

Table 6.6 tabulates the capacity for half rate block codes. Let us compare these results with Table 6.3 for convolutional codes on the basis of equal minimum distance. The $(15, 7, 2)$ block code has $d_{min} = 5$, while the half rate $\nu = 2$ code has $d_{free} = 5$. The convolutional code has a capacity advantage over block codes of approximately 10% for all m. In general, convolutional codes perform better, and consequently higher capacities are possible, when compared to block codes. In addition, convolutional codes have the added advantage that lower rate codes can be used to increase the capacity even further.

6.4 Combined Error Control and RAKE Performance

In this section the influence of a combination of error control coding and RAKE reception are considered. For the purpose of error control coding, as before, convolutional coding and block coding are considered.

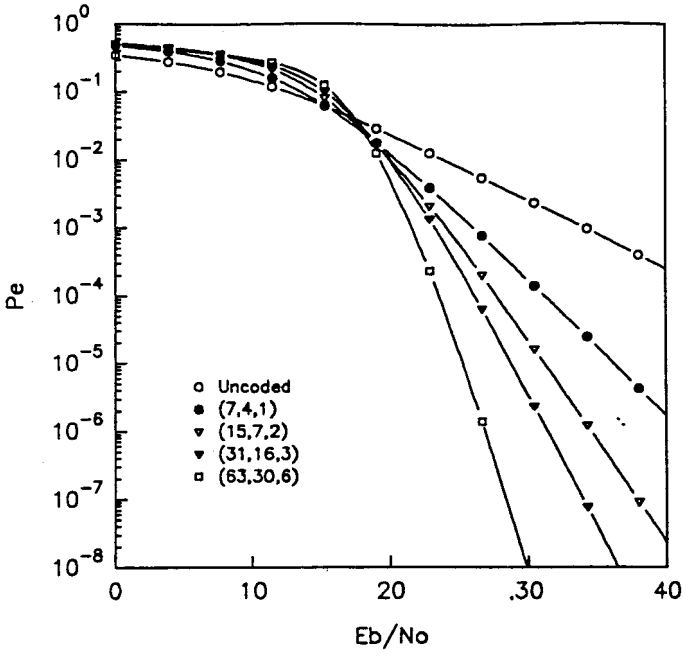

Figure 6.16: Block coded Rayleigh faded performance in the absence of IUI

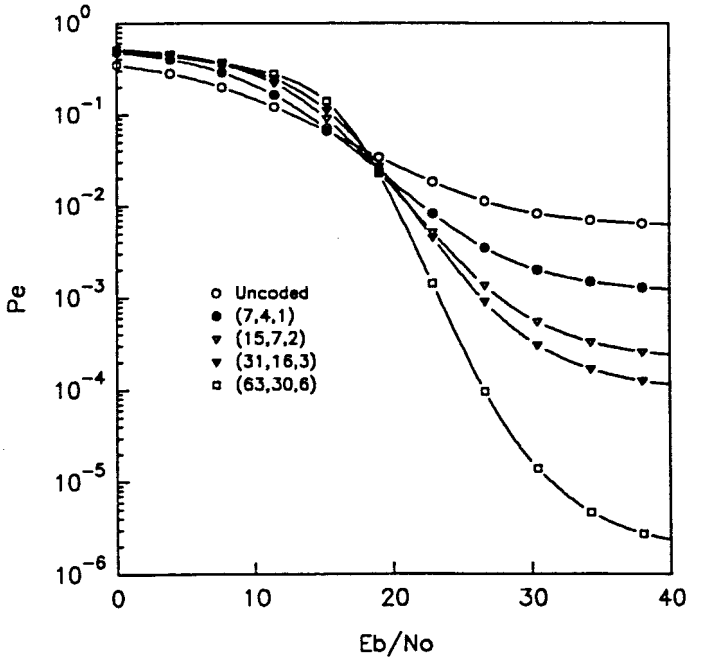

Figure 6.17: Block coded CPSK performance: $K = 20$ and $m = 1$

	P_e	$(7,4,1)$	$(15,7,2)$	$(31,16,3)$	$(63,30,6)$
$m = 1/2$	10^{-3}	-	3	4	9
	10^{-5}	-	-	-	2
$m = 1$	10^{-3}	18	34	37	59
	10^{-5}	3	7	11	26
	10^{-8}	-	-	2	9
$m = 2$	10^{-3}	60	89	94	127
	10^{-5}	16	34	44	74
	10^{-8}	3	10	17	39
$m = 3$	10^{-3}	84	117	123	159
	10^{-5}	30	53	65	101
	10^{-8}	9	21	31	60
$m = 5$	10^{-3}	108	143	150	188
	10^{-5}	48	74	87	126
	10^{-8}	19	36	48	82
$m = \infty$	10^{-3}	136	172	179	218
	10^{-5}	73	101	116	155
	10^{-8}	41	60	74	109

Table 6.6: K for block coded CPSK with $E_b/N_0 = 60$ dB, $P = 1$, $L = 1$, $R_{cd} = \frac{1}{2}$ and $N = 255$

6.4.1 Convolutional Coding and RAKE Reception

Tables 6.7, 6.8 and 6.9 indicate the capacity for $R_{cd} = \{\frac{1}{2}, \frac{1}{4}, \frac{1}{8}\}$ and $P = \{2,3,4,5\}$. It is clear that a combination of low rate convolutional coding and RAKE reception is very effective in increasing the system capacity. For example, by introducing a $R_{cd} = \frac{1}{8}$ convolutional code with a $P = 5$ tap RAKE receiver, the capacity improvement over a non-diversity receiver can be increased by 1500% for $m > \frac{1}{2}$ at $P_e = 10^{-3}$ - a massive increase.

Even more important, for $m = \frac{1}{2}$ the system fails as a multiple access scheme when no diversity is used. Using both convolutional coding and RAKE reception the capacity can be increased to 708 at an error rate of 10^{-3} with a commercially available convolutional coder and a five tap RAKE receiver.

6.4.2 Block Coding and RAKE Reception

Since block coding is not as effective as convolutional coding, we only consider the performance of the $(7,4,1)$ Hamming code. Table 6.10 indicates that a combination of RAKE reception and a simple block code can increase the performance dramatically. Even for $m = \frac{1}{2}$ with a two tap receiver the system can support two users at an error rate of 10^{-5}.

Therefore, a general conclusion is that coding plus RAKE reception is very effective in increasing

	P_e	$P=2$	$P=3$	$P=4$	$P=5$
$m=1/2$	10^{-3}	112	289	493	708
	10^{-5}	35	123	238	367
	10^{-8}	5	35	87	154
$m=1$	10^{-3}	247	466	691	919
	10^{-5}	120	253	395	540
	10^{-8}	45	116	198	286
$m=2$	10^{-3}	346	575	805	1037
	10^{-5}	198	345	494	644
	10^{-8}	100	189	281	375
$m=3$	10^{-3}	384	615	846	1078
	10^{-5}	230	380	530	680
	10^{-8}	127	219	313	408
$m=5$	10^{-3}	416	647	879	1111
	10^{-5}	258	409	560	711
	10^{-8}	151	246	341	436

Table 6.7: K for convolutional coded and RAKE received CPSK at $E_b/N_0 = 60$ dB, $P = \{2,3,4,5\}$, $L = \{2,3,4,5\}$, $R_{cd} = \frac{1}{2}$, $\nu = 4$ and $N = 255$

	P_e	$P=2$	$P=3$	$P=4$	$P=5$
$m=1/2$	10^{-3}	127	247	371	498
	10^{-5}	58	127	202	279
	10^{-8}	21	56	99	144
$m=1$	10^{-3}	187	314	442	571
	10^{-5}	102	180	259	339
	10^{-8}	51	97	145	193
$m=2$	10^{-3}	222	351	481	610
	10^{-5}	130	210	291	371
	10^{-8}	73	122	172	221
$m=3$	10^{-3}	235	364	494	623
	10^{-5}	141	221	302	382
	10^{-8}	82	132	181	231
$m=5$	10^{-3}	245	375	504	634
	10^{-5}	150	230	310	391
	10^{-8}	90	139	189	239

Table 6.8: K for convolutional coded CPSK at $E_b/N_0 = 60$ dB, $P = \{2,3,4,5\}$, $L = \{2,3,4,5\}$, $R_{cd} = \frac{1}{4}$, $\nu = 4$ and $N = 127$

	P_e	$P=2$	$P=3$	$P=4$	$P=5$
$m=1/2$	10^{-3}	324	569	820	1072
	10^{-5}	171	317	468	620
	10^{-8}	83	170	261	354
$m=1$	10^{-3}	411	664	918	1173
	10^{-5}	235	388	542	697
	10^{-8}	131	225	320	415
$m=2$	10^{-3}	460	715	970	1226
	10^{-5}	272	427	582	737
	10^{-8}	161	256	352	448
$m=3$	10^{-3}	478	733	988	1243
	10^{-5}	286	441	596	751
	10^{-8}	173	268	368	459
$m=5$	10^{-3}	492	747	1002	1258
	10^{-5}	296	451	607	762
	10^{-8}	181	276	372	468

Table 6.9: K for convolutional coded CPSK at $E_b/N_0 = 60$ dB, $P = \{2,3,4,5\}$, $L = \{2,3,4,5\}$, $R_{cd} = \frac{1}{8}$, $\nu = 4$ and $N = 63$

the system capacity under fading conditions when CPSK is used as modulation scheme.

6.5 Conclusions

From the numerical work presented in this chapter the following conclusions can be drawn:

If all discrete paths have Nakagami gains with low values of m and guaranteed low average error probability is expected at all times, a simple non-diversity coherent receiver will not be able to cope with the Nakagami channel fading with Gold spread spectrum codes of period $N = 511$. In fact, even for the unfaded $m = \infty$ case (as described in Section 5.1) the capacity is unacceptably low. By using longer sequences to decrease the error probability of the interference limited system, this problem can be partly overcome. However, increasing the spreading code's length is not always a viable option due to restricted bandwidths.

The results indicate that in the absence of diversity even small amounts of multiple access interference can be harmful in a Nakagami fading environment when m is small. However, when either or both RAKE reception and error control coding are introduced the performance and capacity of our SSMA system can be increased dramatically. Also, by introducing voice activity monitoring and a cellular architecture, the capacity as tabulated, can be increased by a factor of five.

Another important result is that low rate convolutional codes can be used to increase the system capacity dramatically, without a penalty paid in bandwidth. This is fundamentally different when

	P_e	$P=2$	$P=3$	$P=4$	$P=5$
$m=1/2$	10^{-3}	34	120	234	361
	10^{-5}	2	21	60	113
	10^{-8}	-	-	7	22
$m=1$	10^{-3}	118	249	389	534
	10^{-5}	31	88	157	232
	10^{-8}	4	23	52	89
$m=2$	10^{-3}	196	341	488	637
	10^{-5}	79	155	235	316
	10^{-8}	27	66	108	155
$m=3$	10^{-3}	228	375	524	673
	10^{-5}	104	184	266	348
	10^{-8}	44	87	139	185
$m=5$	10^{-3}	256	405	554	704
	10^{-5}	127	209	292	375
	10^{-8}	63	112	174	230

Table 6.10: K for the $(7,4,1)$ block code: $E_b/N_0 = 60$ dB, $P = \{2,3,4,5\}$, $L = \{2,3,4,5\}$, $R_{cd} = \frac{1}{2}$ and $N = 255$

compared to narrowband systems. However, low rate block coding can not be used to increase system capacity. The optimum block codes are half rate codes.

When comparing convolutional and block codes, with comparable minimum distances, it is clear that convolutional codes outperform block codes, on average, by 10% when capacity is considered.

From the performance results it is further evident that error control coding combined with RAKE reception are power and bandwidth efficient. All the capacity assessments were made at $\frac{E_b}{N_0} = 60$ dB. However, using these forms of diversity the average error rate saturates at much lower values of signal- to-noise ratio and therefore the transmitted power needed for a given number of simultaneous users can be much lower. This is significant, especially in handhold units where power consumption is critical.

CHAPTER 7

DPSK PERFORMANCE RESULTS IN A NAKAGAMI FADING CHANNEL

This chapter is concerned with the performance of the uplink of the system described in Chapter 2. The same approach as for the downlink (CPSK) will be followed to describe the uplink (DPSK) performance and capacity. The performance and capacity of the uplink is investigated in the presence of impairments due to AWGN, IUI and Nakagami fading.

As a form of diversity it is assumed that the basestation is equipped with a method to obtain diversity (i.e. space diversity) and that the received signals are optimally combined by a Maximum Ratio Combiner (MRC). A second means to obtain diversity is to include error control coding. The effects of these two diversity techniques on the performance and capacity of the system are presented.

As in the downlink, CPSK case, the average path strength of the interfering users are arbitrarily adopted as $\Omega = -10$ dB, with $m = \{\frac{1}{2}, 1, 2, 3, 5\}$, which is typical of the IWC channel [24].

Section 7.1 describes the non-diversity performance, while Section 7.2 investigates the influence of MRC diversity. In Section 7.3 the performance of convolutional and block coding as a means of diversity is investigated, with Section 7.4 discussing the influence on the performance and capacity of a combination of the two diversity schemes.

7.1 Non-diversity Performance

Figure 7.1 and 7.2 indicate the average downlink performance of our system for $m = \{\frac{1}{2}, 1, 2, 3, 5\}$ and $L = \{1, 5\}$ respectively. Gold spreading sequences of length $N = 511$ are assumed with generator polynomials as indicated in Appendix B.

For $m = \frac{1}{2}$ the system fails as a multiple access system, with the average error rate not much different from that of the CPSK uplink. However, as m increases the difference between the uplink and the downlink is more pronounced. For example, for $m = 3$ and $L = 1$ the DPSK (Figure 7.1) and CPSK (Figure 6.1) performance, respectively saturate at approximately 4×10^{-8} and 1×10^{-8}.

Approximately the same ratio in performance degradation between the two modulation schemes is noticed for $L = 5$. It is indeed apparent that decreasing m, i.e. increasing the amount of fading, has a much more noticeable effect on the performance than an increase in L, the number of multipaths. Therefore, as in the downlink, CPSK case, the system performance is mainly limited by fading rather than the multipath spreading.

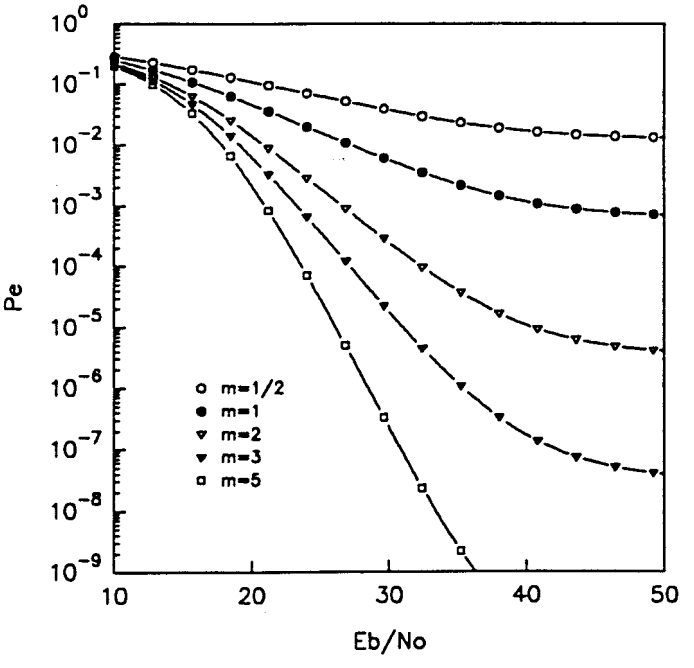

Figure 7.1: Nakagami faded DPSK performance: $K = 2$, $L = 1$ and $N = 511$

Table 7.1 quantifies the capacity for $m = \{\frac{1}{2}, 1, 2, 3, 5, \infty\}$ and $L = \{1, 5, 10\}$. For $m = \frac{1}{2}$, that is severest fading, the uplink fails as a multiple access system, and for $m = 1$ (Rayleigh fading) only two users can be supported at an error rate of 10^{-3}. The latter case, $m = 1$, is 50% less than for the downlink.

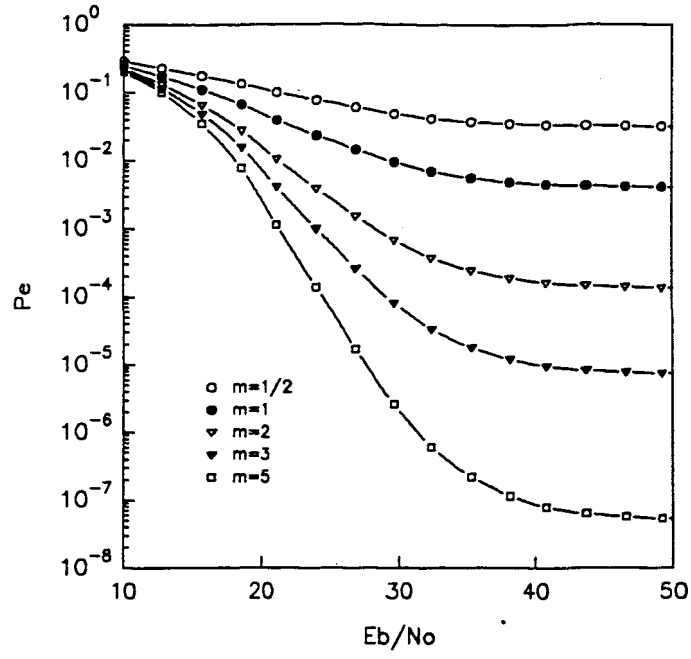

Figure 7.2: Nakagami faded DPSK performance: $K = 2$, $L = 5$ and $N = 511$

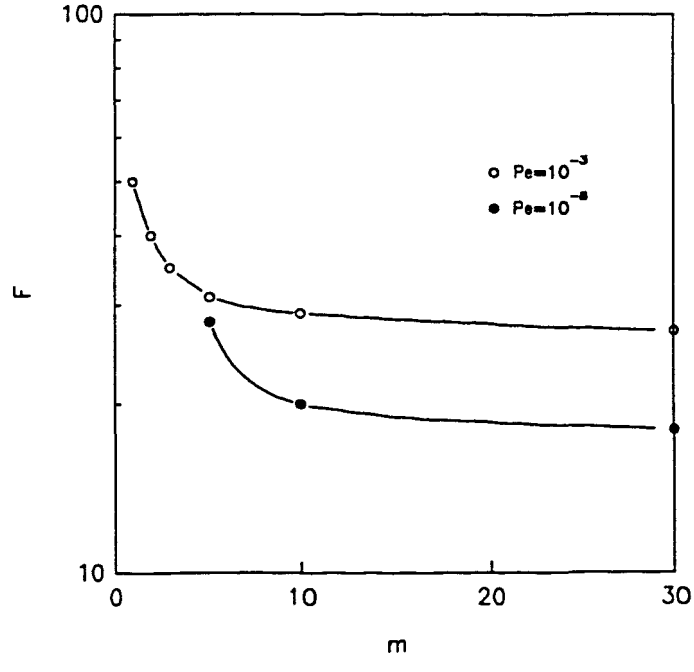

Figure 7.3: Nakagami faded DPSK performance: $K = 2$, $L = 5$ and $N = 511$

Let us define the relative capacity, $\mathcal{F}$, as

$$\mathcal{F} = \frac{\text{Capacity of CPSK-Capacity of DPSK}}{\text{Capacity of CPSK}}. \tag{7.1}$$

Figure 7.3 indicates $\mathcal{F}$ as a function of m for $P_e = 10^{-3}$ and $P_e = 10^{-8}$. It is apparent that as m increases, the DPSK capacity converges quite quickly to roughly 24% and 12% of that of CPSK for $P_e = 10^{-3}$ and $P_e = 10^{-8}$ respectively.

Adding the advantages of voice activity monitoring and cell splitting a gain in capacity of 5 times can be realised. However, it is clear that even then the uplink capacity is not acceptable and that some form of diversity is absolutely essential.

	P_e	$L=1$	$L=5$	$L=10$
$m=1/2$	10^{-3}	-	-	-
$m=1$	10^{-3}	2	-	-
$m=2$	10^{-3}	18	13	7
	10^{-5}	2	-	-
$m=3$	10^{-3}	37	32	26
	10^{-5}	8	2	-
$m=5$	10^{-3}	62	57	50
	10^{-5}	20	15	8
	10^{-8}	5	-	-
$m=\infty$	10^{-3}	115	-	-
	10^{-5}	63	-	-
	10^{-8}	36	-	-

Table 7.1: K for non-diversity DPSK: $E_b/N_0 = 60$ dB, $P = 1$ and $L = \{1, 5, 10\}$

7.2 MRC Diversity Performance

With MRC the L received signals are weighted proportionally to their signal-to-noise power ratios and then summed. The individual signals must be co-phased before the combining process. The combiner that accomplishes this is optimum and is called a Maximum Ratio Combiner. For a detailed description of diversity and combining techniques [72, 98] can be consulted.

The performance results are based on the assumption that the channel attenuations and phase shifts are known perfectly, that is the estimates contain no noise. The analysis, and consequently the resulting performance results, of a RAKE receiver with perfect (noiseless) estimates of the channel tap weights is equivalent to a maximum ratio combiner with P-th order diversity. The

results obtained in this section for MRC can therefore directly be compared to the CPSK RAKE reception results of Chapter 6. Further, the results are valid for a basestation equipped with a RAKE receiver or MRC diversity.

Figure 7.4 indicates the performance of a three path ($L = 3$), three branch ($P = 3$) diversity system, with $K = 30$ and $N = 511$. Recalling from Figures 6.2 and 6.1 where the system failed as a multiple access system, the improvement due to diversity is very noticeable - even for $m = \frac{1}{2}$ the system can support 30 users.

Figure 7.5 depicts the diversity system performance as a function of the multipath parameter L for $P = \{1, 2, 3, 4, 5\}$ branch diversity. As in the CPSK case, a small degree of diversity improves the performance dramatically, although higher order diversity is needed in the DPSK case to achieve performance results equivalent to the CPSK case. The linear increase in average error rate due to an increase in multipaths is also present in the DPSK system due to the approximate Gaussian nature of the IUI.

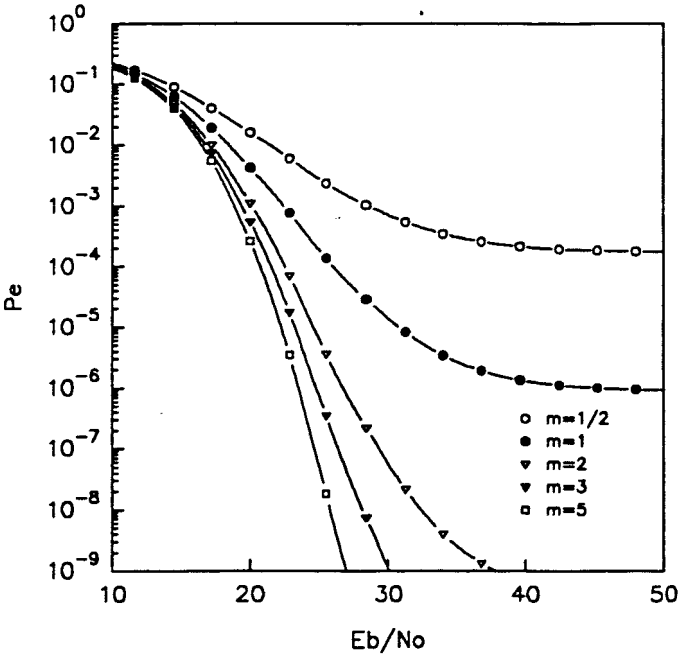

Figure 7.4: Nakagami faded DPSK performance: $K = 30$, $L = 3$, $P = 3$, $N = 511$ and $m = \{\frac{1}{2}, 1, 2, 3, 5\}$

Table 7.2 tabulates the capacity of a P branch MRC diversity system for various values of L, P and m. When comparing this table with Table 6.2, it is interesting to see that the capacity for $P = 5$ and $P = 4$, DPSK and CPSK respectively, is approximately equivalent. In other words, to have equal capacity in the up- and downlink of our system, one more diversity branch is needed in

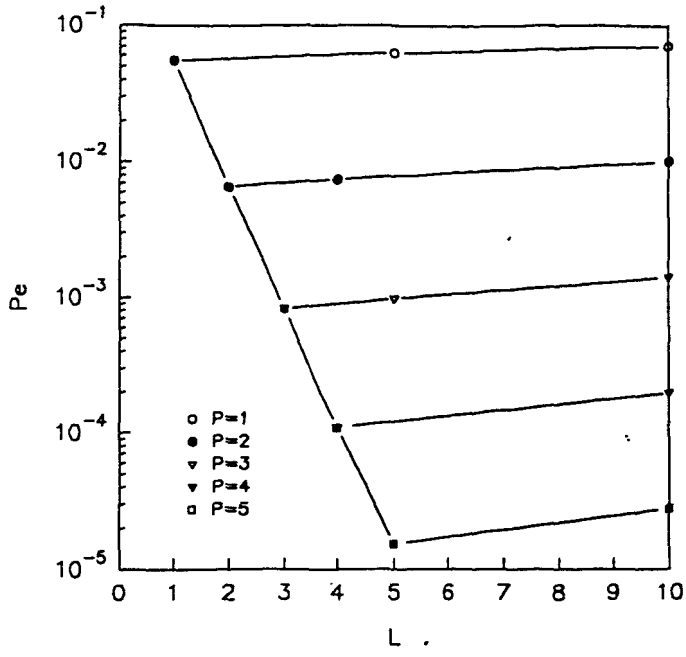

Figure 7.5: P_e as a function of the number of channel paths: $m = \frac{1}{2}$, $K = 20$ and $N = 511$

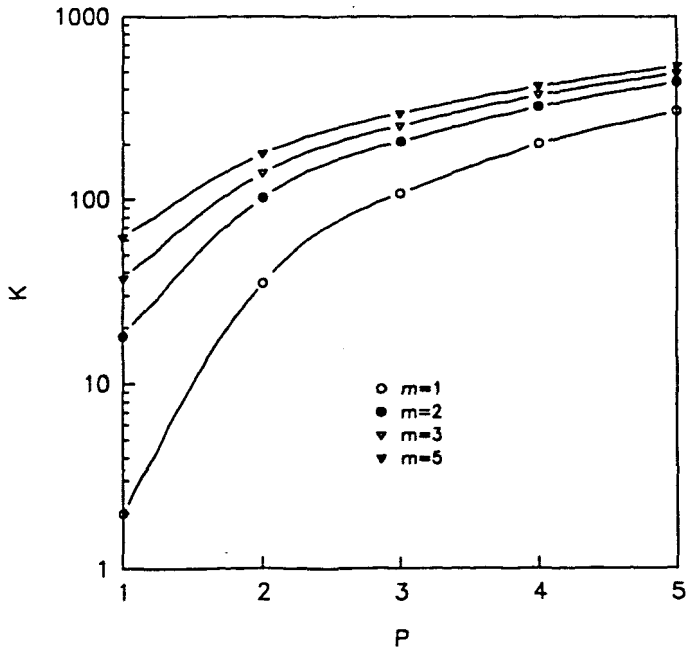

Figure 7.6: Capacity of a P branch DPSK system: $E_b/N_0 = 60$ dB, $P, L = \{1,2,3,4,5\}$ and $m = \{1,2,3,5\}$

	P_e	$P=2$	$P=3$	$P=4$	$P=5$
$m=1/2$	10^{-3}	2	3	68	134
	10^{-5}	-	-	3	16
$m=1$	10^{-3}	35	108	202	305
	10^{-5}	3	19	51	94
	10^{-8}	-	-	6	18
$m=2$	10^{-3}	102	208	322	439
	10^{-5}	27	73	130	191
	10^{-8}	4	19	43	73
$m=3$	10^{-3}	139	254	372	492
	10^{-5}	49	75	171	236
	10^{-8}	13	39	72	108
$m=5$	10^{-3}	177	296	416	537
	10^{-5}	78	142	210	277
	10^{-8}	30	65	104	143

Table 7.2: K for MRC diversity DPSK: $E_b/N_0 = 60$ dB, $P = \{2,3,4,5\}$ and $L = \{2,3,4,5\}$

the uplink, resulting in more complexity of the uplink receiver.

Also noticeable from Table 7.2, is that for $m = \frac{1}{2}$ with two diversity branches the system can operate as a multiple access system. Further, for $m = 5$, $P = 5$ an increase of 766% is realised over the non-diversity ($P = 1$) case at $P_e = 10^{-3}$.

Figure 7.6 indicates the capacity, K, as a function of P for different values of m. When compared to Figure 6.12 it is noticed that K saturates at a lower value as P increases.

In this section it was shown that P branch diversity with MRC can be implemented very efficiently when DSPK is used as modulation scheme. To ensure equal capacity for the up- and downlink of the cellular system, it is necessary to increase the order of diversity by approximately one.

In the next section the influence of error control coding to obtain diversity is investigated.

7.3 Error Control Coded Performance

As explained in Section 6.3, error control coding can effectively be implemented as a means to obtain diversity. In this section the performance and capacity improvements due to convolutional and block coding is investigated.

7.3.1 Convolutional Coding

The convolutional codes as indicated and described in Appendix C are investigated. For reference purposes the performance of a coded DPSK, Rayleigh faded ($m = 1$) signal in the absence of IUI is indicated in Figure 7.7. As in the CPSK case (Figure 6.14) low rate coding enhances the performance significantly.

Figure 7.8 indicates the performance for $K = 20$ and $m = 1$. It is interesting to note that low rate coding improves the performance significantly. However, it is not consistent with the $m = \infty$ case described in Figure 5.10 of Section 5.2.2. This would suggest that as m increases (less fading), low rate coding becomes less efficient. Investigating Tables 7.3, 7.4 and 7.5 this statement is verified. For m small (strong fading), the low rate $R_{cd} = \frac{1}{8}$ code increases the uncoded capacity significantly; for $\nu = 4$ the number of users at $P_e = 10^{-3}$ is 35, where the uncoded case failed as a multiple access system.

By increasing L, the capacities as indicated in Tables 7.3, 7.4 and 7.5 are reduced by approximately 12% for every increase in L by 5. This is 3% more than for the CPSK case.

In general coding is not as effective for DPSK as it is for CPSK. Comparing Tables 7.3 and 6.3 it is seen that DPSK signalling with $\nu = 6$ results in less capacity than CPSK signalling with $\nu = 2$. Therefore, coding in the DPSK case has to be combined with diversity to ensure equal capacity for the up- and downlink.

The most important conclusion to be drawn from this section is that low rate convolutional codes can be used to effectively increase the system capacity if m is small. In other words, in a mobile channel for IWC's, where the channel is severely faded, low rate coding can be implemented with success.

7.3.2 Block Coding

The block codes considered in this section is the same as that investigated for the CPSK case with generator polynomials as indicated in Appendix C.

Figures 7.9 and 7.10 indicate the half rate block coded performance, respectively, under Rayleigh fading ($m = 1$) without and with IUI. In both cases it is clear that an increase in the minimum distance results in an decrease in average error rate. Low rate block codes enhance the system performance for small m, but the performance of block codes is worse than convolutional code performance. For example, Table 7.6 tabulates the performance of half rate block codes. Comparing these entries with that of Table 7.3 on an equatable base, that is equal minimum distance and free distance, it is clear that convolutional codes outperform block codes. The $(15, 7, 2)$ block code has

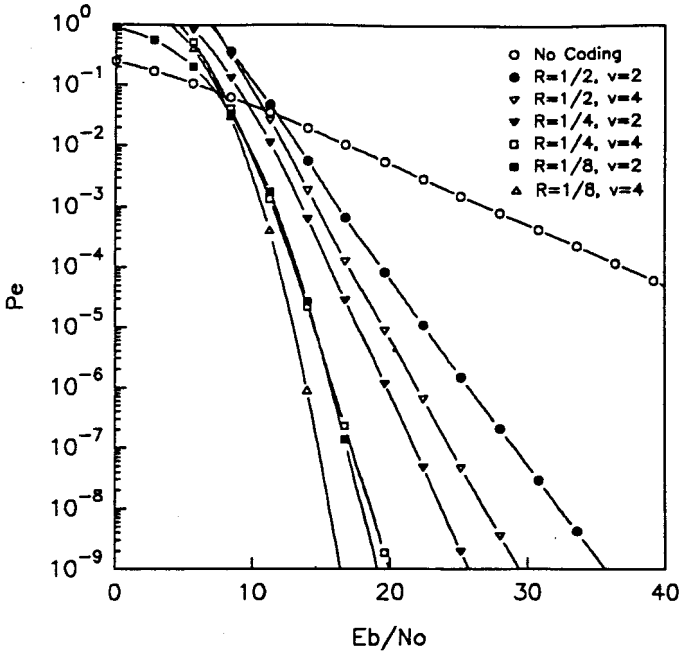

Figure 7.7: Convolutional coded Rayleigh faded performance in the absence of IUI

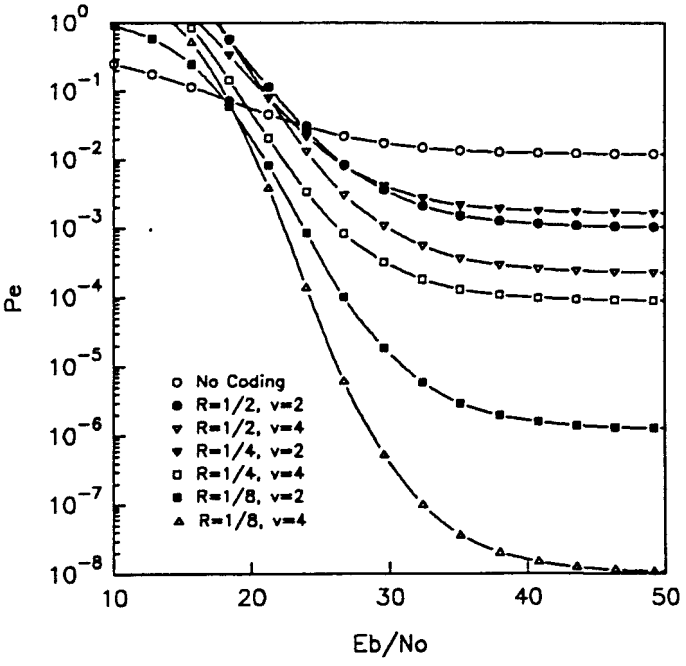

Figure 7.8: Convolutional coded DPSK performance: $K = 20$ and $m = 1$

	P_e	$\nu = 2$	$\nu = 3$	$\nu = 4$	$\nu = 6$
$m = 1/2$	10^{-3}	2	3	4	5
$m = 1$	10^{-3}	19	23	28	35
	10^{-5}	5	6	9	15
	10^{-8}	-	-	2	4
$m = 2$	10^{-3}	54	60	68	79
	10^{-5}	24	28	35	46
	10^{-8}	7	9	14	22
$m = 3$	10^{-3}	74	80	89	101
	10^{-5}	39	43	52	65
	10^{-8}	16	18	26	36
$m = 5$	10^{-3}	94	100	110	121
	10^{-5}	55	60	71	84
	10^{-8}	28	31	40	52
$m = \infty$	10^{-3}	120	128	135	152
	10^{-5}	78	84	94	109
	10^{-8}	49	52	62	75

Table 7.3: K for convolutional coded DPSK at $E_b/N_0 = 60$ dB, $P = 1$, $L = 1$, $R_{cd} = \frac{1}{2}$ and $N = 255$

	P_e	$\nu = 2$	$\nu = 3$	$\nu = 4$
$m = 1/2$	10^{-3}	5	8	11
	10^{-5}	-	2	2
$m = 1$	10^{-3}	18	23	28
	10^{-5}	7	10	14
	10^{-8}	2	3	6
$m = 2$	10^{-3}	31	38	44
	10^{-5}	17	21	27
	10^{-8}	8	11	15
$m = 3$	10^{-3}	37	44	58
	10^{-5}	22	27	33
	10^{-8}	11	15	20
$m = 5$	10^{-3}	42	50	56
	10^{-5}	27	32	38
	10^{-8}	16	19	25
$m = \infty$	10^{-3}	95	112	122
	10^{-5}	62	74	85
	10^{-8}	39	47	57

Table 7.4: K for convolutional coded DPSK at $E_b/N_0 = 60$ dB, $P = 1$, $L = 1$, $R_{cd} = \frac{1}{4}$ and $N = 127$

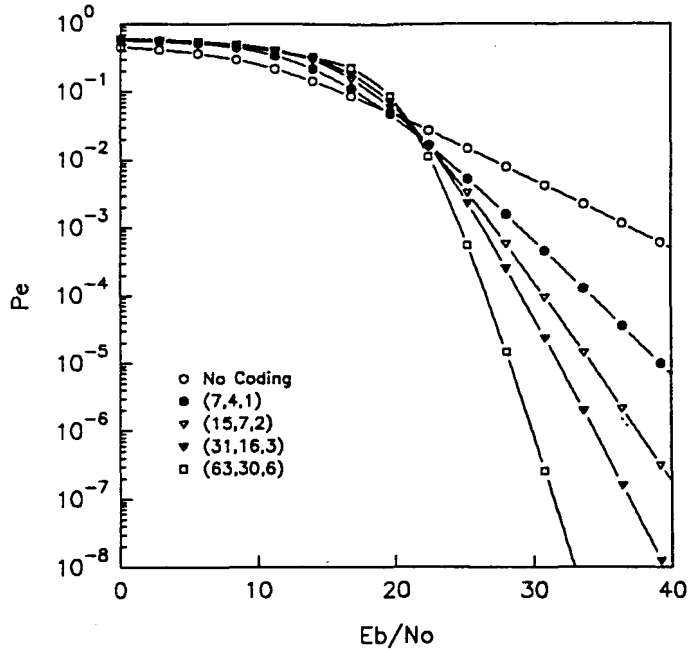

Figure 7.9: Block coded Rayleigh faded performance in the absence of IUI

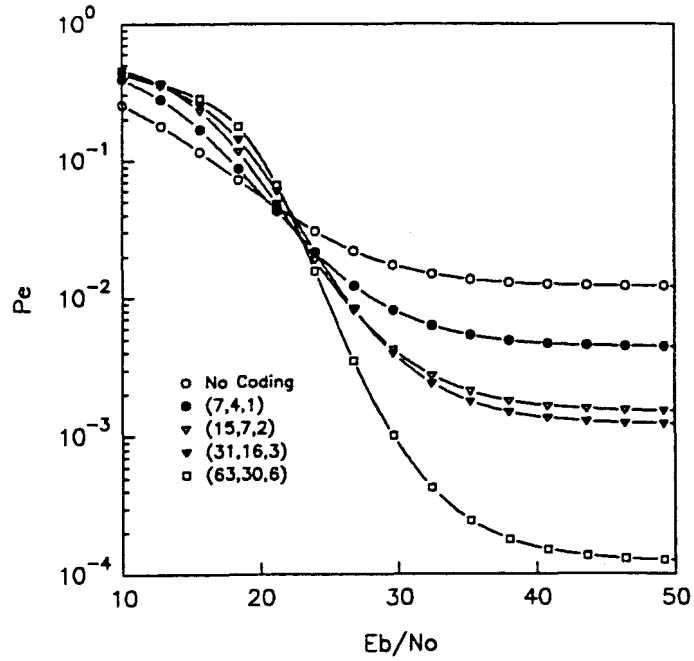

Figure 7.10: Block coded DPSK performance: $K = 20$ and $m = 1$

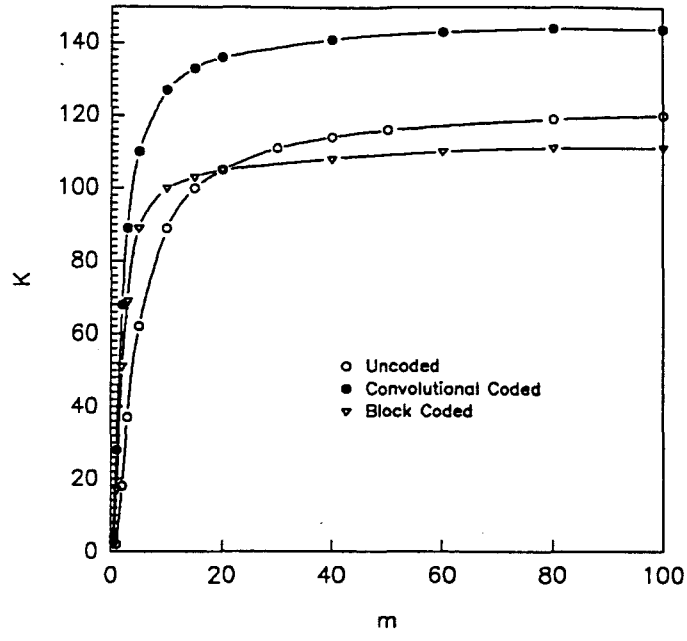

Figure 7.11: K as a function of the Nakagami fading parameter m: $P = 1$, $L = 1$ and $P_e = 10^{-3}$

	P_e	$(7,4,1)$	$(15,7,2)$	$(31,16,3)$	$(63,30,6)$
$m = 1/2$	10^{-3}	-	-	2	4
$m = 1$	10^{-3}	9	17	18	29
	10^{-5}	-	4	5	13
	10^{-8}	-	-	-	5
$m = 2$	10^{-3}	35	51	53	70
	10^{-5}	10	20	26	42
	10^{-8}	2	6	10	23
$m = 3$	10^{-3}	52	69	73	91
	10^{-5}	20	34	41	61
	10^{-8}	6	14	20	38
$m = 5$	10^{-3}	69	89	92	111
	10^{-5}	33	50	58	79
	10^{-8}	14	26	34	54
$m = \infty$	10^{-3}	93	111	115	133
	10^{-5}	56	72	81	102
	10^{-8}	34	46	56	76

Table 7.6: K for block coded DPSK with $E_b/N_0 = 60$ dB, $P = 1$, $L = 1$, $R_{cd} = \frac{1}{2}$ and $N = 255$

7.4 Combined Error Control and MRC

To ensure equal capacities in the up- and downlink directions for DPSK and CPSK respectively, it was seen earlier that a combination of diversity and coding is essential. In this section the influence of a combination of coding and diversity with MRC is investigated for the DPSK uplink.

7.4.1 Convolutional Coding and MRC

It was shown that low rate convolutional coding is not effective when m is small. Therefore, Table 7.7 presents only the performance of half rate convolutional codes combined with a P branch diversity receiver. As in the CPSK case the performance is greatly enhanced by a combination of coding and diversity. The CPSK capacity improvement over the uncoded, non- diversity case is 909% at $m = 5$, $P = 5$ and $P_e = 10^{-3}$. The capacity of DPSK, under the same conditions as above, is 38% less than for CPSK, resulting in unequal capacity of the up-and downlink. Reducing the number of taps (or branches) of the downlink receiver to $P = 3$, result in approximately equal capacity.

This is quite an important result since it indicates that the system capacity is restricted by the uplink performance when equal capacity in the up- and downlink is required.

	P_e	$P=2$	$P=3$	$P=4$	$P=5$
$m = 1/2$	10^{-3}	54	150	267	395
	10^{-5}	17	66	136	217
	10^{-8}	2	18	51	94
$m = 1$	10^{-3}	135	265	401	541
	10^{-5}	69	153	247	344
	10^{-8}	26	74	131	194
$m = 2$	10^{-3}	202	342	484	628
	10^{-5}	124	223	323	425
	10^{-8}	67	131	198	267
$m = 3$	10^{-3}	229	371	515	658
	10^{-5}	149	250	352	455
	10^{-8}	88	156	225	296
$m = 5$	10^{-3}	252	396	540	684
	10^{-5}	171	274	377	480
	10^{-8}	108	178	249	320

Table 7.7: K for convolutional coded and MRC diversity DPSK at $E_b/N_0 = 60$ dB, $P = \{2,3,4,5\}$, $L = \{2,3,4,5\}$, $R_{cd} = \frac{1}{2}$, $\nu = 4$ and $N = 255$

7.4.2 Block Coding and MRC

As in the CPSK case, block coding and DPSK signalling is not very effective, and therefore only the very simple (7,4,1) block code capacity is presented in Table 7.8. Comparing with Table 6.9, the CPSK capacity at $m = 5$ is approximately 33% less than the DPSK capacity.

Also, for $P = 2$ with a simple block code the system can support 16 users at an error rate of 10^{-3} for $m = \frac{1}{2}$. Under the same conditions a non-diversity system fails as a multiple access system.

	P_e	$P=2$	$P=3$	$P=4$	$P=5$
$m = 1/2$	10^{-3}	16	64	133	214
	10^{-5}	-	11	35	69
	10^{-8}	-	-	3	12
$m = 1$	10^{-3}	67	151	244	340
	10^{-5}	18	56	105	159
	10^{-8}	2	14	36	63
$m = 2$	10^{-3}	123	220	320	421
	10^{-5}	54	109	169	230
	10^{-8}	19	48	82	119
$m = 3$	10^{-3}	147	248	349	451
	10^{-5}	73	133	195	257
	10^{-8}	33	67	105	143
$m = 5$	10^{-3}	170	271	374	472
	10^{-5}	93	155	218	281
	10^{-8}	48	87	126	165

Table 7.8: K for the $(7,4,1)$ block code: $E_b/N_0 = 60$ dB, $P = \{2,3,4,5\}$, $L = \{2,3,4,5\}$, $R_{cd} = \frac{1}{2}$ and $N = 255$

7.5 Conclusions

As before, voice activity and a cellular architecture can be incorporated to increase the cellular capacity by approximately a factor of five. Further, convolutional codes outperform block codes, and block codes are not recommended when the channel is very dispersive (i.e. small m) at high error rates - under these conditions, block codes degrade the capacity to worse than the uncoded performance.

One of the main conclusions that is apparent from the results presented in this chapter and Chapter 6, is that the capacity of our spread spectrum system is limited by the uplink performance. Using at least an order higher diversity is in many cases necessary to have approximately equal capacity in both directions. In addition, low rate coding can not be used very effectively to increase system capacity when the channel is not very faded (i.e. large m). Another important point is that power

control in the uplink is more difficult to achieve in a practical system, and therefore the capacity could be even less than predicted in this chapter, resulting in even more diversity branches needed than anticipated.

CHAPTER 8

CONCLUSIONS

This study has proposed and analyzed an asynchronous DS/SSMA system for the IWC channel. For the up- and downlink of the system DPSK and CPSK were assumed as modulation scheme. Actual Gold spreading code correlation parameters of length up to 511 and MaxEnt principles were used to calculate the performance and capacity of this system under Nakagami fading conditions. To extend the capacity results to that of a cellular system, the total interference due to the neighbouring cells were assumed to contribute 50% of the total interference. However, the total interference can be reduced by including a voice activity factor and cell splitting. These features are unique to a spread spectrum system, since it is interference limited and not bandwidth limited like conventional TDMA and FDMA systems.

It was shown that MaxEnt principles can be implemented more successfully than GQR techniques when an unknown pdf and average error rates are calculated. This result is new and laid the foundation to calculate the system performance using MaxEnt techniques.

Closed form expressions for the uplink (CPSK) and downlink (DPSK) performance were derived as a function of the Nakagami fading parameter m and P, the number of taps in a RAKE receiver or the number of branches in a MRC diversity system with P branches. These expressions were derived making use of the Gaussian Assumption. Using these expressions and MaxEnt techniques, the validity of the Gaussian Assumption in SSMA systems has been investigated by comparing the average error rates for different values of m. Also, by calculating the missing information between the actual IUI pdf and a Gaussian pdf with the same second moment as the IUI pdf the Gaussian Assumption was studied, with new results presented for various values of the Nakagami fading parameter m. When m is large, that is no fading, the Gaussian Assumption is more valid than when the channel is highly faded (small m).

When the system is stationary and no scintillating channel effects are present the only form of diversity possible is error control coding. It was shown that low rate convolutional coding is significant in increasing the system capacity of the downlink when CPSK is used as modulation

scheme. Low rate block codes are not as effective and in fact degrades the performance to worse than the uncoded case. For the uplink (DPSK as modulation scheme) it was shown that half rate convolutional and block codes are the most effective. For both modulation schemes it was shown that convolutional codes outperform block codes.

When the Nakagami fading parameter, m, is small, it was shown that some form or forms of diversity are absolutely necessary. The up- and downlink utilised, respectively, MRC diversity and RAKE reception respectively as a form of diversity. As another form of diversity FEC coding was introduced. It was shown that a combination of MRC/RAKE reception and FEC coding is both power and bandwidth efficient. Under these fading conditions it was further shown that convolutional codes outperform block codes.

The capacity and performance of the analyzed system is limited by the DPSK uplink and therefore more diversity is needed in the uplink direction.

To summarize; the proposed cellular IWC system, using DS/SSMA as multiple access scheme, has thoroughly been analyzed under Nakagami channel fading statistics. The main conclusions of the system are reviewed above and reported in e.g. [56, 57, 58, 59, 60, 61, 62, 63, 64, 65, 66, 67].

8.1 Future Work

Since we set out to determine the performance and capacity of a relatively simple system, there is scope to extend the system. The proposed system can be analyzed with higher order modulation schemes such as MPSK, QPSK or GMSK with more efficient spreading sequences. Using complex valued spreading sequences, such as CASAC sequences [99], the capacity of both the up- and downlink can be improved significantly, but with a penalty paid in complexity. Further, instead of using convolutional or block codes, trellis codes, together with the higher order modulation schemes can be incorporated. With regards to trellis coding there are a number of possible areas of future work. The optimum metric for a trellis coded system in the presence of IUI can be determined and the system performance analyzed. Other possible investigations include spreading codes employing higher order alphabets and multidimensional codes. As a further method to enhance the system capacity and performance interference cancellation [100] can be included.

APPENDIX A

DESCRIPTION OF THE NAKAGAMI DISTRIBUTION

Briefly a few comments on the Nakagami-m distribution. In essence, the Nakagami-m fading distribution is a central χ-distribution generalized to a nonintegral number of degrees of freedom (where the number of degrees of freedom is greater than or equal to one). It was introduced by Nakagami [39] as an approximate to two other distributions that he had previously employed, the Nakagami-n and the Nakagami-q distributions. The former of these is the same as the Rician distribution. It is non-central χ-distributed with two degrees of freedom, that is, the distribution of modulus of a complex Gaussian variable whose components are uncorrelated with non-zero mean and equal variance. It is referred to as the Nakagami-Rice distribution by ionospheric physicists, while communication engineers call it simply the Rician distribution [39].

The latter of the two, the Nakagami-q, spans the range from one-sided Gaussian fading to Rayleigh fading. The q- distribution is the distribution of modulus of a complex Gaussian random variable whose components are uncorrelated with zero mean and unequal variance and is commonly referred to as the Nakagami- Hoyt distribution.

In creating the m-distribution, Nakagami was able to span with one distribution the entire range from one-sided Gaussian fading to non-fading. However, the real importance of the Nakagami-m fading model lies in the fact that it can often be used to fit experimental data. The literature contains results of many propagation studies where experimenters have found close agreement between the Nakagami distribution and measured fading scintillation data, i.e. [39, 25, 18].

In addition to providing a useful fading model to fit experimental data, the Nakagami-m distribution offers features of analytical convenience in comparison to the Rician distribution. This is true because the Nakagami-m distribution is a central distribution, while the Rician is not. As a result of this distinction, it is found that analytical results for the Nakagami model possesses greater mathematical simplicity than do those for the Rician.

In fairness, however, it should be mentioned that there are some limitations associated with the Nakagami-m fading model. First, it does not provide a clear intuitive picture of the fading mechanism (in contrast to the Rician model). In addition there is no phase distribution associated with the Nakagami-m amplitude distribution.

All fading statistics in this thesis will assume the Nakagami-m distribution, unless stated otherwise and will be termed simply the Nakagami distribution. For a detailed discussion of all the Nakagami distributions, Crepeau can be consulted [39].

The Nakagami probability density function is given by

$$p_R(r) = \frac{2r^{2m-1}}{\Gamma(m)} \left(\frac{m}{\Omega}\right)^m \exp\left(-\frac{mr^2}{\Omega}\right) \qquad \forall \qquad r \geq 0, \tag{A.1}$$

where $\Gamma(m)$ is the Euler Gamma function, $\Omega = E\{r^2\}$ and $m = \frac{\Omega^2}{Var\{r^2\}}$, with the constraint $m \geq 1/2$.

For $m = 1$ and $m = \frac{1}{2}$, (A.1) reduces to Rayleigh and a one-sided Gaussian distribution respectively. It also approximates, with high accuracy, the Rician distribution and approaches the log-normal distribution under certain conditions [1]. As $m \to \infty$ we have a channel that becomes non-fading (as the pdf tends to an impulse response). Therefore, the amount of fading is indicated by $1/m$.

In our subsequent analysis the Nakagami squared distribution will be needed frequently. That is, we define a random variable γ as

$$\gamma = \mu' R^2. \tag{A.2}$$

where μ' is an arbitrary constant. Applying common statistics [72] we can write (A.1) as

$$p(\gamma) = \left(\frac{m}{\gamma_0}\right)^m \frac{\gamma^{m-1}}{\Gamma(m)} \exp\left(-\frac{m\gamma}{\gamma_0}\right), \tag{A.3}$$

where

$$\gamma_0 = E\{r^2\}\mu'. \tag{A.4}$$

It is easily shown that, for $m = 1$, $p(\gamma)$ reduces to the exponential distribution, which is a Rayleigh squared distributed [72].

We will also need the sum of P Nakagami squared random variables, that is

$$\gamma_b = B \sum_{i=1}^{P} \gamma_i, \tag{A.5}$$

where B is an arbitrary constant.

Each of the $\{\gamma_i\}$ is distributed according to (A.3). Now we must determine the pdf of γ_b. This function is most easily determined via the characteristic function of γ_b. The characteristic function of γ_1 is easily shown to be

$$\psi_{\gamma_1}(jv) = E(e^{jv\gamma_1}) = (1 - jv\frac{\gamma_0}{m})^{-m}, \tag{A.6}$$

where $j = \sqrt{-1}$. Since the i random variables are statistically independent, the $\{\gamma_i\}$ are statistically independent and, hence, the characteristic function for the sum γ_p is simply the result in (A.6) raised to the Pth power

$$\psi_{\gamma_b}(jv) = E(e^{jv\gamma_1}) = (1 - jv\frac{\gamma_0}{m})^{-\epsilon}, \tag{A.7}$$

with $\epsilon = mP$.

Using integration tables from [76] it follows that the pdf $p(\gamma_b)$ is

$$p(\gamma_b) = \left(\frac{m}{\gamma_0}\right)^{\epsilon} \frac{\gamma_b^{\epsilon-1}}{\Gamma(\epsilon)} \exp\left(-\frac{m\gamma_b}{\gamma_0}\right) \qquad \forall \qquad \gamma_b \geq 0. \tag{A.8}$$

It is easily verified that for $P = 1$ we have (A.3) again, and for $\epsilon = 1$, we have a Rayleigh squared pdf again. A final test is to integrate (A.8) over γ_b; the result is indeed one, as it should be for a pdf.

Further, to calculate average error rates, the moments of (A.8) is needed, and is given by

$$\mu_n = \frac{\Gamma(\epsilon + n)}{\Gamma(\epsilon)} \left(\frac{\gamma_0}{m}\right)^n. \tag{A.9}$$

APPENDIX B

GOLD SPREADING SEQUENCES

This appendix describes the spreading code generation method used and tabulates the generator polynomials for $N = \{511, 255, 127, 63, 31\}$ to ensure repeatability of results produced in this thesis.

Generator polynomials and the generation of spreading sequences are not as standard as one would like. Various authors use different notations [101, 70]. The notation of Pursley [70] is used throughout and briefly described below.

Pseudo-noise (PN) sequence codes applied in our numerical evaluations are Gold sequences [102] obtained from multiplying two primitive polynomials. For instance, for $N = 127$ we have

$$h_1(x) = x^7 + x^3 + 1 \tag{B.1}$$

and

$$h_2(x) = x^7 + x^3 + x^2 + x + 1, \tag{B.2}$$

represented by octal numbers 211 and 217, respectively. Hence the resulting sequence is

$$h(x) = x^{14} + x^9 + x^8 + x^6 + x^5 + x^4 + x^2 + x + 1, \tag{B.3}$$

represented by 41567, in octal notation.

To find the actual codes, initial loadings are chosen to generate maximal length sequences, as described by i.e. Dixon and Holmes [19, 102] . In general, with a generator polynomial of the form

$$h(x) = h_0(x)x^n + h_1(x)x^{n-1} + \cdots + h_{n-1}(x)x + h_n \tag{B.4}$$

and for an initial loading of

$$\underline{\alpha}_0 = (\alpha_0, \alpha_1, \cdots, \alpha_{n-1}), \tag{B.5}$$

the following recursive formula to generate the codes can be utilised

$$\alpha_{j+n} = h_1\alpha_{j+n-1} \oplus \cdots \oplus h_{n-1}\alpha_{j+1} \oplus h_n\alpha_j \quad \forall \quad j \geq 0, \tag{B.6}$$

where $\oplus$ stands for modulo-2 addition. Notice that in (B.6) for simplicity the chips are represented by α instead of a_i^k as introduces in (3.10). The generated codes have three-valued autocorrelation function sidelobes and a three-valued cross correlation taking on values from the set $\{+15, -1, -17\}$ for the $N = 127$ example.

In the capacity assessments of Chapters 5, 6 and 7 where $K > \frac{N+1}{2} + 1$ the correlation values for the same family of Gold codes are re-used when a family of Gold codes are not large enough. In other words, the capacity assessments are realistic if there are a large enough family of codes available.

The generator polynomials, $\hbar$, for the Gold sequences adopted in this thesis are presented in Table B.1 in octal. The initial loadings, $\underline{\alpha}_0$, were chosen in such a way to generate maximal length sequences and were obtained by an exhaustive computer search.

N	$\hbar$
511	1510313
255	326161
127	41567
63	14551
31	3013

Table B.1: Generator polynomials for maximal length Gold sequences for $N = \{511, 255, 127, 63, 31\}$

APPENDIX C

ERROR CONTROL CODE PARAMETERS

The coding bounds, code generator polynomials and code parameters used in Chapters 5, 6 and 7 to calculate coded system performance are presented for convolutional and block codes.

C.1 Convolutional Codes

The convolutional codes used in this study are rate $R_{cd} = \{\frac{1}{2}, \frac{1}{4}, \frac{1}{8}\}$ codes, having constrained lengths $\nu = \{2, 3, 4, 6\}$. These binary codes are optimal in the sense that, for a given rate, and a given constrained length, they have the largest possible d_{free}. The generator polynomials are tabulated in C.1 [72, 96].

R_{cd}	ν	d_{free}	Generator polynomials in octal
1/2	2	5	(5, 7)
1/2	3	6	(15, 17)
1/2	4	7	(23, 35)
1/2	6	10	(133, 171)
1/4	2	10	(5, 7, 7, 7)
1/4	3	13	(13, 15, 15, 17)
1/4	4	16	(25, 27, 33, 37)
1/8	2	21	(7, 7, 5, 5, 5, 7, 7, 7)
1/8	3	26	(17, 17, 13, 13, 13, 15, 15, 17)
1/8	4	32	(37, 33, 25, 25, 35, 33, 27, 37)

Table C.1: Generator polynomials of convolutional codes

As explained in [72, 96, 97], when considering maximum likelihood decoding (Viterbi decoding) with hard decision decoding, the probability of selecting an incorrect path in the decoder trellis,

can be represented by

$$P_2(d) = \sum_{k=(d+1)/2}^{d} \binom{d}{k} P_e^k (1-P_e)^{d-k} \quad \forall \quad d \quad \text{odd} \tag{C.1}$$

and

$$P_2(d) = \sum_{k=d/2+1}^{d} \binom{d}{k} P_e^k (1-P_e)^{d-k} + \frac{1}{2}\binom{d}{d/2} P_e^{d/2}(1-P_e)^{d/2} \quad \forall \quad d \quad \text{even.} \tag{C.2}$$

The first event error probability can be overabounded by the sum of the error probabilities $P_2(d)$ over all possible paths which merge with the all zero path at the given node. We therefore obtain the union bound

$$P_u < \sum_{d=d_{free}}^{\infty} a_d P_2(d), \tag{C.3}$$

where the coefficients $\{a_d\}$ represent the number of paths corresponding to the set of distances $\{d\}$. These coefficients are the coefficients in the expansion of the transfer function $T(D)$ [72].

An expression for the upper bound on the bit error probability can be obtained as

$$P_e < \sum_{d=d_{free}}^{\infty} \varrho_d P_2(d) \tag{C.4}$$

where the $\{\varrho_d\}$ are the coefficients of the derivative of the transfer function of the convolutional code.

The coefficients $\{\varrho_d\}$ are only available for $R_{cd} = \{\frac{1}{2}, \frac{1}{3}\}$ from [96]. Using the method described in [103], the coefficients for $R_{cd} = \{\frac{1}{4}, \frac{1}{8}\}$, $\nu = \{2, 3, 4, 6\}$ were calculated and presented in Tables C.3 and C.4. For convenient reference the $\{\varrho_d\}$ is also presented in Table C.2.

Using (C.1), (C.2) and (C.4) together with Tables C.2 to C.4 it is possible to calculate the convolutional coded performance of the system described in Chapter 2.

			ϱ_d for $d =$				
R_{cd}	ν	d_{free}	d_{free}	$d_{free}+1$	$d_{free}+2$	$d_{free}+3$	$d_{free}+4$
1/2	2	5	1	4	12	32	80
1/2	3	6	2	7	18	49	130
1/2	4	7	4	12	20	72	225
1/2	6	10	36	0	211	0	1404

Table C.2: Rate $R_{cd} = \frac{1}{2}$ convolutional code partial weight structure

			ϱ_d for $d =$				
R_{cd}	ν	d_{free}	d_{free}	$d_{free}+1$	$d_{free}+2$	$d_{free}+3$	$d_{free}+4$
1/4	2	10	2	1	4	9	12
1/4	3	13	2	0	4	0	10
1/4	4	16	0	7	0	17	0

Table C.3: Rate $R_{cd} = \frac{1}{4}$ convolutional code partial weight structure

C.2 Block Codes

The error probability bounds derived in text books like [96, 72, 104] are based on the assumption that maximum likelihood decoding is used. Unfortunately, the most common decoding techniques for binary BCH codes are not true maximum likelihood procedures, so that the performance bounds are optimistic. The standard BCH decoding algorithms are bounded distance algorithms and error patterns with more than t error can never be corrected. The bit error probability for these decoders is

$$P_b \leq \sum_{i=t+1}^{n} \frac{i+t}{n} \binom{n}{i} P_e^i (1-P_e)^{n-i}, \tag{C.5}$$

where t is the number of channel errors that can be corrected by the code. The values of n, k and t for all known BCH codes up to length $n = 1023$ are given in Lin and Costello [97]. The block codes investigated in this work is tabulated in Table C.5.

			ϱ_d for $d =$				
R_{cd}	ν	d_{free}	d_{free}	$d_{free}+1$	$d_{free}+2$	$d_{free}+3$	$d_{free}+4$
1/8	2	21	1	2	0	0	0
1/8	3	26	2	4	0	0	0
1/8	4	32	8	0	0	0	4

Table C.4: Rate $R_{cd} = \frac{1}{8}$ convolutional code partial weight structure

n	k	t	Generator polynomials in octal
7	4	1	13
15	7	2	721
31	16	3	107657
63	30	6	157464165547
63	16	11	6331141367235453
127	36	15	3146074666522075044764574721735
127	15	27	2205704244560455477052301376221760435 3

Table C.5: Generator polynomials of block codes

APPENDIX D

MOMENTS OF THE IUI VARIABLE

The average probability of error expressions in (3.25) and (3.53) assumes N_m moments of the random variable α, which is a function of independent random parameters : τ_k, Θ_k and b_1^k. Furthermore, α is independent and symmetrically distributed; hence the odd moments of α_k are all zero. Therefore, having the even moments of α_k, one can determine the moments of

$$\alpha = \sum_{k=2}^{K} \alpha_k, \tag{D.1}$$

using a three step method prescribed in [105], where from the cumulants of the random variables, the moments of α are arrived at.

Since

$$\alpha_k = \frac{V_k}{T} \left\{ b_{-1}^k R_{k,1}(\tau_k) + b_0^k \hat{R}_{k,1}(\tau_k) \right\} \cos \Theta_k, \tag{D.2}$$

then,

$$N_m = E\{\alpha_k^{2j}\} = \frac{1}{T^{2j}} E\left\{ \left[b_{-1}^k R_{k,1}(\tau_k) + b_0^k \hat{R}_{k,1}(\tau_k) \right]^{2j} \right\} E\left\{ [\cos \Theta_k]^{2j} \right\} E\left\{ V_k^{2j} \right\}, \tag{D.3}$$

where j is the number of moments.

Since Θ is an independent random variable, it can be dealt with separately. That is, we first evaluate

$$E\left\{[\cos\Theta_k]^{2j}\right\} = \frac{\binom{2j}{j}}{4^j} \tag{D.4}$$

and then find the first expectation of (D.3) as

$$H = \frac{1}{T}\int_0^T \left[b_{-1}^k R_{k,1}(\tau_k) + b_0^k \hat{R}_{k,1}(\tau_k)\right]^{2j} d\tau_k, \tag{D.5}$$

with the expectation in H is over the random delay τ_k.

The expectation of (D.3) can now be expressed as

$$N_m = E\{z_k^{2j}\} = \frac{\binom{2j}{j}}{4^j}\frac{E\{V_k^{2j}\}}{N^{2j+1}}\sum_{n=0}^{N-1}\sum_{r=0}^{j}\binom{2j}{2r}\Gamma_{j,r,n} \tag{D.6}$$

with $\Gamma_{j,r,n}$ given by

$$\begin{aligned}\Gamma_{j,r,n} = \sum_{i=0}^{2r}(-1)^i \frac{(B_{n_{k,1}})^i}{(\hat{B}_{n_{k,1}})^{i+1}(i+1)} \cdot \frac{\binom{2r}{i}}{\binom{2(j-r)+i+1}{i+1}} \\ \cdot\Big\{(A_{n_{k,1}}+B_{n_{k,1}})^{2r-i}\cdot(\hat{A}_{n_{k,1}}+\hat{B}_{n_{k,1}})^{2(j-r)+i+1} \\ -(A_{n_{k,1}})^{2r-i}\cdot(\hat{A}_{n_{k,1}})^{2(j-r)+i+1}\Big\},\end{aligned} \tag{D.7}$$

where the parameters $A_{n_{k,1}}$, $B_{n_{k,1}}$, $\hat{A}_{n_{k,1}}$ and $\hat{B}_{n_{k,1}}$ are as defined in (3.9).

Further, we notice that for a Nakagami distribution

$$E\{V_k^{2j}\} = \frac{\Gamma(\epsilon+j)}{\Gamma(\epsilon)}\left(\frac{\nu_{0_k}}{m}\right)^j 2^j, \tag{D.8}$$

where $\nu_{0_k} = E\{V_k^2/2\}$ is the average strength of the Nakagami faded path associated with the kth interfering user.

Having the moments of α_k the moments of α can be determined as explained earlier. Equation

(D.6) enables us to accurately evaluate the performance of a DS/SSMA system.

APPENDIX E

MULTIPATH VARIANCE OF IUI

Tables E.1 to E.5 tabulates the variance, σ^2_{ma}, under multipath faded conditions. Equations (3.31) and (3.56) use these tables to investigate the validity of the Gaussian Assumption for $N = \{511, 255, 127, 63, 31\}$ and $E\{\beta^2\} = -10$ dB. Since the variance is only the second moment as calculated in Appendix D, it is not a function of the Nakagami fading parameter m, but nevertheless a function of $E\{\beta^2\}$.

These tables can be generalized to a large extent. If, for example, the variance of $N = 511$, $K = 50$, $L = 5$ is needed, a graph can be drawn from the available data in Table E.1 and extended to $K = 50$. Reasonably accurate estimates can be obtained since the IUI variance has linear characteristics.

Also, the variance for different values of $E\{\beta^2\}$ can be calculated by scaling the tabulated values of Tables E.1 to E.5. For example, for $N = 511$, $K = 20$, $L = 5$, $\sigma^2_{ma} = 0.001584$ from Table E.1. To determine the variance for $E\{\beta^2\} = -20$ dB, $\sigma^2_{ma} = 0.001584$ is multiplied by 0.1, resulting in $\sigma^2_{ma} = 0.0001584$, since $E\{\beta^2\}$ is ten times less for this example.

		K						
		2	**5**	**10**	**15**	**20**	**25**	**30**
L	1	6.68E-05	0.000261	0.000589	0.000911	0.001236	0.001573	0.001833
	2	0.000154	0.000348	0.000676	0.000998	0.001323	0.00166	0.00192
	3	0.00024	0.000435	0.000763	0.001085	0.00141	0.001747	0.002007
	4	0.000327	0.000521	0.000849	0.001171	0.001497	0.001834	0.002094
	5	0.000414	0.000608	0.000936	0.001258	0.001584	0.001921	0.00218
	6	0.000501	0.000695	0.001023	0.001345	0.00167	0.002007	0.002267
	7	0.000588	0.000782	0.00111	0.001432	0.001757	0.002094	0.002354
	8	0.000675	0.000869	0.001197	0.001519	0.001844	0.002181	0.002441
	9	0.000761	0.000955	0.001284	0.001605	0.001931	0.002268	0.002528
	10	0.000848	0.001042	0.00137	0.001692	0.002018	0.002355	0.002614

Table E.1: Variance of Multipath faded SSMA, $N = 511$, $E\{\beta^2\} = -10$ dB

		K				
		2	**5**	**10**	**15**	**20**
L	1	0.000142	0.000537	0.001156	0.001829	0.002386
	2	0.000317	0.000712	0.001331	0.002004	0.002561
	3	0.000492	0.000887	0.001506	0.002179	0.002737
	4	0.000668	0.001063	0.001682	0.002354	0.002912
	5	0.000843	0.001238	0.001857	0.00253	0.003087
	6	0.001018	0.001413	0.002032	0.002705	0.003263
	7	0.001193	0.001589	0.002208	0.00288	0.003438
	8	0.001369	0.001764	0.002383	0.003056	0.003613
	9	0.001544	0.001939	0.002558	0.003231	0.003789
	10	0.001719	0.002115	0.002733	0.003406	0.003964

Table E.2: Variance of Multipath faded SSMA, $N = 255$, $E\{\beta^2\} = -10$ dB

		K				
		2	**5**	**10**	**15**	**20**
L	1	0.000535	0.002111	0.004679	0.007141	0.00981
	2	0.00141	0.002986	0.005554	0.008016	0.010685
	3	0.002285	0.00386	0.006428	0.008891	0.01156
	4	0.003159	0.004735	0.007303	0.009765	0.012435
	5	0.004034	0.00561	0.008178	0.01064	0.013309
	6	0.004909	0.006484	0.009053	0.011515	0.014184
	7	0.005783	0.007359	0.009927	0.01239	0.015059
	8	0.006658	0.008234	0.010802	0.013264	0.015933
	9	0.007533	0.009108	0.011677	0.014139	0.016808
	10	0.008408	0.009983	0.012551	0.015014	0.017683

Table E.3: Variance of Multipath faded SSMA, $N = 127$, $E\{\beta^2\} = -10$ dB

		K				
		2	**5**	**10**	**15**	**20**
L	1	0.000697	0.002498	0.005324	0.008228	0.010797
	2	0.001866	0.003667	0.006493	0.009397	0.011966
	3	0.003035	0.004835	0.007662	0.010565	0.013134
	4	0.004203	0.006004	0.00883	0.011734	0.014303
	5	0.005372	0.007173	0.009999	0.012903	0.015472
	6	0.006541	0.008342	0.011168	0.014071	0.01664
	7	0.00771	0.00951	0.012337	0.01524	0.017809
	8	0.008878	0.010679	0.013505	0.016409	0.018978
	9	0.010047	0.011848	0.014674	0.017578	0.020147
	10	0.011216	0.013016	0.015843	0.018746	0.021315

Table E.4: Variance of Multipath faded SSMA, $N = 63$, $E\{\beta^2\} = -10$ dB

		K			
		2	**5**	**10**	**15**
L	1	0.001342	0.005272	0.011166	0.017023
	2	0.004259	0.008189	0.014083	0.01994
	3	0.007176	0.011106	0.017000	0.022857
	4	0.010093	0.014023	0.019917	0.025774
	5	0.01301	0.01694	0.022834	0.028691
	6	0.015927	0.019857	0.025751	0.031608
	7	0.018844	0.022774	0.028668	0.034525
	8	0.021761	0.025691	0.031585	0.037442
	9	0.024678	0.028608	0.034502	0.040359
	10	0.027595	0.031525	0.037419	0.043276

Table E.5: Variance of Multipath faded SSMA, $N = 31$, $E\{\beta^2\} = -10$ dB

APPENDIX F

GAUSSIAN ASSUMPTION DERIVATION OF CPSK PERFORMANCE

Consider the integral

$$I = K \int_0^\infty \gamma_b^{\epsilon-1} \exp\left(-\frac{m\gamma_b}{\overline{\gamma}_b}\right) \operatorname{erfc}\left(\sqrt{\gamma_b \Lambda}\right) d\gamma_b \tag{F.1}$$

where

$$K = \frac{1}{2\Gamma(\epsilon)} \left(\frac{m}{\overline{\gamma}_b}\right)^\epsilon. \tag{F.2}$$

Letting $t = \sqrt{\gamma_b \Lambda}$ we have

$$I = 2K\Lambda^{-\epsilon} \int_0^\infty \operatorname{erfc}(t) t^{2\epsilon-1} \exp\left(-\frac{mt^2}{\Lambda\overline{\gamma}_b}\right) dt. \tag{F.3}$$

Recalling that $\operatorname{erfc}(x) = 1 - \operatorname{erf}(x)$ and defining

$$G = \int_0^\infty t^{2\epsilon-1} \exp\left(-\frac{mt^2}{\Lambda\overline{\gamma}_b}\right) dt \tag{F.4}$$

and

$$H = -\int_0^\infty \mathrm{erf}(t) t^{2\epsilon-1} \exp\left(-\frac{mt^2}{\Lambda\overline{\gamma}_b}\right) dt. \tag{F.5}$$

Equation (F.3) can therefore be written as

$$I = 2K\Lambda^{-\epsilon}(G + H). \tag{F.6}$$

By making the change in variable

$$x = \frac{mt^2}{\Lambda\overline{\gamma}_b} \tag{F.7}$$

and realising that

$$\Gamma(z) = k^z \int_0^\infty t^{z-1} \exp(-kt) dt, \tag{F.8}$$

G in (F.4) can be evaluated as

$$G = \frac{\Gamma(\epsilon)}{2} \left(\frac{\Lambda\overline{\gamma}_b}{m}\right)^\epsilon. \tag{F.9}$$

Furthermore, using integration tables by Ng and Geller [75], an integral of the form

$$\int_0^\infty \mathrm{erf}(x) \exp\left(-b^2t^2\right) t^r dt = \frac{b^{-(r+2)}}{\sqrt{\pi}} \Gamma\left(\frac{r}{2}+1\right) {}_2F_1\left(\frac{1}{2}; \frac{r}{2}+1; \frac{3}{2}; -b^{-2}\right) \tag{F.10}$$

results.

Using (F.10), it is possible to solve H in (F.5) as

$$H = -\frac{\Gamma\left(\frac{2\epsilon+1}{2}\right)}{\sqrt{\pi}}\left(\frac{m}{\Lambda\overline{\gamma}_b}\right)^{-\left(\frac{2\epsilon+1}{2}\right)} {}_2F_1\left(\frac{1}{2};\frac{2\epsilon+1}{2};\frac{3}{2};-\frac{\Lambda\overline{\gamma}_b}{m}\right). \tag{F.11}$$

Simplification and substituting the results of (F.9) and (F.11) in (F.6) gives

$$I = \frac{1}{2}\left\{1-\frac{2\Gamma\left(\epsilon+\frac{1}{2}\right)}{\sqrt{\pi}\Gamma(\epsilon)}\sqrt{\frac{\Lambda\overline{\gamma}_b}{m}}\,{}_2F_1\left(\frac{1}{2};\epsilon+\frac{1}{2};\frac{3}{2};-\frac{\Lambda\overline{\gamma}_b}{m}\right)\right\}, \tag{F.12}$$

which is the desired result in (3.31).

APPENDIX G

CPSK PERFORMANCE AS $m \to \infty$

As mentioned in Appendix A, $m = \infty$ corresponds to an unfaded signal. Consequently, since $L = 1$, a RAKE receiver would not constitute any advantage, and therefore P and ϵ are equal to one and m respectively for this condition. Now, taking the limit of $m \to \infty$ in (3.31) and making the change in variable $x = \sqrt{\Lambda \overline{\gamma}_b}$, we have

$$I = \lim_{m\to\infty} \frac{1}{2}\left\{1 - \frac{\Gamma\left(m+\frac{1}{2}\right)2x}{\Gamma(m)\sqrt{\pi m}}\, {}_2F_1\left(\frac{1}{2}; m+\frac{1}{2}; \frac{3}{2}; -\frac{x^2}{m}\right)\right\}. \tag{G.1}$$

By definition [76] the Gauss hypergeometric series is defined as

$${}_2F_1(a;b;c;x) = \frac{\Gamma(c)}{\Gamma(a)\Gamma(b)} \sum_{n=0}^{\infty} \frac{\Gamma(a+n)\Gamma(b+n)}{\Gamma(c+n)} \frac{x^n}{n!} \tag{G.2}$$

and the series expansion of the error function as

$$\mathrm{erf}(x) = \frac{2}{\sqrt{\pi}} \sum_{n=0}^{\infty} \frac{(-1)^n x^{2n+1}}{(2n+1)n!}. \tag{G.3}$$

Using the identity of (G.2), (G.1) can be written as

$$I = \lim_{m\to\infty} \frac{1}{2}\left\{1 - \frac{1}{\sqrt{\pi}} \sum_{n=0}^{\infty} \frac{\Gamma\left(n+\frac{1}{2}\right)}{\Gamma\left(n+\frac{3}{2}\right)} \frac{\Gamma\left(m+n+\frac{1}{2}\right) m^{-\left(n+\frac{1}{2}\right)}}{\Gamma(m)} \frac{(-1)^n x^{2n+1}}{n!}\right\}. \quad \text{(G.4)}$$

Making use of the recurrence formulas of the Gamma function [76], we can write

$$\Gamma\left(n+\frac{1}{2}\right) = \frac{1.3.5.7\ldots(2n-1)}{2^n}\Gamma\left(\frac{1}{2}\right) \quad \text{(G.5)}$$

and

$$\Gamma\left(n+\frac{3}{2}\right) = \frac{1.3.5.7\ldots(2n-1)(2n+1)}{2^n}\Gamma\left(\frac{3}{2}\right). \quad \text{(G.6)}$$

Therefore, using (G.5) and (G.6)

$$\frac{\Gamma\left(n+\frac{1}{2}\right)}{\Gamma\left(n+\frac{3}{2}\right)} = \frac{2}{(2n+1)}. \quad \text{(G.7)}$$

Further, let us consider

$$\lim_{m\to\infty} \frac{\Gamma\left(m+n+\frac{1}{2}\right) m^{-\left(n+\frac{1}{2}\right)}}{\Gamma(m)}. \quad \text{(G.8)}$$

Since $\Gamma(m)$ dominates $m^{\left(n+\frac{1}{2}\right)}$ and $\frac{\Gamma\left(m+n+\frac{1}{2}\right)}{\Gamma(m)} = 1$ as $m \to \infty$, (G.8) equals one.

Therefore, substituting (G.7) and (G.8) in (G.4), and making use of (G.3) we have

$$\begin{aligned} I &= \frac{1}{2}\left\{1 - \frac{1}{\sqrt{\pi}} \sum_{n=0}^{\infty} \frac{2}{(2n+1)} \frac{(-1)^n x^{2n+1}}{n!}\right\} \quad \text{(G.9)} \\ &= \frac{1}{2}\{1 - \operatorname{erf}(x)\} \end{aligned}$$

$$= \frac{1}{2}\text{erfc}(x).$$

Substituting $x = \sqrt{\Lambda\overline{\gamma}_b}$ in (G.9) and recalling that

$$\frac{1}{\Lambda} = 1 + 2\frac{E_b}{N_0}\sigma_{ma}^2 \tag{G.10}$$

and

$$\overline{\gamma}_b = \beta_1^2\frac{E_b}{N_0}, \tag{G.11}$$

we have

$$P_e = \frac{1}{2}\text{erfc}\left\{\left(\frac{N_0}{E_b} + 2\sigma_{ma}^2\right)^{-\frac{1}{2}}\right\} \tag{G.12}$$

which is the same as the unfaded CPSK performance derived in (3.35).

APPENDIX H

GAUSSIAN SQUARED VARIABLE

We will derive the statistics of two Gaussian variables, X_1 and X_2, corrupting a conjectural received signal $r(t)$. This scenario can be mathematically expressed as

$$r(t) = A\cos(\omega_c t + \theta_c) + x(t)\cos(\omega_c t + \theta_c) - y(t)\sin(\omega_c t + \theta_c), \tag{H.1}$$

where θ_c is the arbitrarily phase of the received signal and

$$Y = X_1^2 + X_2^2 \tag{H.2}$$

Y is a Gaussian variable with mean $A\cos(\omega_c t + \theta_c)$. We also assume that the variables has the same mean, $m_x = m_y$, and variance $\sigma_x^2 = \sigma_y^2 = \sigma^2$. The joint pdf of x and y is given by

$$p_{X,Y}(x,y) = \frac{1}{2\pi\sigma^2}\exp\left\{-\frac{(x-m_x)^2 + (y-m_y)^2}{2\sigma^2}\right\}. \tag{H.3}$$

Using the transformation $x + A = R\cos\theta$ and $y = R\sin\theta$ we can calculate the new pdf using

$$p_{R,\Theta}(R,\theta) = p_{X,Y}(x,y).\left|J\left(\frac{(x,y)}{(R,\theta)}\right)\right|_{x+A=R\cos\theta, y=R\sin\theta}, \tag{H.4}$$

where $J(\delta)$ is the Jacobian of δ. We therefore have

$$
\begin{aligned}
J\left(\frac{(x,y)}{(r,\theta)}\right) &= Det\begin{vmatrix} \frac{\partial x}{\partial R} & \frac{\partial x}{\partial \theta} \\ \frac{\partial y}{\partial R} & \frac{\partial y}{\partial \theta} \end{vmatrix} \\
&= Det\begin{vmatrix} \cos\theta & -R\sin\theta \\ \sin\theta & R\cos\theta \end{vmatrix} \\
&= R
\end{aligned} \tag{H.5}
$$

Simplifying the terms $(x - m_x)^2$ in (H.3) we have

$$
\begin{aligned}
(x - m_x)^2 &= (R\cos\theta - A)^2 \\
&= A^2 + \frac{R^2}{2} - 2AR\cos\theta + \frac{1}{2}R^2\cos 2\theta
\end{aligned} \tag{H.6}
$$

and

$$
y^2 = R^2\sin^2\theta. \tag{H.7}
$$

Substituting (H.5) and (H.6) in (H.3) we have

$$
p_{R,\theta}(R,\Theta) = \frac{R}{2\pi\sigma^2}\exp\left\{-\frac{A^2 + R^2 - 2AR\cos\theta}{2\sigma^2}\right\}. \tag{H.8}
$$

To have the pdf of (H.8) as a single variable in R, we must perform the following integration

$$
\begin{aligned}
p_R(r) &= \frac{R}{2\pi\sigma^2}\int_0^{2\pi}\exp\left\{\frac{A^2 + R^2 - 2AR\cos\theta}{2\sigma^2}\right\}d\theta \\
&= \frac{R}{2\pi\sigma^2}\exp\left\{\frac{A^2 + R^2}{2\sigma^2}\right\}\int_0^{2\pi}\exp\left\{\frac{AR}{\sigma^2}\cos\theta\right\}d\theta \\
&= \frac{R}{\sigma^2}\exp\left\{\frac{A^2 + R^2}{2\sigma^2}\right\}I_0\left(\frac{AR}{\sigma^2}\right)
\end{aligned} \tag{H.9}
$$

which is the desired result used in Chapter 4.

BIBLIOGRAPHY

[1] H. Hasemi, "The indoor radio propagation channel," *Proceedings of the IEEE*, vol. 81, pp. 941–968, July 1993.

[2] T. Bell, "Telecommunications in the third world," *IEEE Spectrum*, pp. 22–25, January 1994.

[3] R. Hazell, *Electrical Communication*. Paris, France: Alcatel, 2nd quarter ed., 1993.

[4] D. Cox, "Universal portable radio communications," *IEEE Transactions on Vehicular Technology*, vol. 34, pp. 117–121, August 1985.

[5] D. Cox, "Portable radio communications," *IEEE Communications Magazine*, vol. 27, pp. 30–40, July 1989.

[6] K. Raith and J. Uddenfeldt, "Capacity of digital cellular TDMA systems," *IEEE Transactions on Vehicular Technology*, vol. 40, pp. 323–332, May 1991.

[7] K. Murota and K. Hirade, "GMSK modulation for digital mobile radio telephony," *IEEE Transactions on Communications*, vol. COM-29, pp. 1044–1050, July 1981.

[8] "An overview of the application of CDMA to digital cellular systems and personal cellular networks," tech. rep., Qualcomm Inc., San Diego, Ca, May 1992.

[9] W. Lee, *Mobile Communication Fundamentals*. John Wiley & Sons, second ed., 1993.

[10] A. J. Viterbi, "When not to Spread Spectrum-A Sequel," *IEEE Communications Magazine*, vol. 23, pp. 12–17, April 1985.

[11] K. Gilhousen, I. Jacobs, R. Padovani, and L. Weaver, "Increased capacity using CDMA for mobile satellite communications," *IEEE Transactions on Selected Areas in Communication*, vol. 8, pp. 503–514, May 1990.

[12] K. S. Gilhousen, I. M. Jacobs, R. Padovani, and et al, "On the Capacity of a Cellular CDMA System," *IEEE Transactions on Vehicular Technology*, vol. 40, no. 2, pp. 303–312, May 1991.

[13] L. Milstein, T. Rappaport, and R. Barghouti, "Performance evaluation for cellular CDMA," *IEEE Journal on Selected Areas in Communications*, vol. 10, pp. 680–689, May 1992.

[14] W. Lee, "Overview of cellular CDMA," *IEEE Transactions on Vehicular Technology*, vol. 40, pp. 291–302, May 1991.

[15] D. L. Schiling and L. B. Milstein, "Spread Spectrum for Commercial Communications," *IEEE Communications Magazine*, pp. 66–79, April 1991.

[16] R. J. Lambert and J. W. Mark, "Multiple access techniques for indoor radio communications," in *IEEE Pacific Rim Conference*, (Toronto, Canada), May 1989.

[17] M. Spellman, "A comparison between frequency hopping and direct spread PN as antijam techniques," *IEEE Communications Magazine*, March 1983.

[18] M. A. Mokhtar and C. Gupta, "Power control considerations for DS/CDMA personal communication systems," *IEEE Transactions on Vehicular Technology*, vol. 41, pp. 479–487, November 1992.

[19] R. C. Dixon, *Spread Spectrum Systems.* Wiley, New York, 1984.

[20] M. Pursley and D. Sarwarte, "Performance Evaluation for Phase Coded SSMA Communications - Part II: Code Sequence Analysis," *IEEE Transaction on Communications*, vol. COM-25, no. 8, pp. 800–803, August 1977.

[21] J. Mazo, "Some theoretical observations on spread spectrum communications," *Bell Systems Technical Journal*, vol. 58, pp. 2013–2023, November 1979.

[22] K. Yao, "Error performance of asynchronous spread spectrum multiple access communication systems," *IEEE Transactions on Communications*, vol. COM-25, pp. 803–809, August 1977.

[23] G. L. Turin, "The Effects of Multipath and Fading on the Performance of Direct-Sequence CDMA Systems," *IEEE Journal on Selected Areas in Communications*, vol. SAC-2, pp. 597–603, July 1984.

[24] M. Kavehrad, "Performance of Nondiversity Receivers for spread spectrum in Indoor Wireless Communications," *AT&T Technical Journal*, vol. 64, no. 6, pp. 1181–1210, July-August 1985.

[25] H. Xiang, "Binary Code-Division Multiple-Access Systems operating in Multiple Fading, Noisy channels," *IEEE Transactions on Communications*, vol. COM-33, no. 8, pp. 775–784, August 1985.

[26] G. Cooper and R. Nettleton, "A spread spectrum technique for high-capacity mobile communications," *IEEE Transactions on Vehicular Technology*, vol. VT-27, pp. 264–275, November 1978.

[27] E. Geraniotis and M. Pursley, "Performance of coherent DS/SS communications over specular multipath fading channels," *IEEE Transactions on Communications*, vol. COM-33, pp. 502–508, June 1985.

[28] E. Geraniotis and M. Pursley, "Performance of noncoherent DS/SS communications over specular multipath fading channels," *IEEE Transactions on Communications*, vol. COM-34, pp. 219–226, March 1986.

[29] E. Geraniotis, "Direct sequence SSMA communications over nonselective and frequency-selective rician fading channels," *IEEE Transactions on Communications*, vol. COM-33, pp. 102–111, May 1987.

[30] J. Lehnert and M. Pursley, "Error probabilities for binary DS/SSMA with random signature sequences," *IEEE Transactions on Communications*, vol. COM-35, pp. 87–98, January 1987.

[31] W. Lam and R. Steele, "Spread spectrum communications using diversity in an urban mobile radio environment," *IEEE Colloquium on methods of combating multipath effects in wide band digital cellular mobile systems*, October 1987.

[32] C. Gardner and J. Orr, "Fading effects on the performance of a SSMA communication system," *IEEE Transaction on Communications*, vol. COM-27, pp. 143–149, January 1979.

[33] R. Nettleton and H.Alavi, "Power control for a spread spectrum cellular mobile radio system," in *Proceedings of the 33Rd IEEE Vehicular Technology Conference*, pp. 242–246, May 1993.

[34] H. Alavi and R. Nettleton, "Downstream power control for a spread spectrum cellular mobile radio system," in *Procedings of GLOBECOM '82*, pp. 3.5.1–3.5.5, December 1982.

[35] M. Kavehrad and P. McLane, "Performance of Low-complexity Channel Coding and Diversity for Spread Spectrum in Indoor Wireless Communication," *AT&T Technical Journal*, vol. 64, pp. 1927–1965, October 1985.

[36] G. D. Boudreau, D. D. Falconer, and S. A. Mahmoud, "A Comparison of trellis Coded Versus Convolutionally Coded Spread Spectrum Multiple-Access," *IEEE Journal on Selected Areas in Communications*, vol. 8, no. 4, pp. 628–640, May 1990.

[37] R. Skaug and J. Robinson, "Operation of portable HF CDMA networks with controlled transmitter powers," *IEEE Proceedings*, vol. 129, pp. 15–20, December 1982.

[38] U. Charash, "Reception through Nakagami fading multipath channels with random delays," *IEEE Transactions on Communications*, vol. COM-27, pp. 657–670, April 1979.

[39] P. Crepeau, "Uncoded and coded performance of MFSK and DPSK in Nakagami fading channels," *IEEE Transactions on Communications*, vol. 40, pp. 487–493, March 1992.

[40] J. M. Holtzman, "On calculating DS/SSMA error probabilities," in *Proceedings of ISSSTA '92*, (Yokohama, Japan), pp. 23–26, November 29-December 2 1992.

[41] E. Ho and Y. Yeh, "A new approach for evaluating the error probability in the presence of intersymbol interference and Gaussian noise," *Bell Systems Technical Journal*, vol. 49, pp. 2249–2265, November 1970.

[42] O. Shimbo and M. Celebiler, "The probability of error due to ISI and Gaussian noise in digital communication systems," *IEEE Transactions on Communication Technology*, vol. COM-19, pp. 113–119, April 1971.

[43] J. Murphy, "Binary error rate caused by ISI and Gaussian noise," *IEEE Transactions on Communications*, vol. COM-19, pp. 1039–1046, September 1973.

[44] M. Nakhla, "A new method for error rate calculation and its application to fiber optic communication systems," in *Proceedings of Globecom*, (Washington, D.C.), November 1979.

[45] G. Baker and P. Graves-Morris, *Padé Approximations*. Reading, MA: Addison-Wesley, 1980.

[46] G. Golub and J. Welsch, "Calculation of Gauss Quadrature Rules," *Mathematics of Computation*, vol. 26, pp. 221–230, April 1969.

[47] S. Benedetto, "Error probability in the presence of ISI and additive noise for multilevel digital signals," *IEEE Transactions on Communications*, vol. COM-21, pp. 181–190, March 1973.

[48] M. Meyers, "Computing the Distribution of a Random Variable via Gaussian Quadrature Rules," *Bell System Technical Journal*, vol. 61, pp. 2245–2261, November 1982.

[49] J. Shore and R. Johnson *IEEE Transactions on Information Theory*, vol. IT-26, no. 26, 1980.

[50] E. Jaynes, "Information theory and statistical mechanics-I," *Physics Review*, pp. 620–630, 1957.

[51] J. van Campenhout and T. Cover, "Maximum entropy and conditional probability," *IEEE transactions on Information Theory*, vol. IT-27, pp. 483–489, July 1981.

[52] L. Mead and N. Papanicolaou, "Maximum Entropy in the Problem of Moments," *Journal on Mathematical Physics*, vol. 25, pp. 2404–2417, August 1984.

[53] A. Papoulis, "Maximum entropy and spectral estimation: A review," *IEEE Transactions on Acoustics, Speech and Signal Processing*, vol. ASSP-29, pp. 1176–1186, 1981.

[54] M. Kavehrad and M. Joseph, "Maximum Entropy and the Method of Moments in Performance Evaluation of Digital Communication Systems," *IEEE Transactions on Communications*, vol. COM-34, pp. 1183–1189, December 1986.

[55] M. Kavehrad and M. Joseph, "Maximum entropy and the method of moments in the evaluation of probability of error in digital communication systems," in *Proceedings of the Information Theory Science Systems Conference*, (Princeton University, Princeton, NJ), March 1986.

[56] F. Solms, P. van Rooyen, and J. Kunicki, "Maximum entropy in the performance analysis of SSMA systems," in *MaxEnt '94*, (Cambridge, UK), July 1994.

[57] F. Solms and P. van Rooyen, "Maximum entropy and average error rates in digital communication systems," in *MaxEnt '94*, (Cambridge, UK), July 1994.

[58] F. Solms, P. van Rooyen, and J. Kunicki, "Maximum entropy in digital communication systems," in *Proceedings of COMSIG '94*, (University of Stellenbosch), October 1994.

[59] F. Solms, P. van Rooyen, and J. Kunicki, "Maximum entropy and minimum relative entropy in performance evaluation of digital communication systems," *IEE Proceedings-I.* accepted for publication.

[60] P. van Rooyen and H. Ferreira, "Mathematical channel models for spread spectrum multiple access," *IEEE Pacific Rim Conference on Communications, Computers and Signal Processing*, pp. 200–205, 1993.

[61] P. van Rooyen, A. van Heerden, and J. Kunicki, "On the electromagnetic compatability of selected spread spectrum systems," in *Proceedings of the Eighth International Symposium on Electromagnetic Compatability*, (Wraclaw, Poland), pp. 226–230, June 1994.

[62] P. van Rooyen and J. Kunicki, "Performance evaluation of a coded cellular SSMA system," in *Proceedings of COMSIG '94*, (University of Stellenbosch), October 1994.

[63] P. van Rooyen and H. Ferreira, "Capacity evaluation of a DS/SSMA system," in *Proceedings of COMSIG '93*, (Rand Afrikaans University), August 1993.

[64] P. van Rooyen and J. Kunicki, "Performance of cellular SSMA with coding under fading and multipath conditions," **submitted to** *European Transactions on Telecommunications.*

[65] P. van Rooyen, J. Kunicki, and R. Pichna, "Performance of cellular SSMA with block coding under fading and multipath conditions," in *Proceedings of the Third International Symposium on Spread Spectrum Techniques and Applications*, (Oulu, Finland), pp. 263–267, July 1994.

[66] P. V. Rooyen, I. Opperman, and J. Kunicki, "Performance evaluation of Nakagami faded SSMA system," in *Proceedings of ISITA*, (Sydney, Australia), pp. 52–56, November 1994.

[67] P. van Rooyen and J. Kunicki, "Performance evaluation of a Nakagami faded DS/SSMA system with RAKE reception," **submitted to** *Wireless Personal Communications.*

[68] A. J. Viterbi, "Very Low Rate Convolutional Codes for Maximum Theoretical Performance of Spread Spectrum Multiple- Access Channels," *IEEE Journal on Selected Areas in Communications*, vol. 8, no. 4, pp. 641–649, May 1990.

[69] A. J. Viterbi, "Spread Spectrum Communications-Myths and Realities," *IEEE Communications Magazine*, vol. 17, pp. 11–18, May 1979.

[70] M. Pursley, "Performance Evaluation for Phase-Coded SSMA Communications - Part 1: System Analysis," *IEEE Transactions on Communications*, vol. COM-25, no. 8, pp. 795–803, August 1977.

[71] M. Pursley, *Spread spectrum multiple access communications.* Vienna, Austria and New York: Springer Verlag, 1981.

[72] J. G. Proakis, *Digital Communications.* McGraw-Hill, New York, 1983.

[73] Specification, "Wireless Local Access," 1992.

[74] B. Sklar, *Digital communications: Fundamentals and Applications.* Prentice Hall, 1988.

[75] E. Ng and M. Geller, "A table of integrals of the Error functions," *Journal of Research of the National Bureau of Standards*, vol. 73B, pp. 1–20, January-March 1969.

[76] M. Abramowitz and I. Stegman, *Handbook of Mathematical functions.* Washington, D.C.: National Bureau of Standards, 1964.

[77] M. Kavehrad and B. Ramamurthi, "Direct sequence spread spectrum with DPSK modulation and diversity for indoor wireless communications," *IEEE Transactions on Communications*, vol. COM-35, pp. 224–236, February 1987.

[78] L. Couch, *Digital and analog communication systems.* Macmillan Publishing Co., 1983.

[79] C. Cianci, R. Dogliotti, and A. Luvison, "Unified approach to the performance analysis of linear modulation systems with coherent detection," tech. rep., CSELT Rapporti Tecnici, July 1973.

[80] A. Luvison and G. Pirani, "Design and performance of an adaptive Kalman receiver for synchronous data transmission," *IEEE Transactions on Aerospace and Electronic Systems*, vol. AES-15, pp. 635–648, September 1979.

[81] R. Dogliotti, A. Luvison, and G. Pirani, "Error probability in optical fiber transmission systems," *IEEE Transactions on Information Theory*, vol. IT-25, pp. 170–178, March 1979.

[82] D. Laforgia, A. Luvison, and V. Zingarelli, "Bit Error Rate evaluation for Spread Spectrum Multiple-Access Systems," *IEEE Transactions on Communications*, vol. COM-32, no. 6, pp. 660–669, June 1984.

[83] R. Sack and A. Donovan, "An algorithm for Gaussian quadrature given modified moments," *Numerische Mathematik*, vol. 18, pp. 465–478, 1972.

[84] W. Gautschi, "On the construction of Gaussian quadrature rules from modified moments," *Mathematics of Computation*, vol. 24, pp. 245–260, April 1970.

[85] G. Golub, "Some modified matrix eigenvalue problems," *SIAM Review*, vol. 15, pp. 318–334, April 1973.

[86] A. Luvison, S. Benedetto, E. Biglieri, and V. Zingarelli, "Moment based performance evaluation of digital communication systems," *IEE Proceedings-I*, vol. 139, pp. 258–266, March 1992.

[87] C. Shannon *Bell systems technical journal*, no. 27, p. 379, 1948.

[88] A. Tagliani *Journal on Mathematical Physics*, no. 34, p. 326, 1993.

[89] N. Agmon, Y. Alhassid, and R. Levine *Journal on Computational Physics*, no. 30, p. 250, 1979.

[90] W. Press, W. Flannery, and S. Teukolski, *Numerical recipes in C.* Cambridge, UK: Cambridge university press, 2nd ed., 1992.

[91] K. Morletta and L. Lennert, "On the calculation of average error rates in spread spectrum systems," *Proceedings of ISSSTA '92*, pp. 25–29, 1992.

[92] A. Luvison, "Interpolatory quadrature rules and error rate of digital communication systems," *Electronic Letters*, vol. 16, pp. 16–17, January 1980.

[93] M. Pursley, D. Sarwate, and W. Stark, "Error probability for DS/SSMA communications - Part II: upper and lower bounds," *IEEE Transactions on Communications*, vol. COM-30, pp. 975–984, May 1982.

[94] M. Pursley and H. Roefs, "Numerical evaluation of correlation parameters for optimal phases of binary shift register sequences," *IEEE Transactions on Communications*, vol. COM-27, pp. 1597–1604, October 1979.

[95] R. Pickholtz, "Theory of Spread Spectrum Communications - A Tutorial," *IEEE Transactions on Communications*, vol. COM-30, no. 3, pp. 855–884, May 1982.

[96] G. C. Clark and J. Cain, *Error-Correcting Coding for Digital Communications.* Plenum Press, 1981.

[97] S. Lin and D. Costello, *Error Control Coding: Fundamentals and Applications.* Prentice Hall, 1983.

[98] W. C. Jakes, *Microwave Mobile Communications.* New York: Wiley, 1974.

[99] M. Lotter and L. Linde, "A comparison of three families of spreading sequences for CDMA applications," in *COMSIG-94 Proceedings*, (University of Stellenbosch), pp. 68–75, October 1994.

[100] R. Kohno, "Pseudo-noise sequences and interference cancellation techniques for spread spectrum systems," *IEICE Transactions on Communications, Electronics, Information and Systems*, vol. E74, pp. 23–35, May 1991.

[101] W. Peterson and W. Weldon, *Error Correcting Codes.* MIT Press, Cambrige, Ma, 1972.

[102] J. K. Holmes, *Coherent Spread Spectrum Systems.* Wiley and Sons, New York, 1982.

[103] A. J. Viterbi and J. Omura, *Principles of Digital Communications and Coding.* New York: McGraw-Hill, 1979.

[104] R. Ziemer and R. Peterson, *Digital Communications and Spread Spectrum Systems.* MacMillan Publishing Co., New York, 1985.

[105] D. Laforgia, A. Luvison, and V. Fingarelli, "Bit error rate evaluation for spread spectrum multiple access systems," *IEEE Transactions on Communications*, vol. COM-32, pp. 660–669, June 1984.